COMMONWEALTH OF AUSTRALIA
DEPARTMENT OF EXTERNAL AFFAIRS

AUSTRALIAN NATIONAL ANTARCTIC RESEARCH EXPEDITIONS

ANARE SCIENTIFIC REPORTS

SERIES A (IV) GLACIOLOGY

PUBLICATION No. 103

A STUDY OF THE LOCAL ICE CAP NEAR WILKES, ANTARCTICA

by

W. A. McLAREN

ISSUED BY THE ANTARCTIC DIVISION
DEPARTMENT OF EXTERNAL AFFAIRS, MELBOURNE
1968

Registered at the G.P.O. Melbourne
for transmission by post as a book.

Printed in Australia by
Brown Prior Anderson Pty Ltd 5 Evans Street Burwood Victoria

CONTENTS

LIST OF PLATES

LIST OF FIGURES

PREFACE

It was found during the field work of the ANARE at Wilkes 1960-61-62 that the local ice cap near Wilkes was in the form of a dome rising about 1400 m in the centre and with a radius of about 100 km. As such, it acted as an independent ice cap joined to the main Antarctic ice cap through the Totten-Vanderford glacier trench into which both glaciers flow. This local ice cap is in the medium-scale range between ice caps of the size of Drygalski Island (10 km radius) and the large ice caps of Greenland (500 km) and East Antarctica (1400 km). As a consequence, this Wilkes ice cap provides an ideal model for studying the dynamics of ice masses generally.

There is still not sufficient known about the flow law of natural ice to be able to calculate the movement of the interior of the large ice masses precisely. Hence, by conducting comprehensive measurements of the horizontal and vertical movement of the Wilkes ice cap as well as its temperature distribution, its elevation and ice thickness everywhere, its nourishment, wastage and its change in form, the theoretical equations of the dynamics of ice masses can be tested and developed to sufficient accuracy to enable the application of them generally and the ealculation of the dynamics of the large ice masses which, owing to their size, are much more difficult to measure. Furthermore, as a result of these measurements for the Wilkes ice cap, an accurate determination will be obtained of the present state of balance of this region of the Antarctic. With the addition of the information obtained from deep-core drilling through the ice cap, the history of the ice and climate in this region can be examined.

The Wilkes ice cap project is a long-term programme over many years designed to carry out the above measurements. The work is being performed by one Antarctic Division glaciologist at Wilkes each year, with logistic support making traverses in autumn, spring and summer of each year since 1964. In some years extra support has been provided by a surveyor from the Antarctic Mapping Branch of the Division of National Mapping, and a geophysicist from the Bureau of Mineral Resources, Geology and Geophysics. The programme has been under the general supervision of Dr. U. Radok of the Department of Meteorology of the University of Melbourne.

The first phase of the project was begun in 1964 with the location of the Wilkes Ice Dome centre (P. J. Morgan, glaciologist; K. Budnik, surveyor; R. Whitworth, geophysicist) and measurements of accumulation, elevation, and gravity around the northern triangle. The second phase consisted of two tellurometer traverses around the triangle by W. A. McLaren in 1965, and the establishment of a system of strain grids. The second traverse resurvey by McLaren obtained the first movement and strain measurements over the region. Ice thickness by gravity and seismic measurements were carried out by G. Allen. The present report by McLaren con-

tains the analyses of the work to this stage, which indicates a definite negative mass budget and net lowering of the ice cap. As McLaren's first tellurometer survey did not include angle measurement on two legs of the triangle, the complete velocity vectors were first obtained accurately in 1966 by L. Pfitzner who resurveyed the northern triangle, extended the study to the southern triangle, and optically levelled accurately to the Dome summit.

In 1967, D. Carter, using a precise Lacoste gravimeter, measured the rate of change of gravity over the region, due to the subsidence of the ice cap, to check on the mass flux divergence calculations from the movement measurements. A Scott Polar Research Institute-designed radio-echo sounder was used successfully to obtain detailed profiles around the triangle. The 1968 programme at present in operation aims at completing the radio-echo sounding over the region and repeating the optical levelling to determine directly the surface-lowering rate.

For 1969, the major aim is to study the deep inner structure and temperature distribution of the ice cap using a CRREL thermal drill and quartz thermometer. The information provided by these measurements is being used to test theoretical investigations of dynamics and temperature distributions.

The results of each year's work are being published as ANARE research reports.

W. Budd,
Senior Glaciologist.

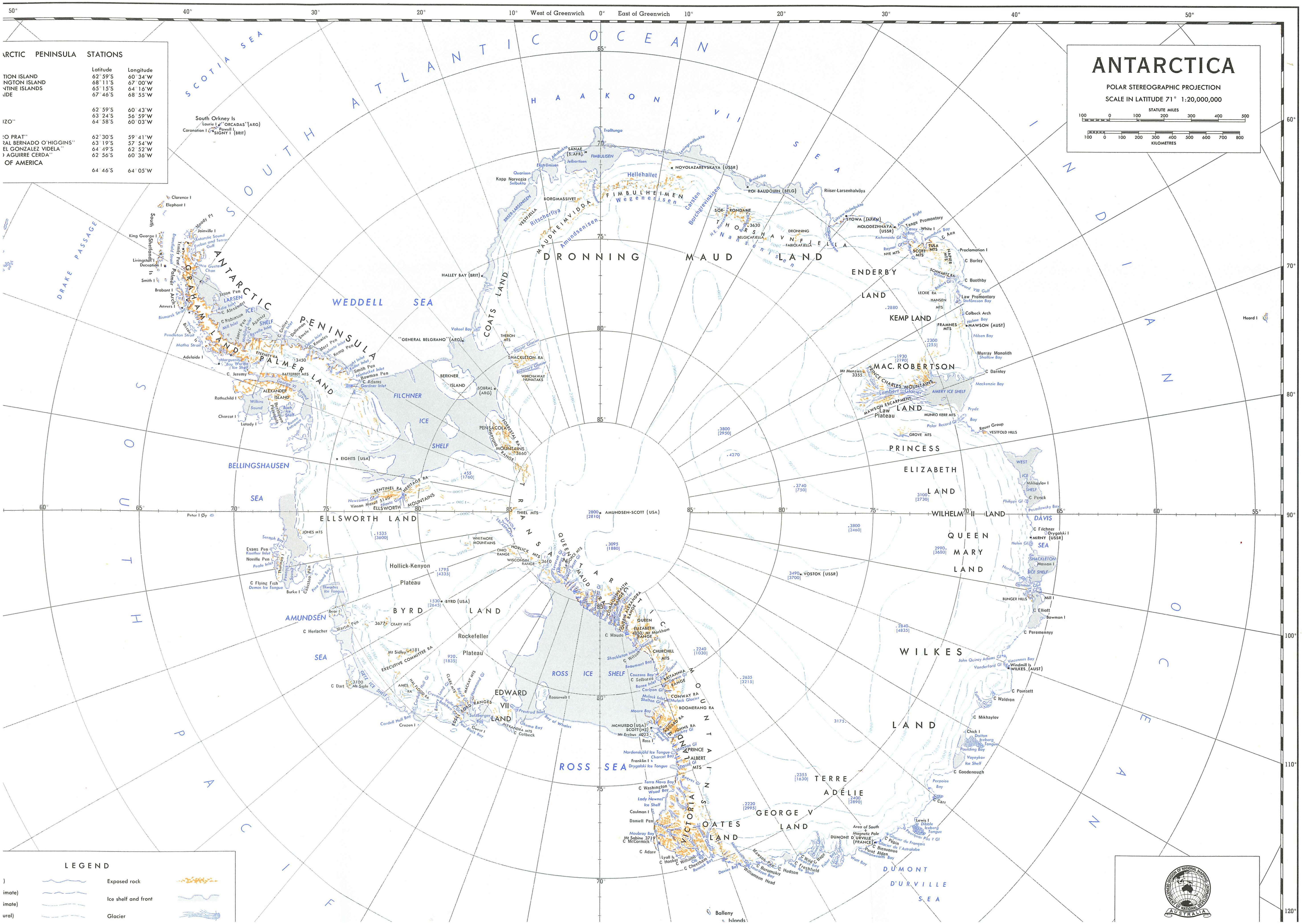
ANTARCTICA
POLAR STEREOGRAPHIC PROJECTION
SCALE IN LATITUDE 71° 1:20,000,000
STATUTE MILES
100 0 100 200 300 400 500
100 0 100 200 300 400 500 600 700 800
KILOMETRES
ARCTIC PENINSULA STATIONS
Latitude Longitude
TION ISLAND 62°59'S 60°34'W
NGTON ISLAND 68°11'S 67°00'W
NTINE ISLANDS 65°15'S 64°16'W
IDE 67°46'S 68°55'W
62°59'S 60°43'W
63°24'S 56°59'W
IZO" 64°58'S 60°03'W
O PRAT" 62°30'S 59°41'W
RAL BERNADO O'HIGGINS" 63°19'S 57°54'W
EL GONZALEZ VIDELA" 64°49'S 62°52'W
AGUIRRE CERDA" 62°56'S 60°36'W
OF AMERICA
64°46'S 64°05'W
West of Greenwich
East of Greenwich
SOUTH ATLANTIC OCEAN
SCOTIA SEA
DRAKE PASSAGE
HAAKON VII SEA
INDIAN OCEAN
SOUTH PACIFIC
WEDDELL SEA
BELLINGSHAUSEN SEA
AMUNDSEN SEA
ROSS SEA
DAVIS SEA
DUMONT D'URVILLE SEA
South Orkney Is
Laurie I "ORCADAS" (ARG)
Coronation I
Powell I
SIGNY I (BRIT)
Clarence I
Elephant I
South Shetland Is
King George I
Livingston I
Deception I
Smith I
ANTARCTIC PENINSULA
GRAHAM LAND
PALMER LAND
LARSEN ICE SHELF
ALEXANDER ISLAND
FILCHNER ICE SHELF
BERKNER ISLAND
SOBRAL (ARG)
"GENERAL BELGRANO" (ARG)
HALLEY BAY (BRIT)
COATS LAND
DRONNING MAUD LAND
SANAE (S. AFR)
NOVOLAZAREVSKAYA (USSR)
ROI BAUDOUIN (BELG)
SYOWA (JAPAN)
MOLODEZHNAYA (USSR)
ENDERBY LAND
KEMP LAND
MAWSON (AUST)
MAC. ROBERTSON LAND
PRINCE CHARLES MOUNTAINS
Lambert Glacier
AMERY ICE SHELF
PRINCESS ELIZABETH LAND
WILHELM II LAND
QUEEN MARY LAND
MIRNY (USSR)
WILKES LAND
WILKES (AUST)
TERRE ADÉLIE
DUMONT D'URVILLE (FRANCE)
GEORGE V LAND
OATES LAND
VICTORIA LAND
TRANSANTARCTIC MOUNTAINS
QUEEN MAUD RA
ROSS ICE SHELF
MCMURDO (USA)
SCOTT (NZ)
Mt Erebus 4023
Ross I
EDWARD VII LAND
Roosevelt I
BYRD LAND
BYRD (USA)
Hollick-Kenyon Plateau
Rockefeller Plateau
ELLSWORTH LAND
ELLSWORTH MOUNTAINS
Vinson Massif 5140
EIGHTS (USA)
AMUNDSEN-SCOTT (USA)
2800 [2810]
VOSTOK (USSR)
3490 [3700]
Peter I Øy
Heard I
Balleny Islands
Area of South Magnetic Pole
LEGEND
Exposed rock
Ice shelf and front
Glacier
DIVISION OF NATIONAL MAPPING
DEPARTMENT OF NATIONAL DEVELOPMENT
AUSTRALIA

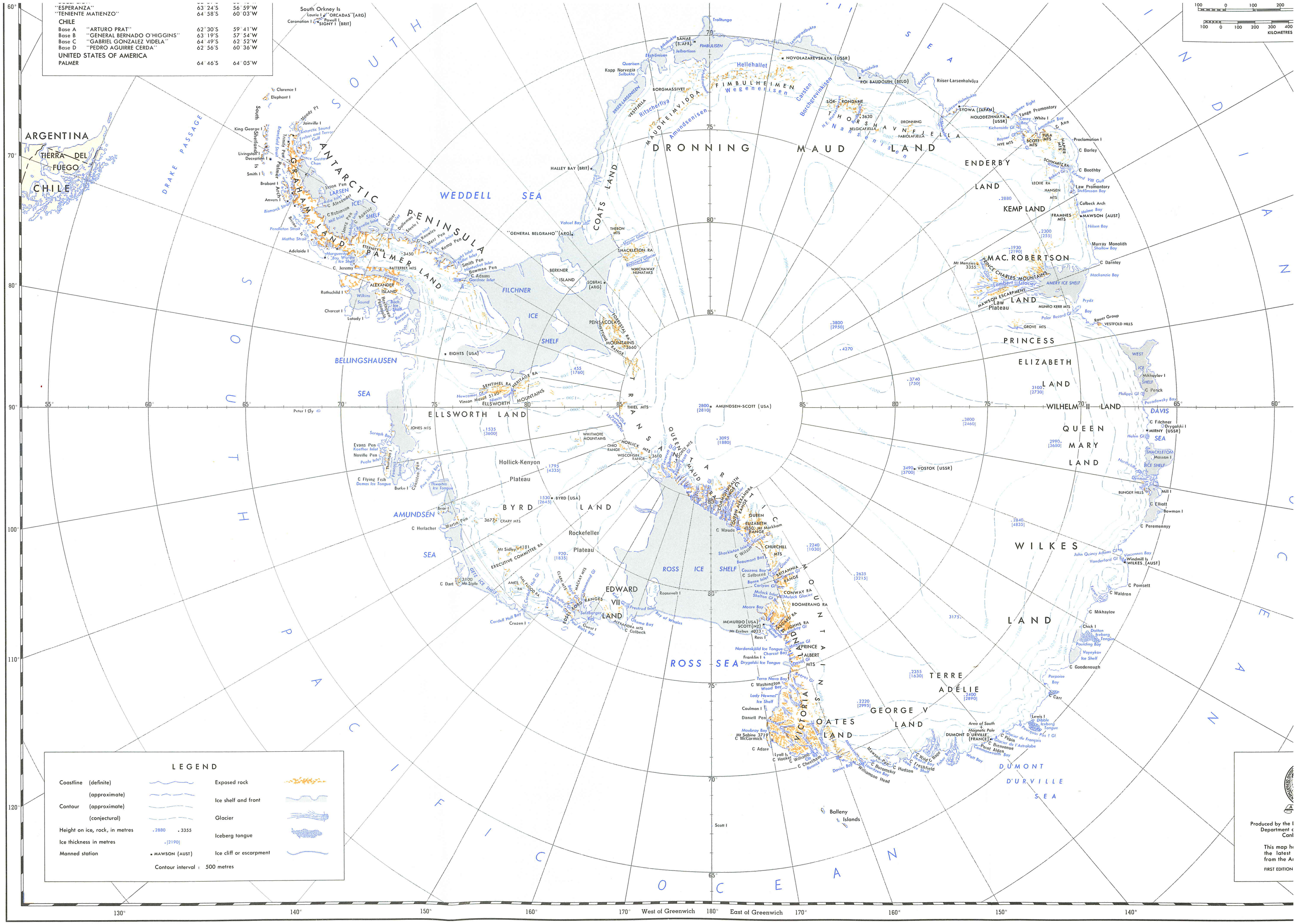

FIG. 1. Map of Antarctica.

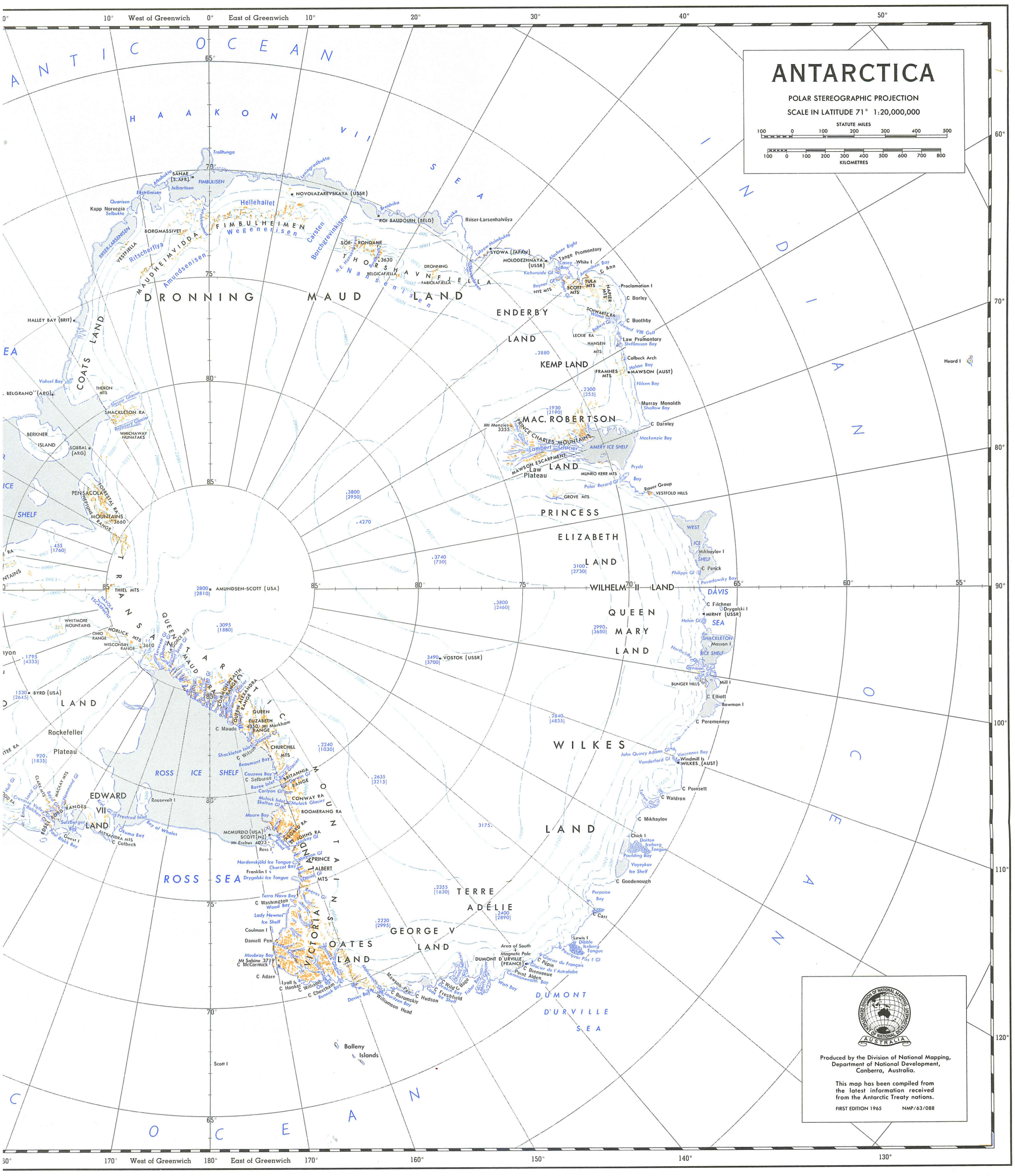

FIG. 1. Map of Antarctica.

ANTARCTIC PENINSULA STATIONS

		Latitude	Longitude
BRITAIN			
Base B	DECEPTION ISLAND	62°59'S	60°34'W
Base E	STONINGTON ISLAND	68°11'S	67°00'W
Base F	ARGENTINE ISLANDS	65°15'S	64°16'W
Base T	ADELAIDE	67°46'S	68°55'W
ARGENTINA			
"DECEPCIÓN"		62°59'S	60°43'W
"ESPERANZA"		63°24'S	56°59'W
"TENIENTE MATIENZO"		64°58'S	60°03'W
CHILE			
Base A	"ARTURO PRAT"	62°30'S	59°41'W
Base B	"GENERAL BERNADO O'HIGGINS"	63°19'S	57°54'W
Base C	"GABRIEL GONZALEZ VIDELA"	64°49'S	62°52'W
Base D	"PEDRO AGUIRRE CERDA"	62°56'S	60°36'W
UNITED STATES OF AMERICA			
PALMER		64°46'S	64°05'W

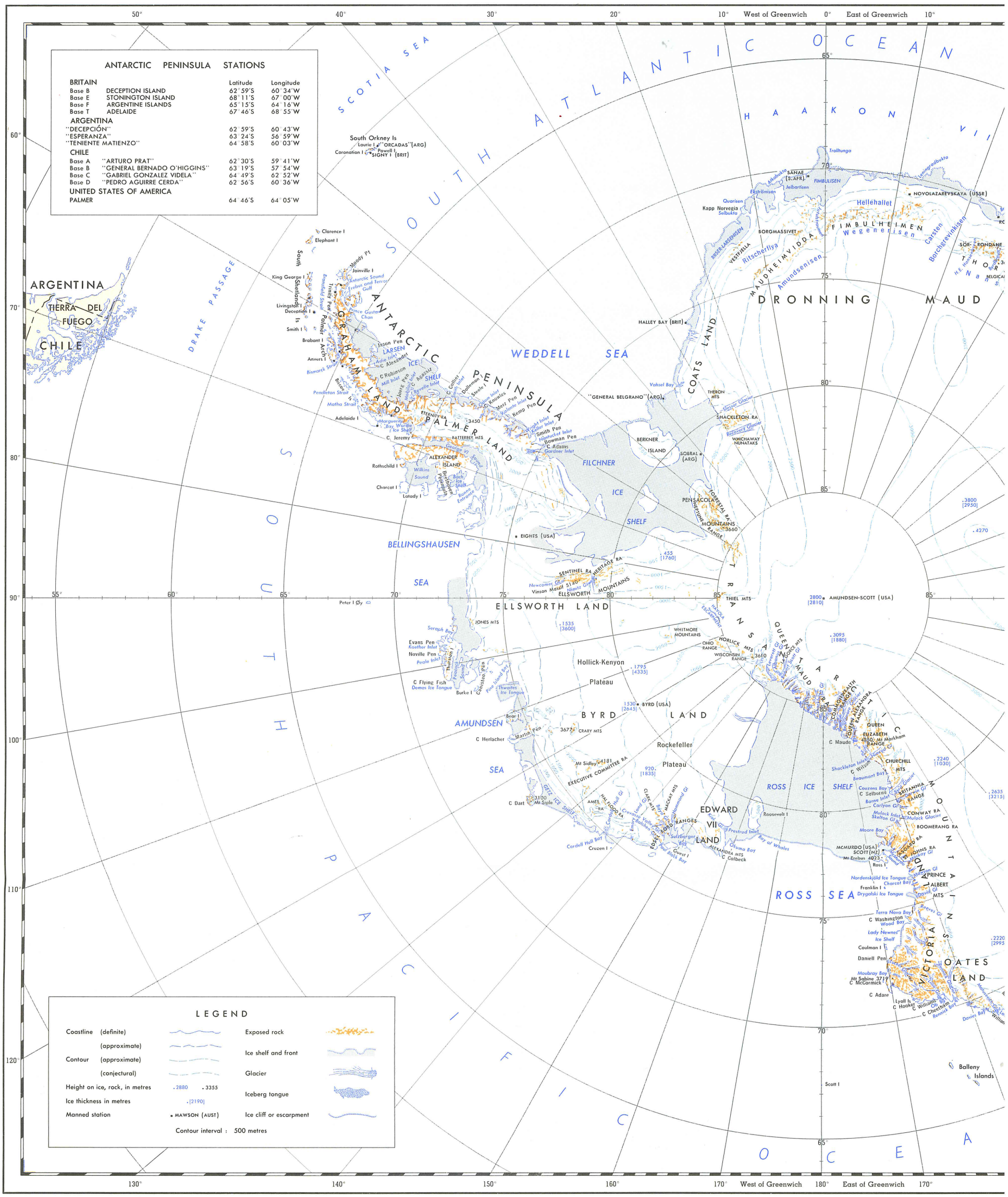

LEGEND

Coastline (definite)
(approximate)
Contour (approximate)
(conjectural)
Height on ice, rock, in metres .2880 .3355
Ice thickness in metres .[2190]
Manned station * MAWSON (AUST)

Exposed rock
Ice shelf and front
Glacier
Iceberg tongue
Ice cliff or escarpment

Contour interval : 500 metres

FIG. 1. Map of Antarctica.

A STUDY OF THE LOCAL ICE CAP NEAR WILKES, ANTARCTICA

by
W. A. McLaren

Antarctic Division, Department of External Affairs, Melbourne
and
Department of Meteorology, University of Melbourne

(Manuscript received January 1968)

ABSTRACT

The Wilkes Ice Dome project is both an investigation into the regime of an independent Antarctic ice cap, with regard to determining its state of mass balance, and a means of applying practical results to the theoretical work of other glaciologists.

The 1965 ANARE glaciological programme at Wilkes concerned the interrelation of surface and bedrock topography, accumulation, ice flow, surface strain rates and shear stresses over a triangular sector of this ice cap. The instruments and techniques used, the errors incurred, the methods of analyzing the field data and of obtaining the final results, are discussed.

The results show that the Wilkes Ice Dome does not correspond to an ideal ice cap and that it is not in a steady state of equilibrium. Lacking further studies on possible fluctuations of the coastline, it cannot be discerned whether the ice cap is becoming smaller, as calculations indicate, or is in the process of changing form while retaining a balanced mass budget.

Measurements made over the ice cap have been applied to theoretical works by Nye (1959A), Shumskiy (1961) and Budd (1967). The results indicate that, over the Wilkes ice cap, ice flow is governed largely by features of bedrock topography and that velocities are in accordance with the more recent glaciological theories of Shumskiy and Budd.

Parameters have been determined for the stress—strain relationship in both the basal layers of the ice and for the large mass of ice above the base. Values of $n = 3{\cdot}4$ and $B = 0{\cdot}85 \times 10^9$ dynes/cm^{2}sec$^{1/3}$ were found to apply in the basal layers over the triangle area, where stresses were about one bar and temperatures estimated at about -5°C; and values of $n = 1{\cdot}2$ and $B = 1{\cdot}3 \times 10^9$ dynes/cm^2 sec$^{1/3}$ were found for the upper ice along the Dome—Cape Poinsett leg where stresses averaged 0·1 bar and temperatures were about $-15°$ to -20°C. Due to the large lateral strains caused by bedrock topography, the investigation could not be carried out in the upper ice of the Dome—Cape Folger leg. The values of the stress parameters are in good agreement with those found by other workers for the stress and temperature ranges involved.

1. INTRODUCTION

A. BACKGROUND

Wilkes is located at about 66°15′S, 110°32′E (Fig. 1). It is situated at the western edge of a middle-sized ice cap whose bedrock is separated from the major Antarctic mass by the Vanderford-Totten Glacier trough, described by Cameron (1964). The area covered by the ice cap is roughly square, about 160 km across its N-S and E-W diagonals (see Fig. 2), with bedrock rising to over 400 m above sea level. The ice flow from the major continental plateau is diverted from the area by the Vanderford and Totten Glaciers allowing the ice cap, whose summit is known locally as "the Dome", to exist unaffected by external pressures.

From 1957 to 1962, glaciological programmes at the station were mainly concerned with accumulation, coastal ice movement and mass budget studies, often involving long traverses onto the continental plateau. In 1963 an initial attempt was made to obtain a continuous core through the local ice cap in order to study the effects of flow and pressure on ice petro-fabrics. While carrying on the deep drilling project in 1964, efforts were also made towards locating the exact position of the Dome summit and a start was made on an intensive study into the mechanics of ice flow throughout the local ice cap.

B. WILKES ICE DOME PROJECT

The Wilkes Ice Dome project is an investigation by glaciologists of the Australian National Antarctic Research Expeditions into all aspects of the regime of an independent Antarctic ice cap. The programme, to be spread over several years, calls for a detailed knowledge of surface and bedrock topography; accumulation rates; surface and subsurface velocities and strain rates along 3 major axes; rate of iceberg calving along the coast; and ice properties, temperatures and thermal gradients through the ice cap. From this information, studies such as the following are possible:

(i) the mass balance of the ice cap may be determined: such a study would be one of many called for around the periphery of Antarctica by the SCAR conference of 1963 to determine the state of balance of the continent;

(ii) an examination of the stress-strain relationship in polar glacial ice, to further investigate the flow laws of Glen (1955), Nye (1959A), Mellor and Smith (1965), Steinemann (1954), Butkovitch and Landauer (1958, 1960) and others;

(iii) determination of the effects of bedrock and surface topography on stresses within an ice cap, and comparison of theoretical works by Nye (1957, 1959A), Weertman (1957), Shumskiy (1961) and Budd (1967), with the actual behaviour of natural ice;

(iv) an examination of the effect of temperature on the flow law parameters;

(v) an examination of the effects of ice flow and accumulation on thermal

gradients in the ice cap to further the investigations of Jenssen and Radok (1963);

(vi) the determination of the effects of stress on the orientation of ice crystals and hence a basic study into the mechanism of ice flow.

Due to its surface regularity, the sector of the ice cap between Capes Folger and Poinsett has been chosen for the first part of the study into the state of mass balance, the relationship of stress and strain, and the effects of surface and bedrock topography on stresses in the ice cap.

The instrumentation used to date has involved barometers, optical levels and gravimeters for determining surface elevations; gravimeters and geophysical seismic equipment (operated by the Bureau of Mineral Resources, Geology and Geophysics) for bedrock elevations; theodolites, Tellurometer Micro-Distancer MRA-2's and invar tapes for distance, strain and flow measurements; and a photo-theodolite and aerial photography for determination of iceberg loss and coastal movement. New instruments are continually being introduced to the work for more accurate and detailed results over these and further fields of study.

This report describes the work done and results obtained during 1965, the second year of the project.

2. FIELD PROGRAMMES

A. 1964

In the autumn of 1964 the highest point of the ice cap was located by barometrie and optical levelling. A microgravity survey, using a Worden "Prospector" gravimeter, was made over the summit area and an X-pattern of accumulation stakes set out at 1·6 km spacing.

In the following spring, stake lines connecting the Dome, Cape Folger and Cape Poinsett were set out. Using intermediate poles, marker stakes at 1·6-km intervals were placed to within 4 minutes of a straight line (Plate 1). Accumulation and gravity readings were taken at each stake and elevation differences along the route measured barometrically every 0·3 km. Crevassing along the coast prevented the route approaching closer than 6 miles to the sea (Plate 2). Approximate surface and bedrock profiles were calculated from the barometric and gravity measurements (Morgan, unpublished).

B. 1965

1. *Proposed.*

The "Proposed 1965 Wilkes Glaciological Programme" requirements were:

a. Surface velocities were to be found by repeated surveys of marker stakes using Wild T-2 theodolites and tellurometer MRA-2's. Survey procedures, to be selected in the field, were to give an accuracy of between 1:10,000 and 1:20,000. Three such surveys were planned, in the autumn, spring and summer, to determine the difference between winter and summer strain rates.

b. Square strain grids were to be set out at selected positions around the triangle to determine the strain vectors in directions other than along the route. Their number and location were to be determined in the field, at least six being envisaged.

c. Ice thickness and rock topography measurements were to be made, supplementing those of 1964.

d. Accumulation readings were to be taken at all stakes around the triangle.

e. If time permitted, efforts to drill a deep hole through the ice cap, using the ANARE drill, were to be continued and temperature profiles measured.

f. Other work programmed, and generally carried out successfully, has no bearing on the Ice Dome Project and is not discussed below.

2. *Accomplished.*

a. In the autumn of 1965, a second set of stakes was placed along the previously marked route at distances of maximum intervisibility, i.e., between 1·5 and 9 km but averaging 4·5 km. Distances between the stakes were measured to an accuracy of better than one part in twenty-five thousand with the tellurometers. Horizontal and vertical angles were measured from Wilkes as far as the Dome

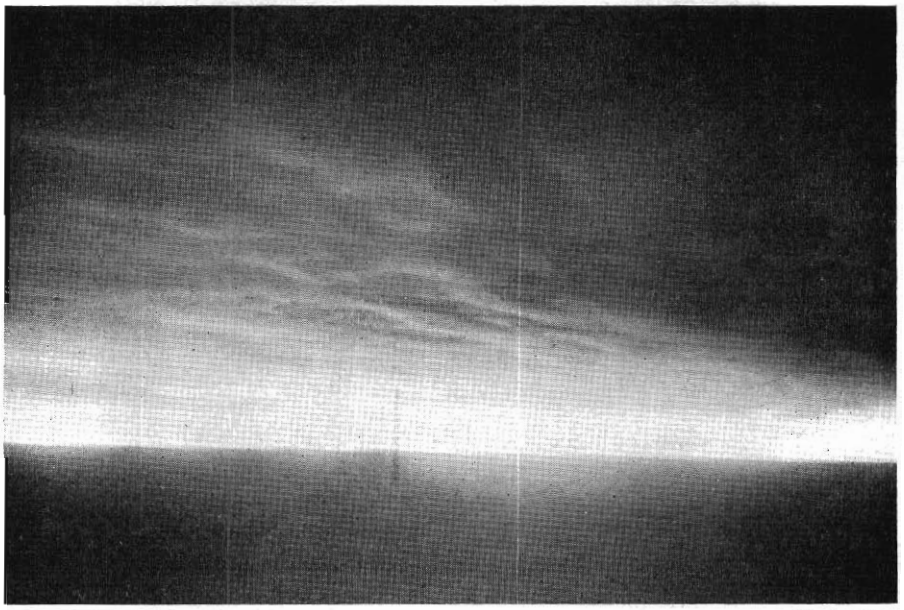

ANARE photo W. A. McLaren

PLATE 1
Marker stake along triangle route.

ANARE photo W. A. McLaren

PLATE 2
Hazards of working near the coast: crevassing prevented the route approaching closer than 6 miles to the sea.

summit via Cape Folger. Decreasing daylight and excessive shimmer caused by the sun's low altitude precluded theodolite work on the other two legs.

Instead of the square strain grids, three-arm rosettes with radii of 100 m were established at the corners and approximate third points of each side of the triangle. For greater accuracy, the rosette at the Dome summit had radii of 200 m. A six-arm rosette with radii of over 1·5 km was also established at the summit and measured with the tellurometers.

Gravity readings were taken with a Worden Prospector gravimeter, borrowed from the Bureau of Mineral Resources, Geology and Geophysics, at each of the route-marker and survey stakes. The ice thickness was measured directly by seismic reflection shots every 16 km around the triangle and, later in the year, at the corners of 16 km squares within the triangle area by G. A. Allen, the field seismologist for the Bureau.

Snow accumulation measurements were taken at each stake along the route and at as many of those in the previously established Dome network as could be found.

b. Due to a shortage of vehicles and personnel at the station, the early spring traverse was deleted from the programme, and the start of the summer traverse moved forward to November. On this trip, a complete survey of the stakes set out the previous autumn was accomplished to an accuracy of one part in ten thousand. Due to improved visibility, theodolite observations proceeded more quickly than in the previous autumn and the 340 km traverse was completed in six weeks, despite several lengthy blizzards.

All strain rosettes and accumulation stakes were remeasured and further markers set out at the edge of the crevassed area at Capes Folger and Poinsett.

c. No work was done with the ANARE drill. It was returned to Australia at the end of the year.

c. 1966-67

In the autumn of 1966, L. Pfitzner remeasured the leg from Cape Folger to the Dome summit by tellurometers. A second triangle was installed and surveyed, connecting the summit with strain grids 24 km SE and SW, in order to determine flow conditions on the southern slopes of the ice cap.

The leg between strain grid "A" and the summit was optically levelled during the winter and tied in to the bench mark at Wilkes, producing a surface profile with a probable error of ± 2 ft.

A complete survey of both triangles was again accomplished in the summer of 1966 which, when the results are analyzed, will give the first direct measurements of flow around the triangle taken over a period greater than one year.

Further work in 1967 includes the use of an optical level and precise gravimeter on each of the traverse legs to provide more accurate profiles and to give direct measurements of surface vertical velocities, and extending the area already covered by seismic and gravity readings, using gravimeter and radio echo-sounder to gain a more complete picture of the bedrock topography.

3. 1965 PROCEDURES AND ACHIEVEMENTS

A. ICE VELOCITY SURVEY

1. *Choice of survey methods.*

The ice flow rates were to be found by comparison of the geographic positions of stakes after repeated surveys. Three survey methods were considered: a. triangulation; b. trilateration; c. traverse.

a. Triangulation. In autumn 1964, an attempt to position the stakes by triangulation had failed, due to the heavy refraction and shimmering experienced over flat snow surfaces with the sun low in the sky. For most of the time, theodolite observations were limited to less than one mile, introducing too much error and lost time into the work.

b. Trilateration. The tellurometer MRA-2's were known to operate satisfactorily in conditions where, due to fog, light drift or shimmer, theodolite observations were impossible. To overcome the above problem in 1965, therefore, consideration had been given to doing the survey by trilateration.

As this requires many redundant measurements to determine accurately each new position, the survey stakes would need to have been few and widely spaced in order to complete the work in the allotted time. Two 20 ft-high collapsible aluminium towers were constructed to enable long tellurometer shots to be made over the curving plateau surface. Once on site, however, a shortage of personnel and serviceable vehicles precluded the economic use of trilateration and the survey was accomplished using tellurometer traverse methods.

c. Traverse. Due to the lack of rock outcrops along the Budd Coast, the tellurometer traverse had both to start and close at the second order trig. station NM/S/6 (formerly US Survey Station G-5) near Wilkes (Plate 3). Directions of lines were taken from the known azimuth from NM/S/6 to NM/S/7 on Chappel Island, 10·5 km away. Data sheets for these stations, supplied by the Division of National Mapping, are given in Appendix I.

2. *Survey specifications.*

At the time of departure for the Antarctic, there were no available Australian specifications relating traverse survey procedures to resulting accuracy. Canadian specifications, as given in the booklet "Specifications for Control Surveys" by the Department of Mines and Technical Surveys (1961), were therefore used.

The desired accuracy of 1:20,000 called for a second order survey. In the field, optical conditions and the lack of time combined to prevent this from being feasible, and third order procedures were adopted. The specifications state that a line joining any two points in a third order survey would have a maximum anticipated error after adjustment of 1 part in 10,000 in length and 20 seconds in azimuth.

"The term maximum anticipated error is used to indicate the greatest error that

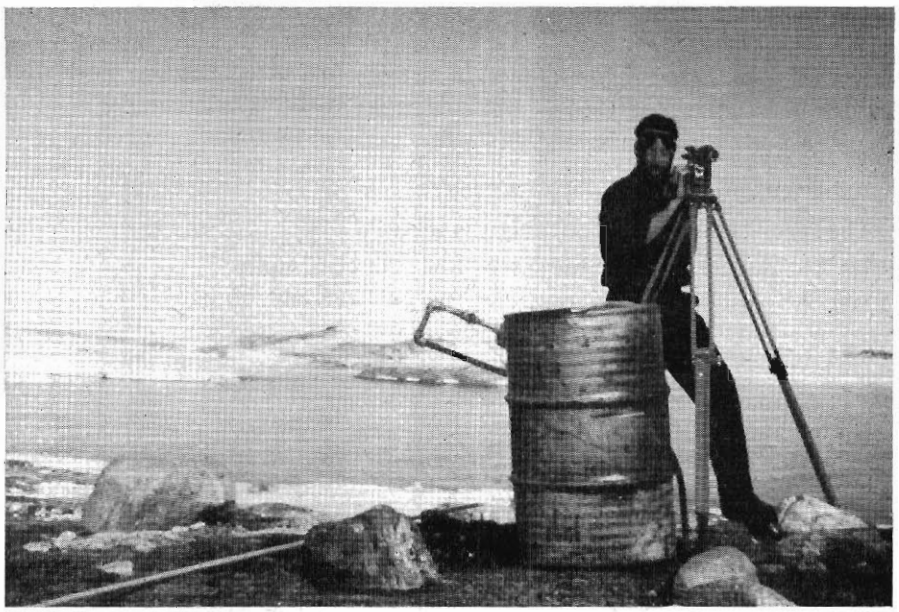

ANARE photo W. A. McLaren

PLATE 3

Theodolite set up over NM/S/6, near Wilkes.

may reasonably be expected, taking account of systematic as well as accidental errors. While this error cannot be computed accurately, it is believed more meaningful than a previously calculated probable or standard error in whose computation some sources of error may be neglected."

a. Aims.

The specifications used were:

(i) Length of traverse should not exceed 200 miles.

(ii) The maximum anticipated error in measured lengths should not exceed 1:15,000.

(iii) Three complete rounds should be read of each angle on a one-second reading theodolite, each round deviating from the accepted mean by no more than six seconds.

(iv) Astronomic azimuths, accurate to within three seconds, should be used as angular control every 15 stations.

(v) The closure in azimuth to not exceed the smaller of either 3 N or 10 $\sqrt{}$ N seconds, where N is the number of intermediate stations between control points.

(vi) The closure in position, after azimuth adjustment, should not exceed 1:5000.

As stated in "Specifications for Control Surveys", "the above detailed requirements should not be taken too rigidly but should be regarded as examples of the class of work necessary to attain the specified accuracy. In some cases, one requirement may be relaxed if another is tightened. For example, the length of a circuit

may be increased if the accuracy of individual measurements is increased accordingly."

It was found necessary at times to modify the specifications, particularly in regard to theodolite observations, but it is believed that this is compensated for by the high accuracy in distance measurements attained by the tellurometers.

b. Achievement.

The specifications were adhered to as follows:

(i) The overall length of the survey was about 212 miles.

(ii) All distances were measured to an accuracy of better than 1:25,000, averaging about 1:50,000 over the survey.

(iii) Wild T-2 or Kern DKM2 theodolites were used for all angular measurements.

On the autumn traverse it was not found possible to adhere to the specification. Of 27 angles measured between Wilkes and the Dome, 13 fitted the specification, 6 had one of the 3 rounds deviating up to 7 seconds, 6 more were taken as the mean of only 2 closely agreeing rounds, and 2 were calculated from a network of tellurometer measurements after lengthy delays due to fog and/or refraction. No angles were measured beyond the Dome.

On the summer traverse, 2 angles were taken as the mean of only 2 rounds. At 5 other stations the specification was met but the angle was considered to have slightly less weight than normal due to possible refractive effects. All other angles were measured satisfactorily.

(iv) Due to the 24-hour daylight, control azimuths were taken from the sun. Thirty readings were made on each face of the theodolite at both the Dome and Cape Poinsett. Due to a combination of errors, however, these turned out valueless, so that there is no azimuth control between the beginning and the end of the survey.

(v) Seventy-four theodolite stations were required to complete the survey. The closure in azimuth on the summer traverse was 30 seconds.

The azimuth of the last of the 27 traverse legs between Wilkes and the Dome on the autumn traverse agreed within 11 seconds of its value determined on the summer traverse.

(vi) The closure in position after the summer traverse was 24 m ESE, or 1:14,000. This included the effect of ice movement during the survey. The position of the Dome summit calculated from the autumn traverse was within 2·1 m, or 1:60,000 of the adjusted summer traverse position.

3. *Instrument operation.*

a. Tellurometer.

(i) Procedure. Basic tellurometer operating procedures are described in the manufacturer's instruction manual (Tellurometer Pty Ltd, 1963).

Three sets of coarse readings were taken on all lines. Taking these readings required negligible time, the third set being used to resolve any ambiguities or mistakes which later showed up in the office.

Twelve fine readings were taken on each line, and the arithmetic mean used for the transmit time. Ground swing was in all cases small, usually only one to two millimicroseconds (mμs). On many grazing shots it was doubtful if a complete cycle had been observed, but in these conditions the amplitude of the swing would be small, perhaps a small fraction of a foot, and inseparable from the other errors (Wadley, 1957).

Dry-bulb temperatures were read to 0·1°F before and after the measurement, using a Lambrecht-Assman psychrometer. This instrument tends to get clogged with drift in moderate winds.

Due to the low absolute humidity, wet-bulb temperatures were not read below freezing. In calculating distances a relative humidity of 50% was assumed, with little consequent error (see Section III.A.4).

Barometric pressures were read to 0·01 mbar before and after the measurement, using "Mechanism" digital aneroid barometers. Readings at each end of the line were taken on the snow surface simultaneously, to provide a check on elevation differences.

(ii) Performance. No major difficulties were experienced with the instruments in temperatures down to —45°C. Using muffs supplied by the manufacturers, the instrument warm-up times were less than ten minutes if left standing, or five minutes if coming from a vehicle. The plastic headphones fractured easily in the cold, however, and the mouth-pieces required a plastic cover to prevent the operator's breath penetrating and freezing, stopping vocal communication. Such stoppages were overcome on several occasions by auxiliary radios, Verey flare signals and a pre-arranged code of instructions sent by the speech-measure switch.

It was found impossible, due to low signal strength, to measure lines longer than 4 km over flat snow surfaces using optionally provided 17-inch circular reflectors on the instruments. Even this limited range was unattainable using the rectangular 17-inch reflectors normally provided. For grazing shots of greater distance, a 48-inch circular reflector was used on the master instrument (Plates 4 and 5). This was sufficient for all distances encountered, although a second 48-inch reflector was kept available for use at the remote instrument.

The dipole used with the 48-inch reflector is stated by Tellurometer Pty Ltd (1964), to add a constant 16·5 cm to the measurement. Two measurements made as a check over distances of 5 km and 6 km on the summer traverse showed an increase in length of only 10 cm. This value was used as the dipole correction in the calculations. Further investigation in 1967 showed that the amount of correction depended on the master instrument and the large dipole being used. It ranged between 8 cm and 25 cm with the various instrument combinations tested. No tests were made into the variation, if any, of this correction with distance. By using the correction measured in the field, no additional errors were introduced into calculated summer traverse distances. All autumn traverse distances between stakes 505/65 and H-1/65, however, and the longer intervals along the coastal leg, may be in error up to ±3 cm more than the normal tellurometer errors calculated in Section III.A.4. Due to the late determination of this information, it has not been considered in working out the results nor in anything said in the present report.

It was necessary to make an expanding screw-leg to support the 48-inch reflec-

PLATE 4. Tellurometer with 17-inch circular reflector. The muff-cover around the instrument reduced heat losses from crystal oven.

ANARE photo
W. A. McLaren

tor when mounted on the instrument. Prior to this, the increased reflector weight had pulled the instrument mounting boss away from the casing, causing the casing to buckle slightly. The threaded leg allowed the support to be adjusted to the height required by the tripod stance.

A sail-like effect of the large reflector in moderate winds was overcome by guying the instrument to ice pitons or other suitable anchors.

Attempts to gain ground clearance for the rays by operating the tellurometers from the Snowtrac roof (Plate 6) did not improve signal reception sufficiently to justify the risk to operator and instrument. Such procedure is impracticable with Snowtracs unless a suitable platform is mounted on the vehicle beforehand.

b. Theodolite. Poor optical conditions were the cause of most difficulties and of lost time on the surveys. At the start of the autumn traverse, shimmering, haze and refraction limited practical observing time to between 11 a.m. and 4 p.m. and eventually forced the angles to be dropped from the programme altogether. Shimmer and haze were less severe on the summer traverse, due to the higher altitude of the sun and, unless lifting was obviously significant, angular observations were taken neglecting the effects of vertical or horizontal refraction.

ANARE photo W. A. McLaren

PLATE 5. Tellurometer with special 48-inch reflector and 6½-inch dipole. A 48-inch reflector on one instrument doubled the normally received signal strength. The expanding screw leg, in this case assisted by a SIPRE corer, gave necessary snpport to the reflector. A plastic cover, taped over the mouthpiece, prevented moisture in the operator's breath from entering and freezing, and so stopping vocal communication.

A set of horizontal angles consisted of a reading on the preceding stake, the following stake and the preceding stake. If the initial and final readings to the back stake were more than ten seconds apart, the set was rejected. Two sets, with the instrument upright and inverted and circling clockwise and anti-clockwise, made up one round of angles. Three rounds with initial readings at zero, 60 and 120 degrees were taken at each stake, each round agrceing within six seconds of their mean. These angles were worked out by the notekeeper as observing progressed, so that additional rounds could be taken if necessary. In severe cold, the horizontal circle, despite special lubricants, dragged slightly after the telescope, causing rejection of many sets of readings.

ANARE photo W. A. McLaren

PLATE 6. Tellurometer with 48-inch reflector mounted on Snowtrac roof. Slippery footing and open hatch made this operation risky.

Minor difficulties often experienced with the theodolite in cold weather were:

(i) icing of the telescope eyepiece, which was avoided by the rigorous holding of one's breath while observing and avoiding close contact with the lens;

(ii) settlement of the tripod into soft snow, which was overcome by packing snow about the legs to keep off solar radiation and prevent melting (Plate 7).

Observing in hazy visibility was greatly facilitated by flagging made from PVC-coated cotton cloth. The luminescent cloth could be discerned as a patch of colour at 2 to 3 times the normal range of vision. Orange and pink were the most distinctive of the colours available. When the bamboo pole could not be seen, observations were made to the up-wind edge of the flagging. This material became very brittle and easily torn in low temperatures. It was best attached to the pole by making several horizontal slits near one edge and threading it over the top of the pole, the bamboo knobs holding it up. This allowed the flag to revolve in the wind and prevented its tearing, as happened when wired on.

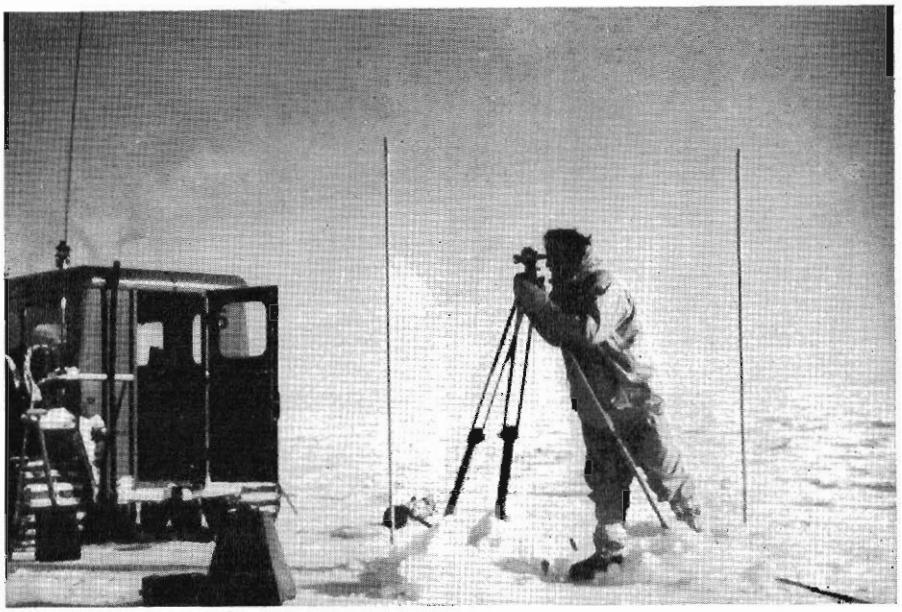

ANARE photo W. A. McLaren

PLATE 7

Kern DKM-2 theodolite being used near coast. Snow piled about tripod feet prevented settlement by melting into surface during operation.

4. *Errors.*

a. Tellurometer. The formulae used in reducing the transit time of a radio wave over double the length of a line to the actual distance are:

$$D = \frac{V}{2} \times \frac{\text{transit time}}{n},$$

where D = length of the line;

V = velocity of electromagnetic waves in vacuo = 299793 0 km/sec;

n = refractive index.

The value of n is calculated from

$$(n - 1)10^6 = \frac{77{\cdot}7}{273 + t}(P + E),$$

where P = barometric pressure in millibars;

t = dry-bulb temperature in °C;

E = equivalent pressure in millibars.

$$E = \frac{4744e}{273 + t},$$

where e = vapour pressure in mbars.

Sources of error in tellurometer measurements, as given by Edwards (unpublished) are:

(i) crystal frequencies, affecting transit times;
(ii) meteorological factors, affecting n;
(iii) reading accuracy and error distribution;
(iv) zero error of the instrument.

(i) Crystal frequencies. These were set to ± 1 cps before leaving Melbourne and checked as follows at Wilkes every six months.

An oscilloscope connected to a radio receiver compared the frequencies transmitted by each A master crystal (10·000 Mc/s) with WWV (10 Mc/s $\pm$ 0·1 cps). The A master crystals were trimmed to remove any beat from the CRO tube. This was estimated as accurate to ± 3 cps or 0·3 ppm.

The oscilloscope was then arranged to compare simultaneously the beat between an A master crystal and an A remote crystal, of a different instrument, with a generated 1 Kc/s signal. The A remote crystals of the second instrument were then trimmed to $\pm$ 10 cps.

Other master frequencies were checked by a frequency meter to ± 200 cps and the remote crystals set 1 Kc below.

The checks showed that a maximum error of 3 ppm may have been introduced into the autumn measurements through crystal frequency drift, but that none was likely in the summer results.

The MRA2 oven keeps the crystal temperature at 50°C $\pm$ 3°C. With a temperature deviation of 0·4 ppm/°C this allows a maximum accidental error of ± 1 ppm.

(ii) Meteorological factors. An error of 3 mbars in barometric pressure introduces an error of 0·90 ppm into the calculation of the refractive index n. The digital aneroids used had a maximum error in reading, calibration and temperature correction of 2 mbars, or well under 1 ppm.

Wet-bulb temperatures were not read below freezing point and a relative humidity of 50% was assumed. The vapour pressure is given by

$$e = e' - [0{\cdot}000660(1 + 0{\cdot}00115t')]P(t - t')$$

where t' and e' are the wet bulb temperature and saturation vapour pressure respectively.

At zero degrees C, e' is 6·107 mb. By assuming 50% humidity, therefore, the maximum error introduced into e is 3·05 mb. With a barometric pressure always about 950 mb when these temperatures were experienced (i.e., on the summer traverse between Wilkes and Cape Folger and on several shots along the coastal leg), the maximum error which can be introduced into n is less than 15 ppm. At a temperature of -10°C and pressure of 825 mb the error is less than 7 ppm and at the normal working temperatures below -20°C is completely negligible.

Dry bulb temperatures, measured by aspirating Lambrecht-Assmann psychrometers with calibrated thermometers, had an error of $\pm 0{\cdot}2$°F, affecting n by 0·4 ppm. Despite efforts to keep them free of vehicle heating effects, errors up to 3°F were detected on occasions. As the dry bulb temperature used in the calculation was the mean of 4 readings, such an error in one recording would only affect the calculated distance by 1 ppm.

Apart from the summer traverse measurements along the coastal leg, where

temperatures above —10°C were experienced, the probable error due to meteorological conditions is therefore $\pm 1/3 \times (7 + 1)$ or about the ± 3 ppm usually attained by the instruments (Telluronieter, 1963) (Kelsey, 1959A, B) (Edwards, unpublished) (Wadley, 1957) (Humphries and Brazier, 1958).

(iii) Empirically, it has been found by Edwards that the probable error of a series of fine readings is

$$PE = \frac{\text{(range of ground swing)}}{20\sqrt{f}}, \text{ in } m\mu s,$$

where f = number of fine readings.

On the Dome traverses, 12 fine readings were taken over each line with the swing rarely exceeding 2 mμs. The probable error is thus 0·06 mμs or 1 cm.

(iv) A zero error or index error of ± 5 cm is assigned by the manufacturers to all tellurometer measurements. This is said to be the difference between the electrical centre of the instrument and the physical centre, which is the hole for the bolt (McLellan 1959), and includes mounting errors, minor effects at the dipoles and electrical delays in the circuitry (Wadley 1958).

The combined probable error of each measurement therefore totals ± 6 cm ± 3 ppm, which gives an overall accuracy of 1:50,000 to the tellurometer work. The minimum accuracy over any line was 1:25,000.

b. Theodolite.

The standard deviation of the three rounds of angles measured at each of the 74 survey stations on the summer traverse averaged 2·20 seconds. The traverse closure of 30 seconds was 1/3 the maximum allowed by the specifications. However, due to the non-observance of control azimuths, and the possible effects of lateral refraction, the maximum anticipated error of an azimuth joining any two points in the adjusted triangle may not be regarded as better than the ± 20 seconds suggested in the specifications.

c. Flow and strain rates.

Before correcting for the ice movement during the 10 days' stop at Cape Poinsett, the unadjusted closure of the summer traverse was 24 m. Taking the ice movement into account, the unadjusted closure due to survey errors was 22·9 m or 1:14,800.

The Canadian specifications assigned a maximum anticipated error to an adjusted survey of this order of one part in ten thousand in both distance and azimuth between any two points on the survey. Taking the maximum anticipated error as limiting the 95·5% probable value, and noting that the accuracy of both distance and angular measurements fall within the specifications, the probable error in the final position of each survey stake is one part in thirty thousand of its distance from Wilkes. Flow velocities, found by comparing positions and multiplying by a time factor, have a probable error in m/yr of around 1/15,000 the magnitude of this distance.

Each strain value calculated from comparative tellurometer measurements has a probable error of $\pm 8{\cdot}5$ cm ± 4 ppm of the distance measured. The larger the strain rate, therefore, the smaller its probable error.

B. STRAIN RATES

Three-arm rosette strain grids were used to determine the strain picture around the triangle instead of the square stake patterns originally planned (Nye 1959B). The time saved in setting out the rosettes on the autumn traverse justified the decreased accuracy resulting from fewer measurements. Rosettes were placed at the corners and approximate third points of each leg (see Fig. 2).

The strain grids were composed of a centre stake and three others, 99 m away, spaced around it at intervals of 120° ±10′. The rosette at the Dome had arms of 200 m. Measurements of each arm were made three times to within 0·001 m between metallic markers at the pole centres. A 100 m invar tape was used, laid along the surface under a tension of 20 lbs. Surface temperatures were recorded to 1°F before and after the taping. On the summer traverse it was found that some metallic markers had shaken loose or rotated with the pole due to wind action. Measurements were therefore taken from the visual centres of the stakes.

As the same tape was used for measurements on both autumn and summer traverses, only corrections for temperature and surface irregularities were applied in calculating the changes in length of the arms. Leaning of the pole, causing horizontal displacement of the measuring point, was never great, and only occurred on the eastern leg of the triangle where large strains minimized the error. Measurements at these stakes were made to the pole centre at the autumn snow surface level. No correction was made for leaning in the calculations.

ANARE photo S. Harvey

PLATE 8

Carrying the 100-m invar tape between strain rosette arms to avoid damaging it on surface protrusions. The snow surface is typical of all the rosettes, low sastrugi about 6-inches high. The centre pole of the rosette also acts as a survey station.

CAPE POINSETT

110° E
66°S
111°
BALAENA IS.
114°
115°
116°E
66°S

CAPE FOLGER
CHAPPEL IS.
WILKES
VINCENNES BAY
PETERSON GLACIER
VANDERFORD GLACIER
S2 TRAIL
CAPE WALDRON.
TOTTEN GLACIER.

66°30'
67°
67°30'

SG.A
SG.B
SG.C
SG.G
SG.H
SG.K
SG.L
SG.'s D&E
S2
M1
H1
G1
D1
E1

LEGEND

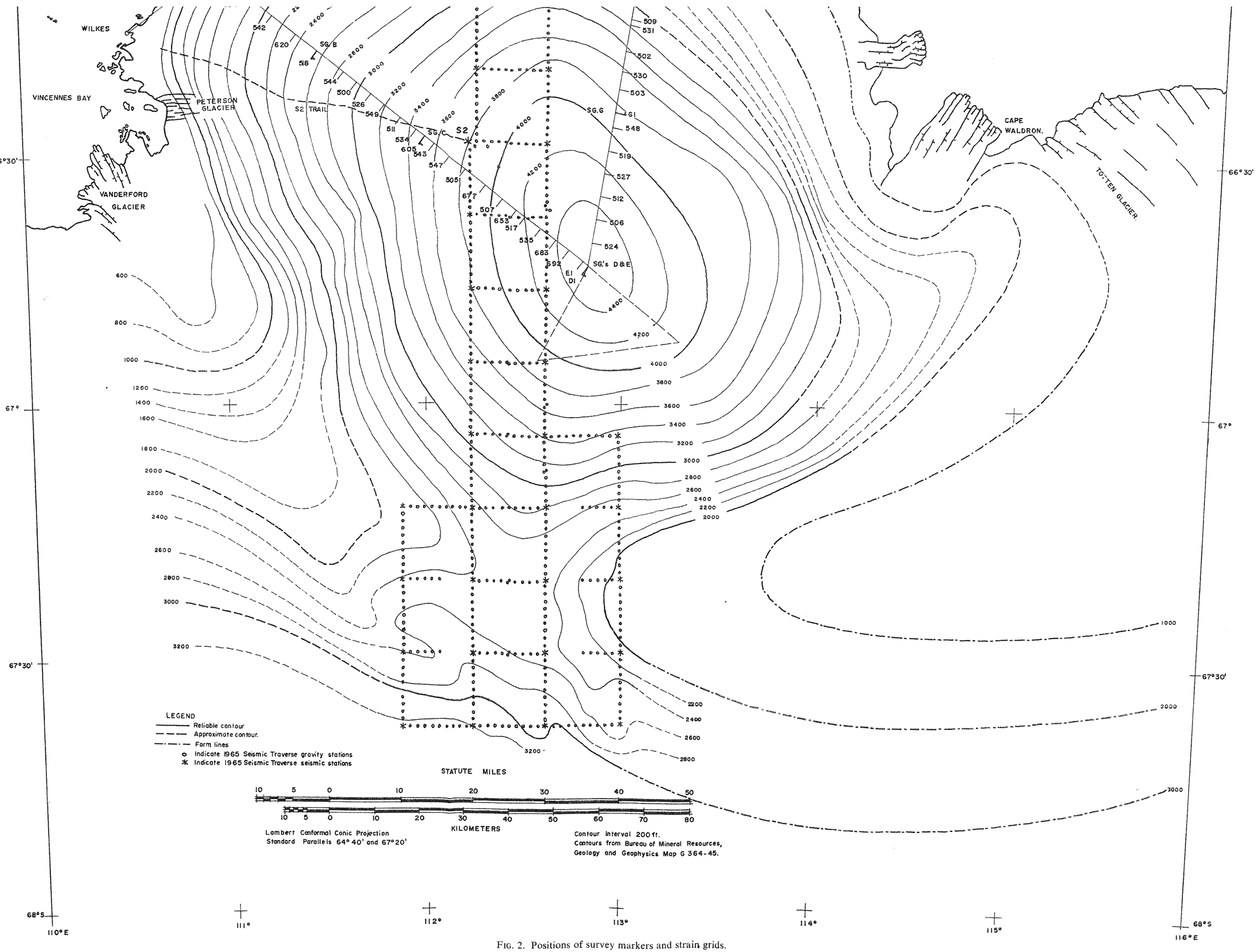

FIG. 2. Positions of survey markers and strain grids.

A probable error of one centimetre in each measurement is the result of difficulties in estimating the pole centre and in assessing the effect of surface irregularities (Plate 8).

In rosettes A, B, C, D, K and L, strain values varied in magnitude from zero to 7 cm. Probable errors in the calculated strain rates averaged ±35%. Rosettes G, H and J showed strain values varying between two and 72 cm. These grids have probable errors of 15%, 7% and 2%.

A rosette of six arms between 1·5 and 2 4 km, spaced at 60° intervals, was installed at the Dome summit and measured by tellurometer to better than 1:25,000. Strain rates calculated from these measurements have a probable error of ±11%.

C. SURFACE MEASUREMENTS AND ICE THICKNESS

1. *Surface elevation.*

Reeiprocal vertical angles were read between survey stakes from Wilkes to the Dome in the autumn, and around the triangle in the summer, to determine surface elevations. Two readings to 0·1 minute were taken on both faces of a theodolite. Angles were measured to the equivalent, often estimated, instrument height at all stakes.

As only one theodolite was used, the reciprocal angles were not observed simultaneously, but separated by at least one hour, and sometimes several days. Over some lines, the change in refractive coefficient K during this interval was such as to prevent the slope being measured from one end. Values of K ranged from (—)1·27 to (+)3·51, somewhat higher than the maximum value of 3·16 found by Lazarev (1962) on the Mirny-Komsomolskaya traverse. Where angles had been observed at only one end of a line, the normal K value of (+)0·07 (Admiralty 1938; Clark 1961) was used in compensating for effects of refraction and earth curvature.

As a check that refraction had not introduced large errors into the work, elevation differences were also computed from the pressure readings required for the tellurometer work. Corrections were applied for barometric error, based on intercomparisons made twice daily in the field, air temperature and latitude, to give values accurate to ±3 m.

Elevation differences between stakes were taken from the two sets of theodolite measurements, with consideration to recorded optical conditions, and, where necessary, from the barometric differences. These produced a closure of 14·4 metres which was distributed amongst all stations in the survey. Optical levelling in 1966 showed that the unadjusted elevations of 382 m at Cape Folger and 1395 m at the Dome summit were both correct, and that the misclosure of 14 m therefore lies in the other two legs. Adjusted figures have, however, been used in the calculations and drawings. These are 0·2 m low at Cape Folger and 6·0 m too low at the Dome.

Elevations of points between survey stakes were calculated by tying in barometric readings taken in 1964 with the adjusted survey heights.

2. *Gravity and seismic work.*

A bedrock profile along each triangle leg was computed in 1964 from gravity measurements made with a Worden "Prospector" gravimeter, loaned to the glaciologist by the Bureau of Mineral Resources, Geology and Geophysics. Bouguer

Anomalies were deduced and plotted at each point, and the resulting curve tied every 16 km to bedrock elevations determined seismically in 1965. Bedrock elevations between seismic control points were calculated from the relationship

$$H = \frac{(H_1 + 13{\cdot}5\Delta g_1)x_2 + (H_2 + 13{\cdot}5\Delta g_2)x_1}{x_1 + x_2}$$

where H is the bedrock elevation at the point in question;

H_1 is the bedrock elevation at control point 1;

H_2 is the bedrock elevation at control point 2;

x_1 and x_2 are distances from the point to control points 1 and 2;

Δg_1 and Δg_2 are the differences in Bouguer Anomalies between the point in question and control points 1 and 2.

The factor of 13·5 metres/milligal was calculated assuming a density contrast between ice and bedrock of 1·77 gm/cc over the entire triangle area (Morgan unpublished).

A second set of readings was taken at each point around the triangle by the glaciologist in 1965 and over a 56 × 16 km area inside the triangle by the seismologist. Seismic bedrock control was continued every 16 km along this latter route. The results of the work will be incorporated in a forthcoming map produced by the Bureau of Mineral Resources, Geology and Geophysics.

Pending completion of this map, a bedrock topography plan (Fig. 3) has been prepared from preliminary information supplied by the Director of BMR and incorporating the ice thickness measurements of Jewell (1962) and Walker (unpublished). Bedrock elevations between seismic control points were calculated by

$$H = H_1 + 13{\cdot}5\Delta g_1 - Rp,$$

where Rp = Residual Bouguer Anomaly in terms of height,

$$Rp = \frac{x_1}{x_1 + x_2}\left[13{\cdot}5(G_2 - G_1) - (H_2 - H_1)\right],$$

where G_1 and G_2 are the Bouguer Anomalies at control points 1 and 2.

This expression produces the same results as Morgan's but involves fewer, more simple calculations and is believed to lead to a clearer understanding of what is involved.

Alterations were made to the previous bedrock profile between Cape Folger and the Dome in the light of further studies. The original bedrock elevations obtained by Morgan were, however, used in the calculations in this work. These only introduce minor errors into the determination of vertical surface velocities, shown in Fig. 4, between stakes 542 and 605.

3. *Accumulation.*

The accumulation studies started at 1·6 km intervals in 1964 were continued in 1965. Snow densities were measured in autumn and spring, using a US Forestry Service sampler. Accumulation was also measured at all survey markers and at additional stakes placed around the Dome summit.

As 1965 and 1964 readings were not taken exactly a year apart, seasonal

corrections were applied in obtaining the annual accumulation. At all stakes between Cape Folger and the Dome, measurements showed either a net ablation or greatly reduced accumulation rate between January and April 1965. This was assumed to apply over the whole triangle, and proportional corrections were made to the accumulation rates on the other two legs. To smooth the overall pattern, the value at each stake was meaned with the average of its two neighbouring stakes. Smoothed accumulation isolines, along with prevailing wind directions determined from sastrugi observations in 1964 and 1965, are shown in Fig. 5.

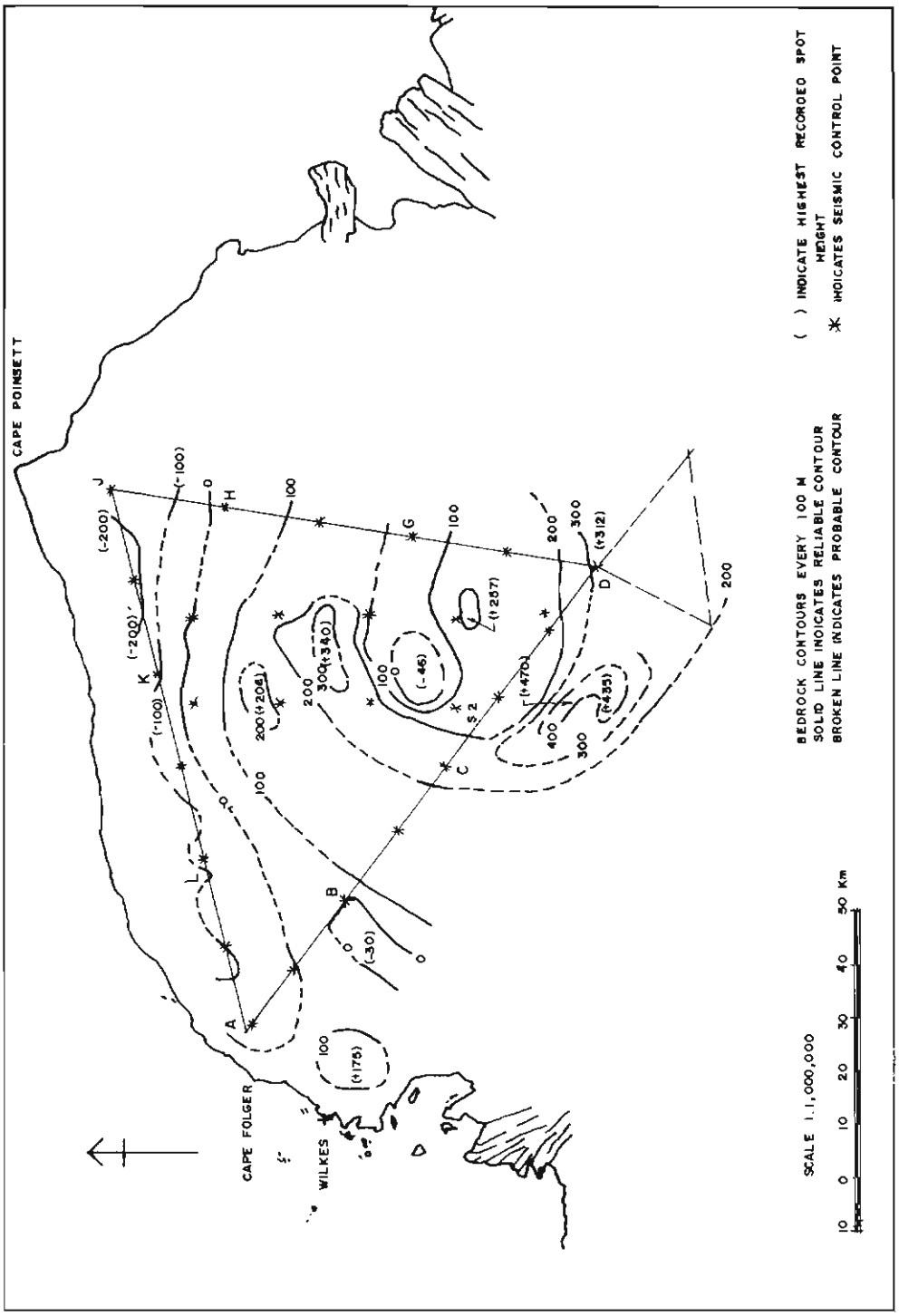

FIG. 3. Wilkes local ice dome; bedrock elevations.

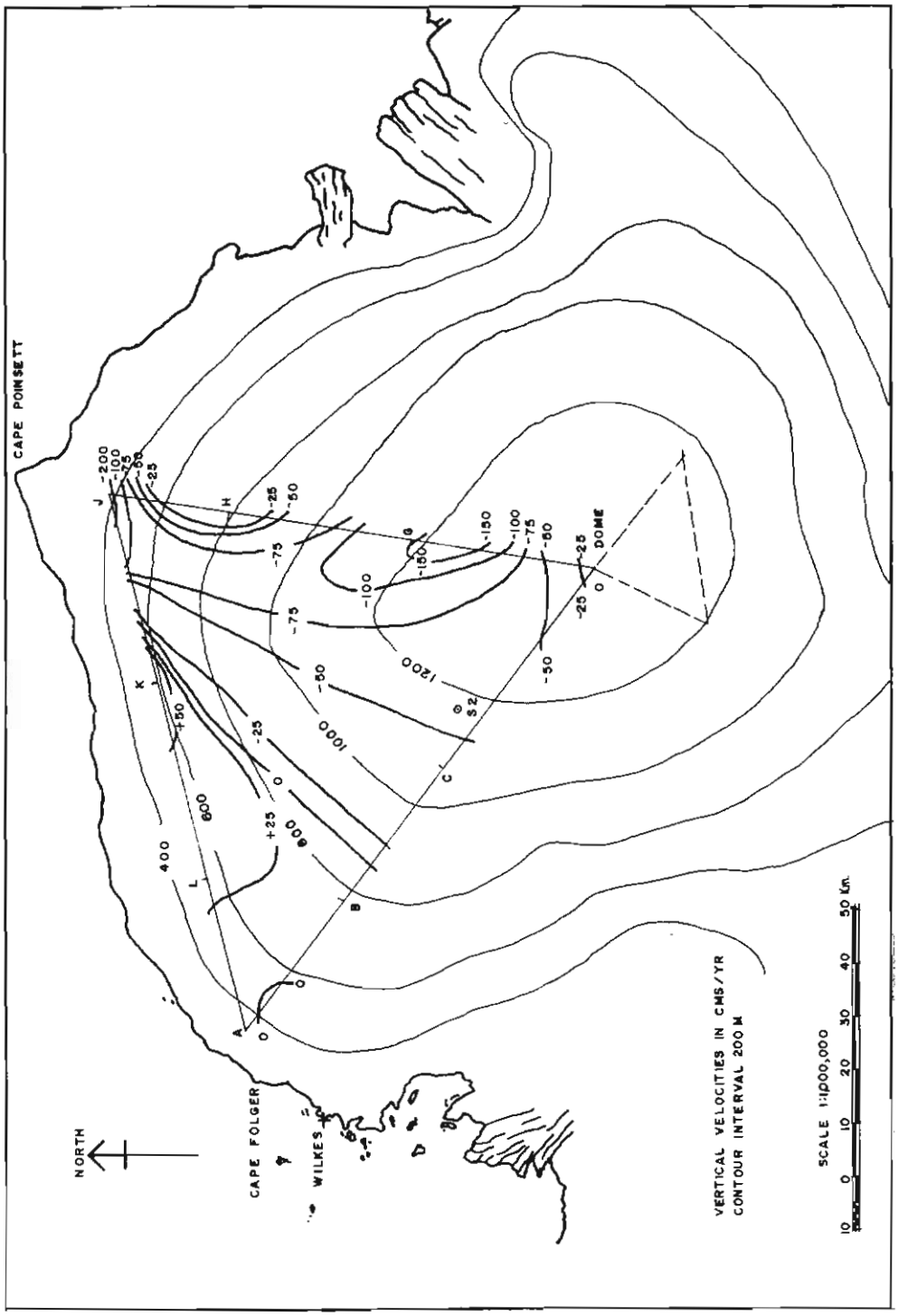

FIG. 4. Vertical surface velocity isolines.

C

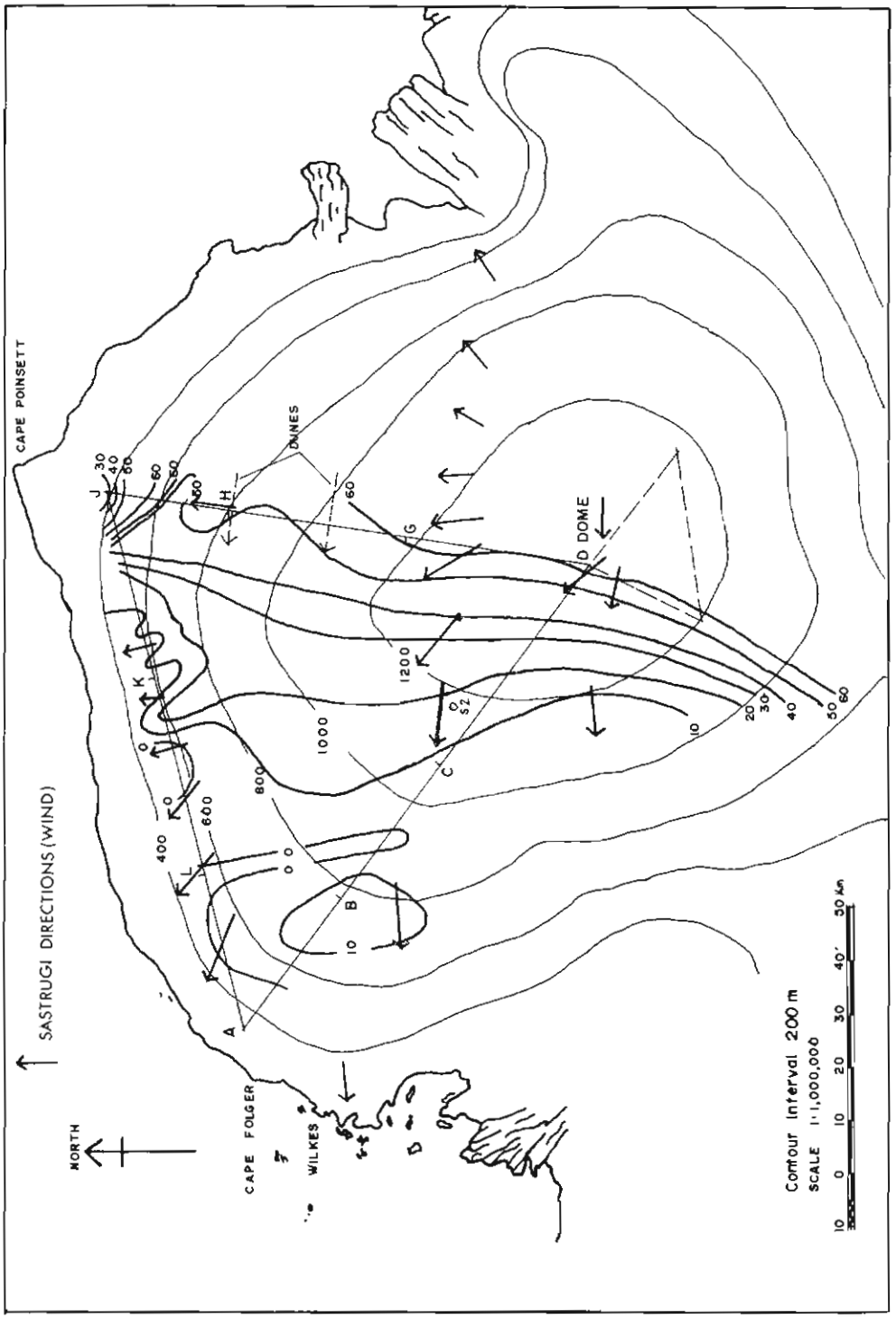

FIG. 5. Smoothed accumulation isolines.

4. RESULTS

A. REDUCTION OF FIELD DATA

1. *Survey adjustment.*

Field note calculations were reduced and checked in the Antarctic. On return to Australia, corrections for eccentric stations were made, the spherical excess of the triangle calculated as 21·9″, and the horizontal angles of the closed summer traverse balanced. Angular closure on this traverse was minus 30 seconds. The solar control azimuths were worked out but, due to an undetermined error, could not be used.

The tellurometer readings and vertical angles from both traverses were fed into a Sirius computer at I.T. & C. Pty Ltd, Melbourne, using a programme compiled for the Division of National Mapping called "Metric Traverse Heights and Tellurometer Distances". This gave the slope distance in feet, the refractive coefficient K, and both the elevation difference and sea-level horizontal distance in feet and metres. The survey stake elevations were adjusted as previously discussed (see Sect. 3.C.1.) and resubmitted to the computer which recalculated the horizontal sea-level distances. Following the procedure used by the Division of National Mapping, the International Spheroid, having a Major Semi-Axis of 20926469·66 ft and an eccentricity squared of 0·0067226700, was used in all calculations as the figure of the earth.

The adjusted angles and sea-level distances were sent to Mr. A. G. Bomford of the Division of National Mapping in Canberra where they were submitted to the CSIRO CDC 3600 computer for determination of the geodetic positions of each stake, using Clark's formula (Clark 1961). These positions were then converted to Universal Transverse Mercator (U.T.M.) co-ordinates, using Redfearn's formula in full by the computer.

The closure of the summer traverse was 24 m ESE or 1:14,000, which included errors due to the ice movement during the survey as well as normal survey errors. A stop of ten days due to bad weather had been made at Strain Grid "J" during the summer traverse. To eliminate the effect of ice flow during this time, the velocity at J was calculated as described below, and the actual amount of displacement during this period determined. This amount of 1·5 m was subtracted from all stations beyond J before the closure error was removed by the application of Bowditch's rule (Clark 1961). Adjusted positions of the survey stakes are given in Appendix II.

2. *Rosette strain grids.*

The major and minor strain vectors ($\dot{E}_1$ and $\dot{E}_2$) were calculated from the corrected rosette measurements, using the following relationships proposed by

Kehle (Zumberge *et al.* 1960; Zumberge 1964). Starting with the corrected lengths of the arms *oa*, *ob*, *oc* and *oa'*, *ob'* and *oc'*,

$$\dot{E}aa = \frac{oa' - oa}{oa} \quad \frac{365}{\Delta t(\text{days})}$$

$$\dot{E}bb = \frac{ob' - ob}{ob} \quad \frac{365}{\Delta t(\text{days})}$$

$$\dot{E}cc = \frac{oc' - oc}{oc} \quad \frac{365}{\Delta t(\text{days})}$$

$$\dot{E}_1 = 1/3\ (\dot{E}aa + \dot{E}bb + \dot{E}cc) + (\text{I} + \text{II} + \text{III})^{\frac{1}{2}}$$

$$\dot{E}_2 = 1/3\ (\dot{E}aa + \dot{E}bb + \dot{E}cc) - (\text{I} + \text{II} + \text{III})^{\frac{1}{2}},$$

where $\text{I} = 1/9\ (\dot{E}aa + \dot{E}bb + \dot{E}cc)^2$

$$\text{II} = 1/3\ (\dot{E}cc - \dot{E}bb)^2$$

$$\text{III} = -2/3\ \dot{E}aa\ (\dot{E}bb + \dot{E}cc - \tfrac{1}{2}\dot{E}aa).$$

The angle θ between *oa* and one of the principal horizontal strain axes is given by

$$\tan 2\theta = \frac{1{\cdot}73205(\dot{E}cc - \dot{E}bb)}{2\dot{E}aa - \dot{E}bb - \dot{E}cc}.$$

Results of the strain rosette calculations are given in Appendix III and are shown graphically in Fig. 6.

The large six-arm rosette at the Dome summit (Fig. 7) was worked out, considering the sum of diametrical arms as being one line.

From the principal strain vectors, the longitudinal strain rate (i.e., $\dot{E}x$, along the triangle leg) and lateral strain rate ($\dot{E}y$, at right angles to the leg) were deduced from:

$$\dot{E}x = \dot{E}_1 \cos^2 \psi + \dot{E}_2 \sin^2 \psi$$

$$\dot{E}y = \dot{E}_1 \sin^2 \psi + \dot{E}_2 \cos^2 \psi,$$

where ψ is the angle between E_1 and the triangle leg (Jaeger 1962).

The shear component (γ_{xy}) at each rosette was calculated by

$$\gamma_{xy} = (\dot{E}_1 - \dot{E}_2) \sin 2\psi.$$

The values of $\dot{E}x$, $\dot{E}y$ and γ_{xy} from the strain rosettes are shown in Figs. 8 to 10, along with the values of $\dot{E}x$ found by tellurometers. It can be seen that, while the two determinations of $\dot{E}x$ are in general agreement, the strain rosettes are strongly affected by local peculiarities. The worst examples of this are the three strain grids G, H and J on the Dome—Cape Poinsett line. Strain Grid G is in a local area of compression, while rosettes H and J, due to their proximity to the tops of steep slopes, are in areas of high expansion. Measurements from these grids are not representative in magnitude of conditions along the whole line.

B. ICE FLOW VELOCITIES

A comparison of the adjusted summer and unadjusted autumn U.T.M. co-ordinates at the Dome showed a movement of 2·08 m eastwards, with a probable error

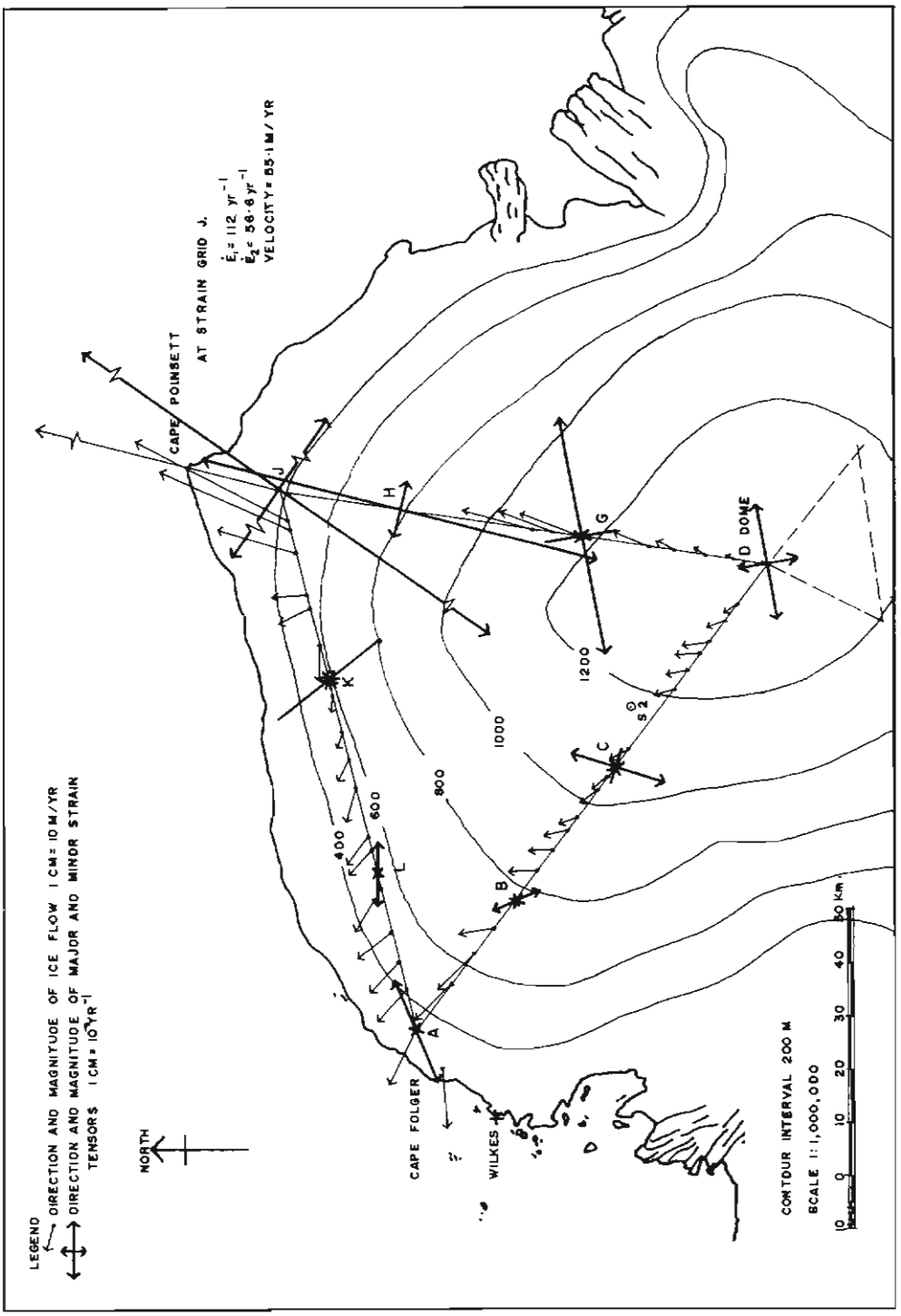

FIG. 6. Ice velocities and strain rates.

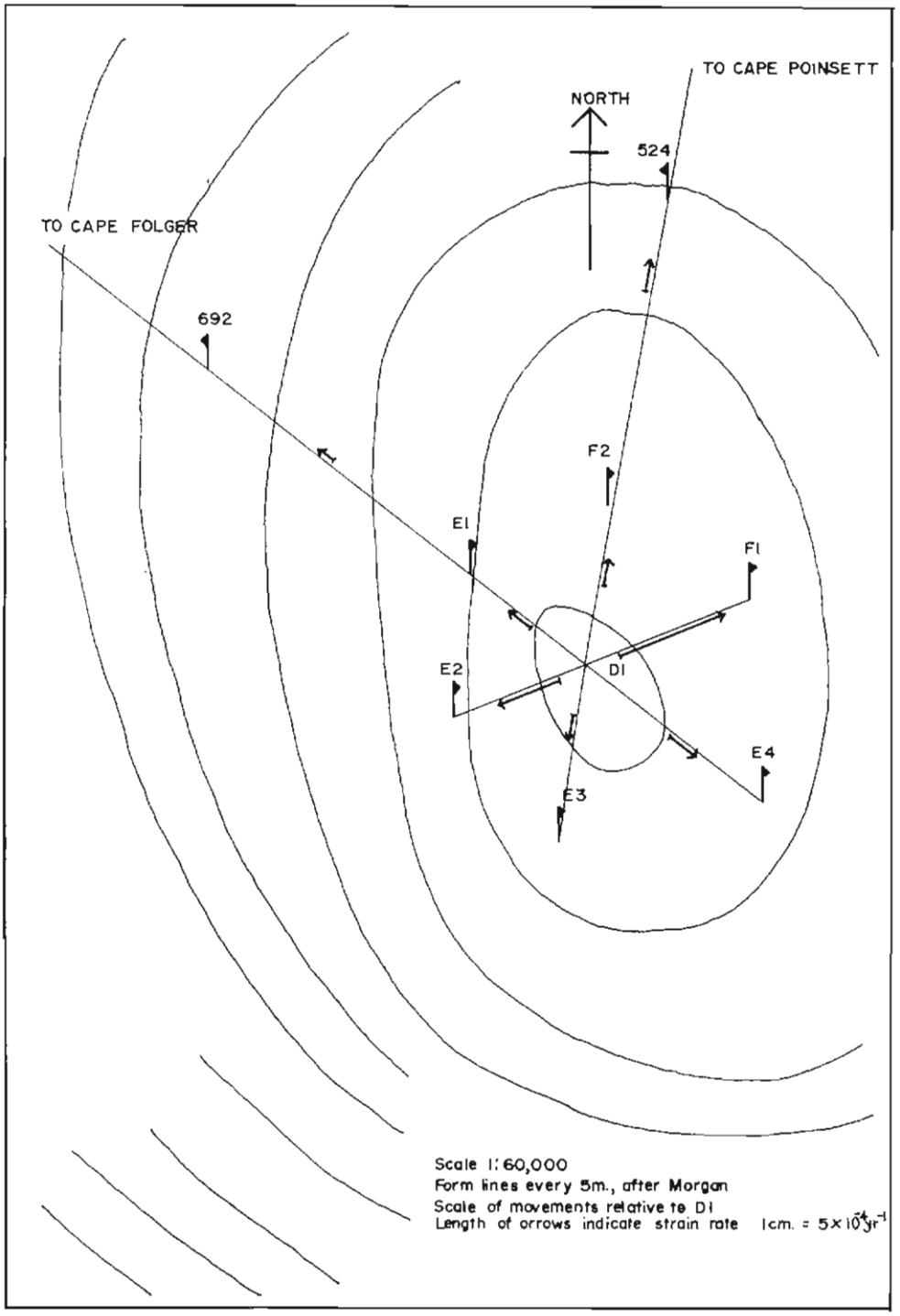

FIG. 7. Strain rates around Dome by tellurometers.

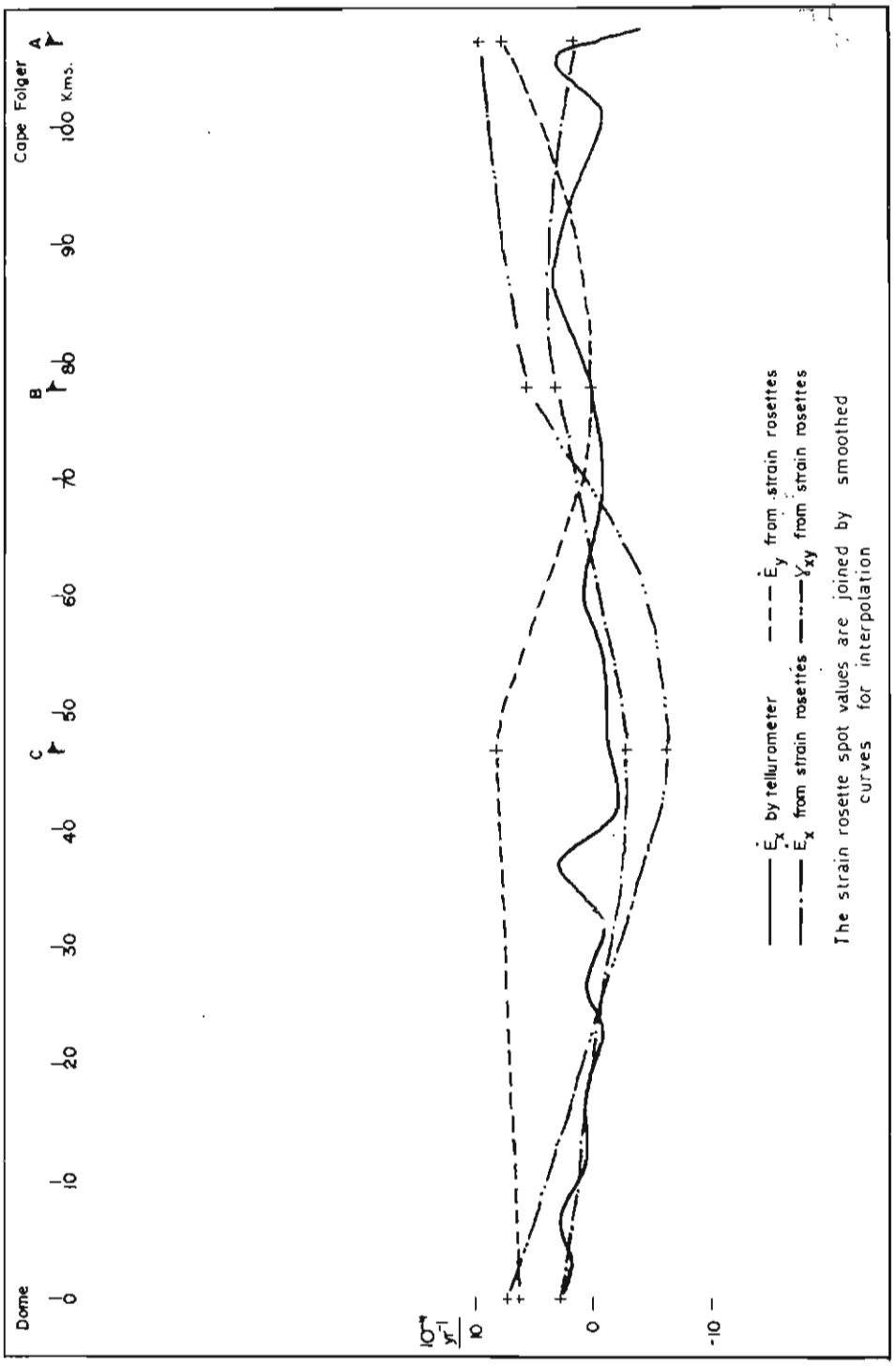

FIG. 8. Comparison of strain rates from strain rosettes and tellurometer work: Dome summit—Cape Folger leg.
+ indicates strain grid measurement.

of ±6·0 m. This is equivalent to a velocity of 3·0 m/yr ±8·7 m/yr. In view of the probable errors, and to simplify further calculations, zero horizontal velocity was assumed at this point. The autumn traverse positions of the stakes between Cape Folger and the Dome were adjusted by Bowditch's rule on tbis assumption. Comparison of adjusted autumn and summer coordinates gave movement, and hence flow velocities, along this line. Tbe velocity at Strain Grid A was 10·0 m/yr ±2·0 m/yr.

The extensions, betwcen traverses, of the two legs meeting at Cape Poinsett were found by comparing their total sea-level tellurometer distances. The stakes on these lines had been planted in as near straight lines as possible and large differential lateral movements would be required to cause significant ehanges in their lengths. The total extensions, therefore, were taken as being along the mean azimuths of the legs. Using the above ice velocities at Strain Grids A and D, the flow rate at Strain Grid J was calculated as 55·1 m/yr ±13·7 m/yr bearing 007° from North.

To determine flow rates at survey stakes along legs D-J and J-A, the total velocity V was broken into two components, the longitudinal velocity (Vx) along the line, and the lateral velocity (Vy) at right angles to the line. Vx was determined at each stake by summating the strains outwards from the known points, A and D:

$$Vx_n = Vx_o + \Sigma_o^n \dot{E}x.$$

An attempt to determine the lateral velocities by multiplying the distances between survey stakes by the graphically interpolated shear strain rates, γ_{xy}, and summing towards Cape Poinsett, produced considerably higher values there than determined by tellurometer measurements.

$$Vy_n = Vy_A + \Sigma_A^n \gamma_{xy} \cdot d.$$

Some values of Vy along the coastal leg were directed inland. A similar calculation along the Dome—Cape Folger leg gave results at variance in sign with the surveyed values. This is believed to be due to the strain rosettes not showing results typical over large areas. These results were therefore rejected and the method considered unsatisfactory.

The lateral velocity of Strain Grid J was then determined with respect to each leg from the known velocity vector. This was divided by the value of $\dot{E}y$ appropriate to that leg given by the strain rosette (Figs. 9, 10). The lateral velocity at each survey stake along the line D-J, was estimated by multiplying the resulting factor by the local value of Ey graphically interpolated from Fig. 9,

$$\text{i.e., at Stake 502, } Vy502 = \frac{Vy_{\text{Poinsett}}}{\dot{E}y_{\text{Poinsett}}} \dot{E}y_{502}.$$

On the line A-J, the lateral velocity of 6·70 m/yr seaward at A was considered a basic seaward velocity along the leg. This was added algebraically to the values of Vy determined at each stake similarly to those determined along leg D-J,

$$\text{i.e., at Stake 599, } Vy599 = \frac{(Vy_{\text{Poinsett}} - 6{\cdot}70)}{\dot{E}y_{\text{Poinsett}}} \dot{E}y_{599} + 6{\cdot}70.$$

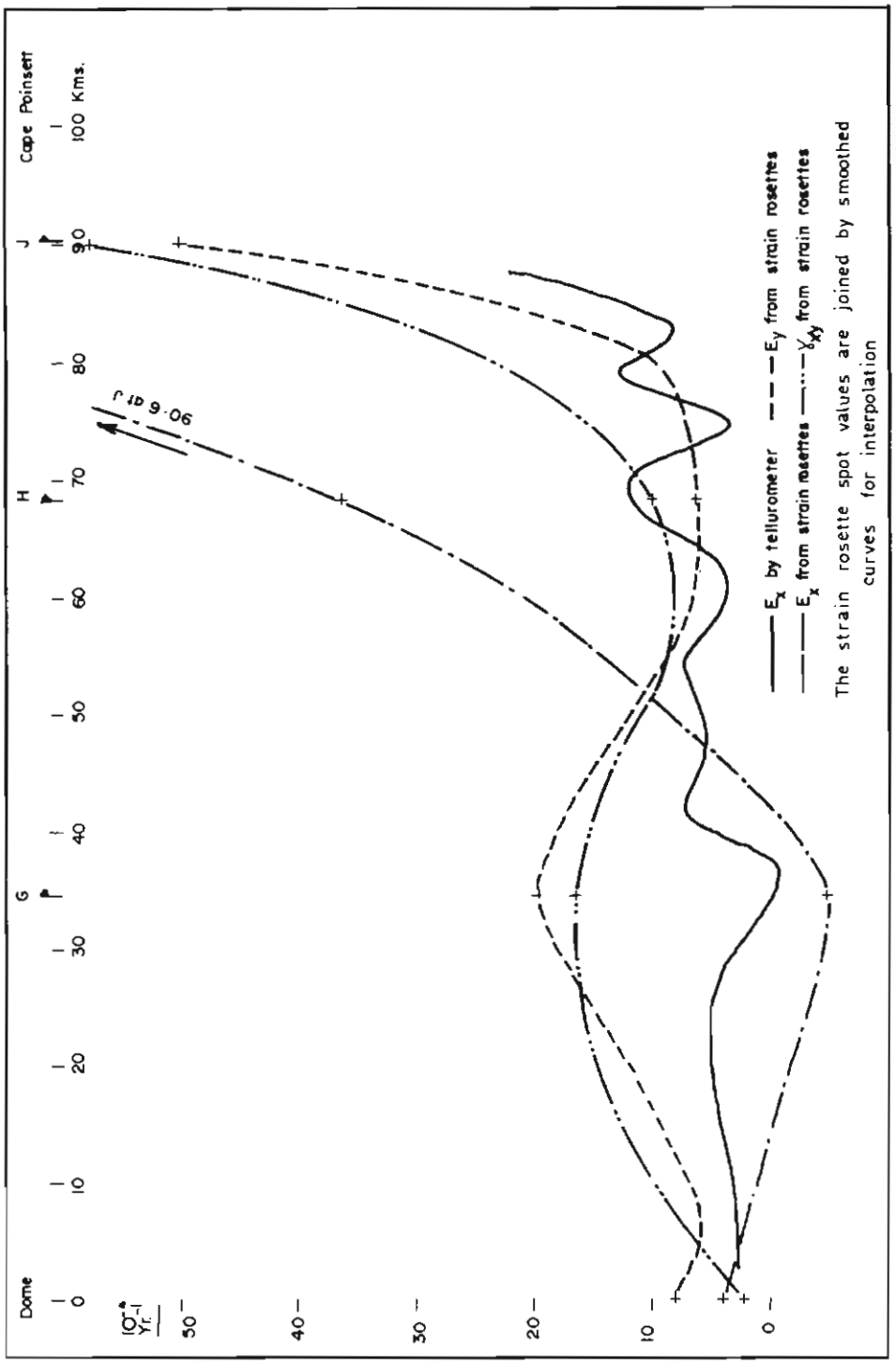

FIG. 9. Comparison of strain rates from strain rosettes and tellurometer work: Dome summit—Cape Poinsett.
+ indicates strain grid measurement.

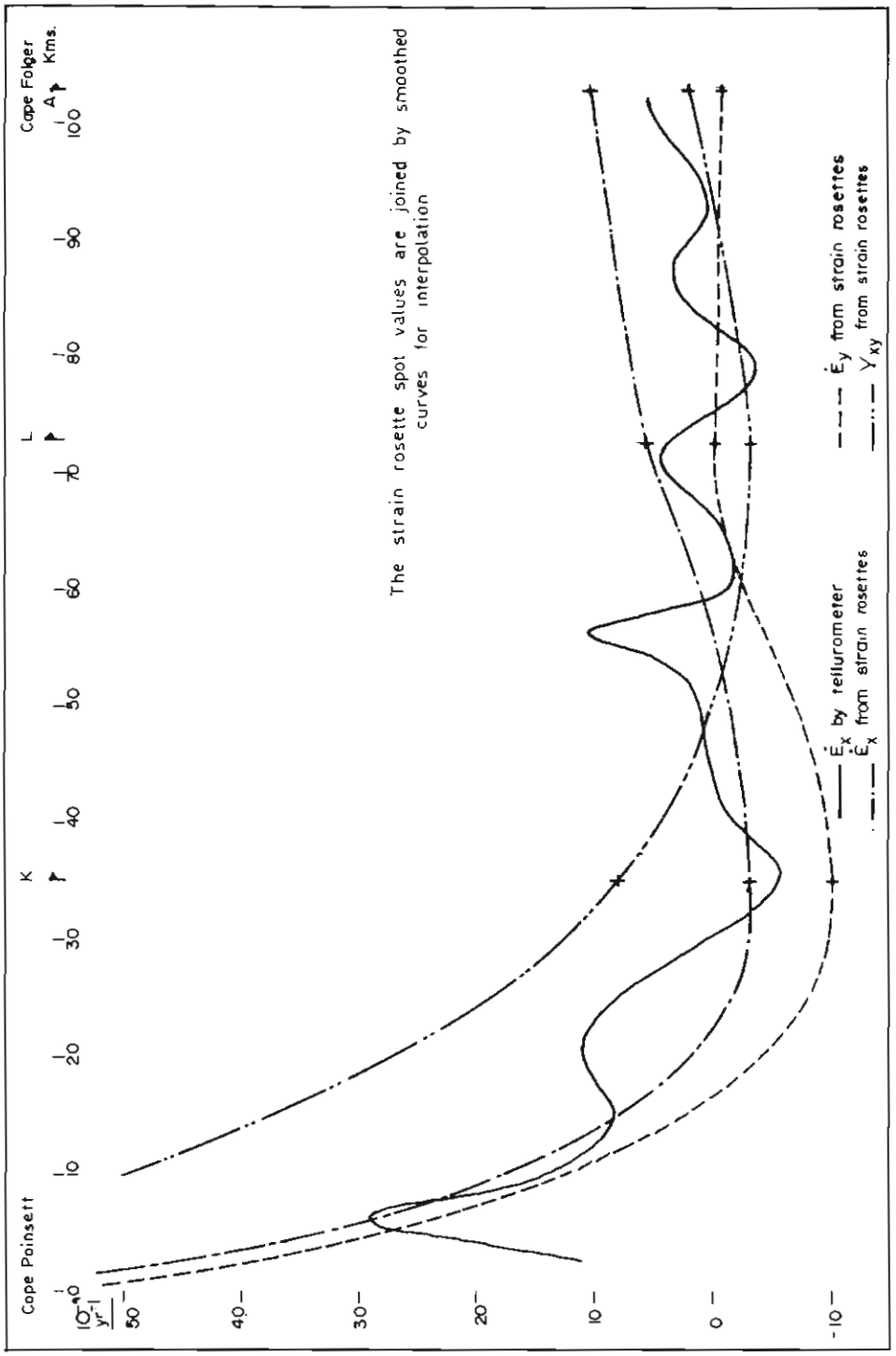

FIG. 10. Comparison of strain rates from strain rosettes and tellurometer work:
Cape Poinsett—Cape Folger leg.
+ indicates strain grid measurement.

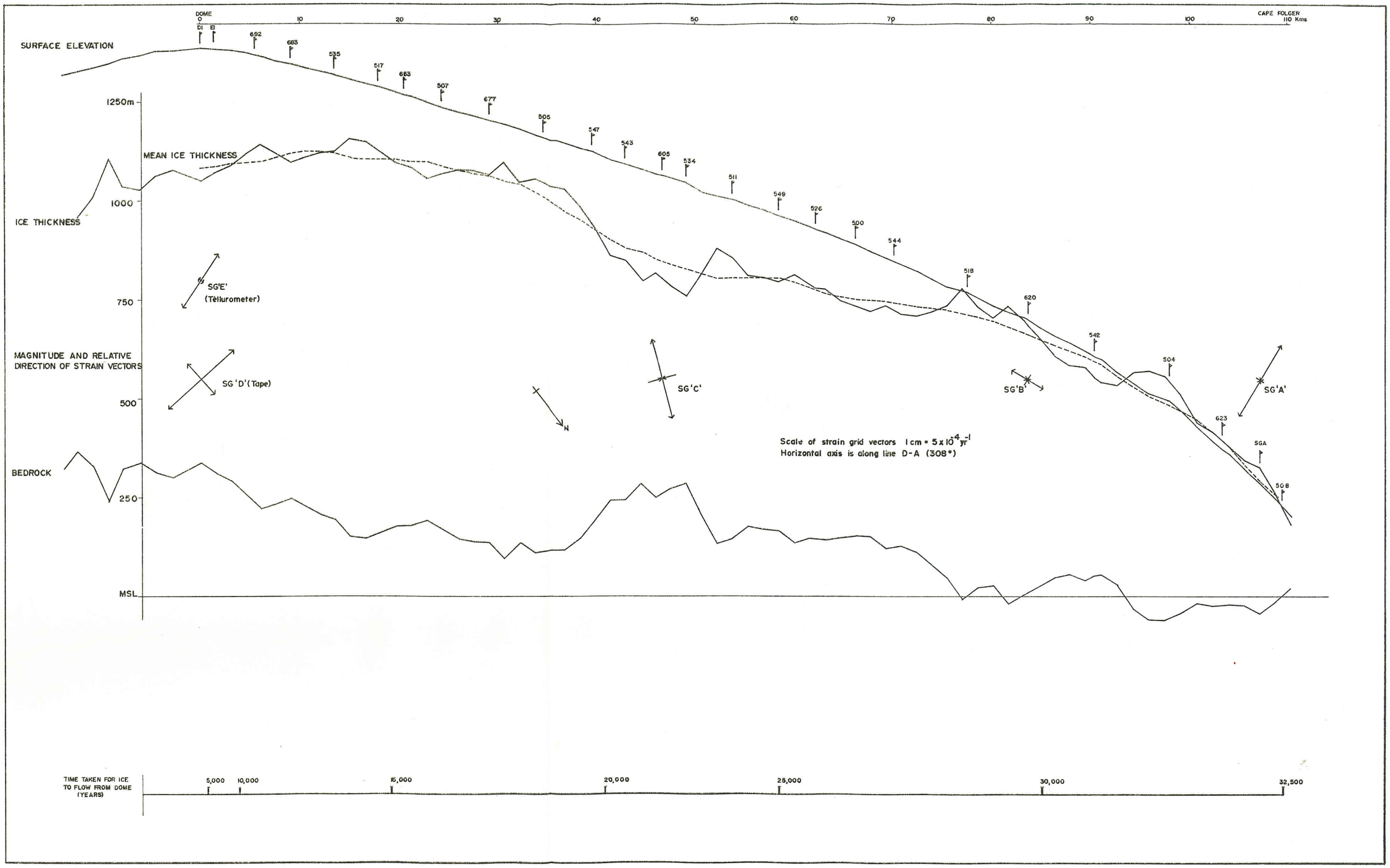

FIG. 11. Physical profiles: Dome—Cape Folger.

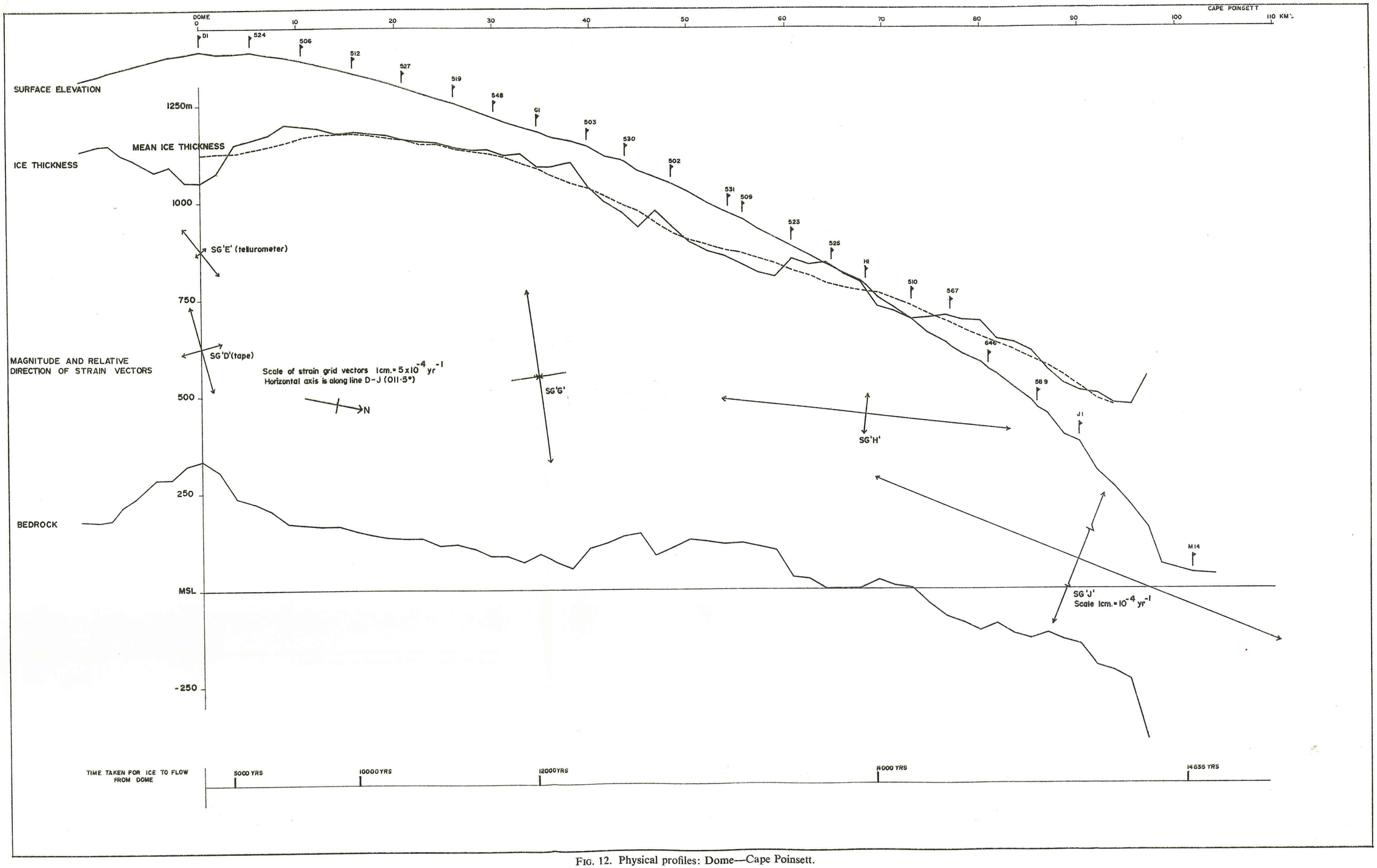

FIG. 12. Physical profiles: Dome—Cape Poinsett.

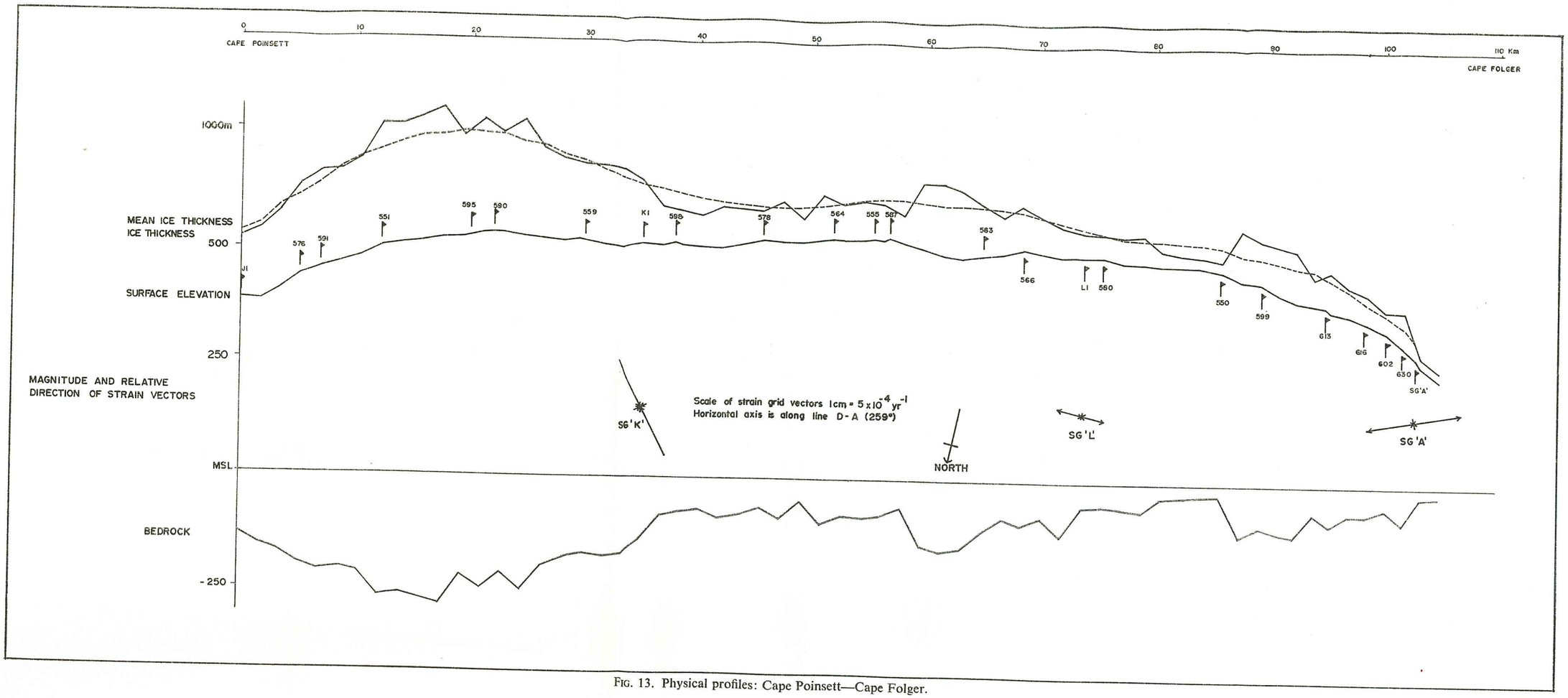

FIG. 13. Physical profiles: Cape Poinsett—Cape Folger.

While only approximate, the method gives values of magnitude and sign for Vy which agree with known values at each end of the lines and which are proportional to the lateral strain tensors, and hence stresses, at intermediate points.

The ice flow vectors representing the combined values of Vx and Vy are given in Appendix IV and are shown in Fig. 6.

C. DETERMINATION OF STRESS PARAMETERS

1. *Stresses near bedrock.*

The ice thickness at each trail-marker stake had been determined by gravity measurements in 1964 and checked every 16 km by seismic work in 1965. Surface elevation, ice thickness and bedrock profiles are shown in Figs. 11 to 13. The running mean ice thickness was computed over 8 km on either side of each stake to eliminate minor bedrock effects.

Shear stresses at the bottom of the ice cap were calculated at each survey marker along the two arms radiating from the Dome, according to the well-known equation (Nye 1952)

$$\tau = \rho g h \sin \alpha,$$

where τ = shear stress at depth h;
α = mean surface slope of the ice cap between preceding and following survey stakes;
ρ = mean density of ice, taken as 0·90 gms/cc;
g = gravity constant.

Surface velocities along the two legs were plotted against the bottom shear stresses (Fig. 14), showing good general agreement up to a stress of 1 bar for the Dome—Cape Poinsett leg and up to 0·8 bars for the Dome—Cape Folger leg. Above these levels, velocities appeared independent of stress, suggesting either bottom-sliding, as ice temperatures reach the pressure melting point, or a change in ice properties near that point. Considering Nye's (1959A) assumed flow law,

$$V = \left(\frac{\tau}{A}\right)^m \qquad (1)$$

where A and m are parameters dependent on bed roughness, ice temperature and ice constitution, values of $m = 2{\cdot}7$ were obtained for the two legs.

2. *Stress parameters near bedrock.*

The surface strain rates represent the combination of strains occurring near the bottom of the ice cap and strains occurring in the main block of ice above the bottom. These strains are completely independent of one another. Nye (1959A) has shown that, away from the centre of the ice cap, the strain at the bottom is generally the larger of the two. Glen (1955) proposed a power law for the flow of ice,

$$\dot{E} = \left(\frac{\sigma}{B}\right)^n \qquad (2)$$

where $\dot{E}$ is the strain rate,
σ is the normal stress,
and B and n are parameters.

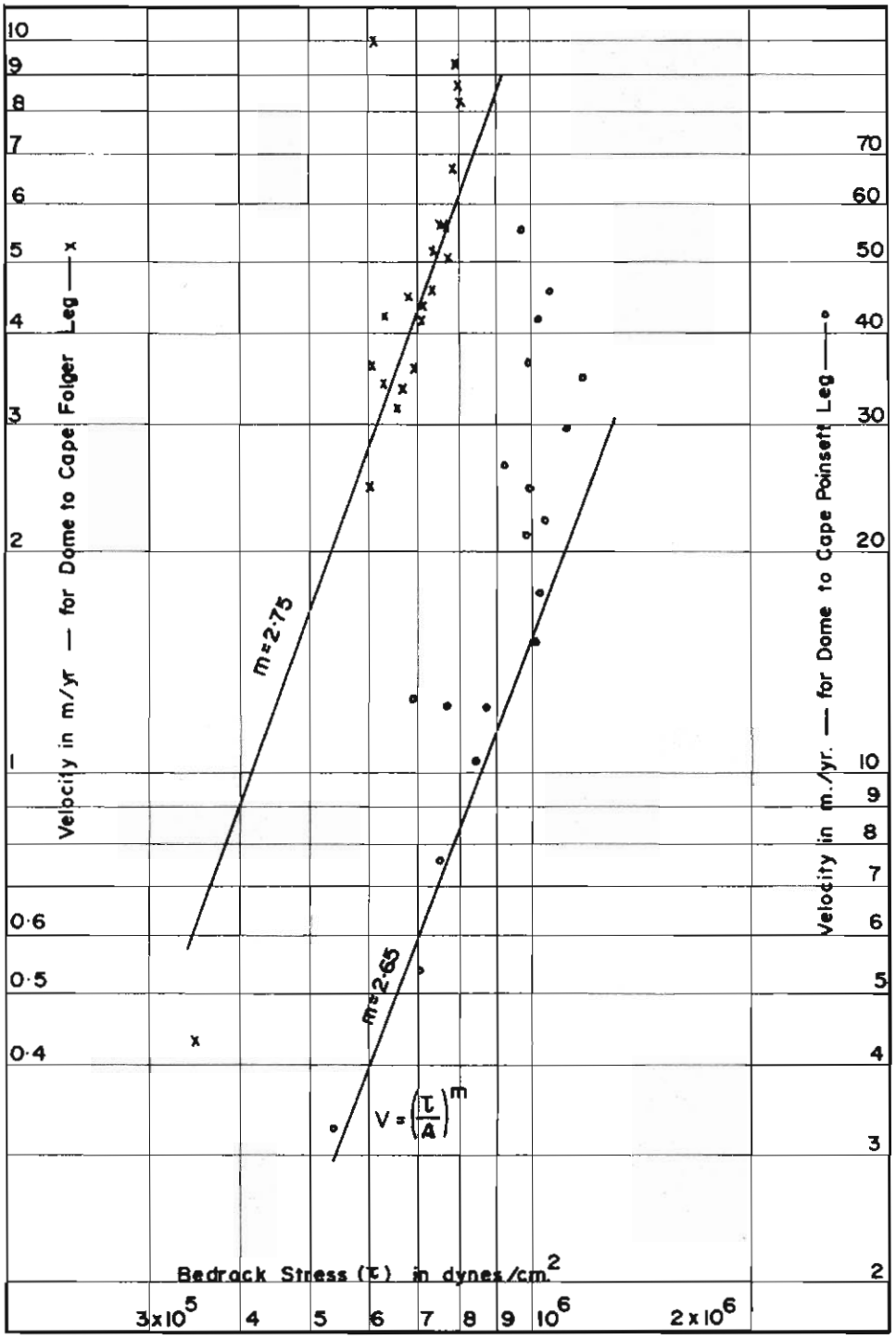

FIG. 14. Surface velocities versus basal stress as calculated from mean slope between preceding and following survey stakes.

Budd (1966A) showed that n varies over different ranges of stress. Shumskiy (1961) quotes Royen (1922) and Voitkovskiy (1959) as showing that the rate of flow is inversely proportional to the coefficient $(\theta - 1)$ and gives the flow law in the form

$$\dot{E}_x = \frac{1}{1-\theta} \left(\frac{\sigma_x}{k}\right)^n \tag{3}$$

where θ is the mean temperature of the ice in °C,
and k is the stress for unit strain at 0°C.

The ice near the bedrock would have a different temperature, and be under different stresses, from those of the main block of ice above. It would therefore react to different parameters in the flow law. An attempt was made to determine the parameters suitable to these two areas of strain, and from these make an estimate of their significant temperatures.

The magnitude of the parameter B depends, through its units, on the values of n and τ. Budd (1966A) uses $B_2 = B_1\, n_1/n_2\, \tau(n_2 - n_1)/n_2$. For comparison with other works, values of B given hereafter have been converted to values of $n = 3$ and $\tau = 10^6$ dynes/cm^2, i.e., in units of dynes/cm^2 sec$^{1/3}$. Where temperature compensation to B has been required in solving for n, Shumskiy's expression

$$B = k(1-\theta)^{1/n} \tag{4}$$

has been used. θ was taken as the mean surface temperature, from Cameron (1964), at the elevation of the point in question. The inherent assumption that the significant temperature of the ice equals that of the mean surface temperature is based on works by Jenssen and Radok (1963), Bogoslovski (1958) and Hansen and Langway (to be published), and is considered sufficiently accurate until actual thermal measurements are made.

From Shumskiy (1961)

$$\dot{E}_x = \frac{1}{1-\theta} \left(\frac{\sigma_x}{k}\right)^n,$$

and $\sigma_x = \frac{1}{2}\left[\frac{1}{2}\rho g h \cos^2\beta + \frac{1}{h}\int_x^1 \rho g h \cos^2\beta\,(\tan\beta - f)\,dx\right]$,

where β is the bedrock slope
and f is a coefficient of friction between the ice and bedrock, Budd (1967) (personal communication) had deduced

$$\frac{\partial}{\partial x}(hB\dot{E}^{1/n}) \simeq \tfrac{1}{2}\rho g h(\alpha - f) \tag{5}$$

where α is the surface slope.

Plotting $\frac{\partial h\dot{E}}{\partial x}$ and $h\bar{\alpha}$ against distance for the Dome—Cape Poinsett leg gave similar curves, with the latter being always positive, while $\frac{\partial}{\partial x} h\dot{E}$ alternated between positive and negative signs. From a comparison of these curves, f was deduced to approximate $\bar{\alpha}$, the mean surface slope over the length of the undulations.

If it is assumed that there is no basal sliding,

from $\tau_b = \rho ghf = \rho gh\bar{\alpha}$, and $\tau_b = h(\frac{dp}{dx})$,

where $\frac{dp}{dx} = B\left[\frac{(n+1)V}{2h^{n+1}}\right]^{1/n}$ is the uniform pressure gradient along the leg (Budd 1966A; Jaeger 1956), we get

$$B^n \frac{V}{h} = \frac{2(\rho gh\bar{\alpha})^n}{n+1}. \qquad (6)$$

Substituting equation (4) in (6) gives

$$(1-\theta)\frac{V}{h} = \frac{2(\rho gh\bar{\alpha})^n}{(n+1)k^n} \qquad (7)$$

Mean values of $\frac{V}{h}$ over 8 km on either side of each survey stake on the Dome —Cape Poinsett leg were adjusted for surface temperature and plotted (Fig. 15) against equally smoothed values of $\bar{\alpha}h$. The resulting line gave a value of $n = 4{\cdot}3$ and, from equation (6) a value of $B = 0{\cdot}74 \times 10^9$ dynes/cm^2 sec$^{1/3}$. A comparison of B with values from other works [Fig. 16 (Budd 1966A)] indicated that the mean bottom temperature of the ice was about —3°C or about 14° higher than the mean assumed surface temperature. A value of θ equal to the mean surface temperature plus 10°C was then taken, values of $(1-\theta)\frac{V}{h}$ calculated along the two legs radial from the Dome and plotted vs. $\bar{\alpha}h$ (Fig. 15).

Lines of slope $n = 3{\cdot}4$ were obtained for both legs, giving a value of $B = 0{\cdot}85 \times 10^9$ dynes/cm^2 sec$^{1/3}$ for the Cape Poinsett leg, and $B = 0{\cdot}96 \times 10^9$ dynes/cm^2 sec$^{1/3}$ for the Cape Folger leg.

3. *Stress parameters in upper ice mass.*

To determine the parameters governing strain in the main mass of ice above the bottom, a comparison was made between deviations of strain rates and slopes from their respective mean values at intervals of 1·75 km over the surface undulations. Most of the longitudinal strain rates measured on the Dome—Cape Folger leg were small, being strongly influenced by bedrock obstructions. This leg, and the coastal leg where down-slope strain rates were not available, were therefore omitted from further consideration, and the investigation confined to the Dome—Cape Poinsett leg.

The surface undulations were noted to average about 15 km in length. The mean strain rate over 8·75 km on either side of each stake was computed, using values scaled every 1·75 km from Fig. 9. The mean value was subtracted from each individual value to give the residual strain rate ($\Delta\dot{E}_x$) caused by surface topography,

$$\Delta\dot{E}_x = \dot{E}_x - \bar{\dot{E}}_{17.5}.$$

Surface slopes were similarly treated to give values of $\Delta\alpha = \alpha - \alpha_{17.5}$. Values of $\Delta\dot{E}_x$ and $\Delta\alpha$ were plotted in Fig. 17.

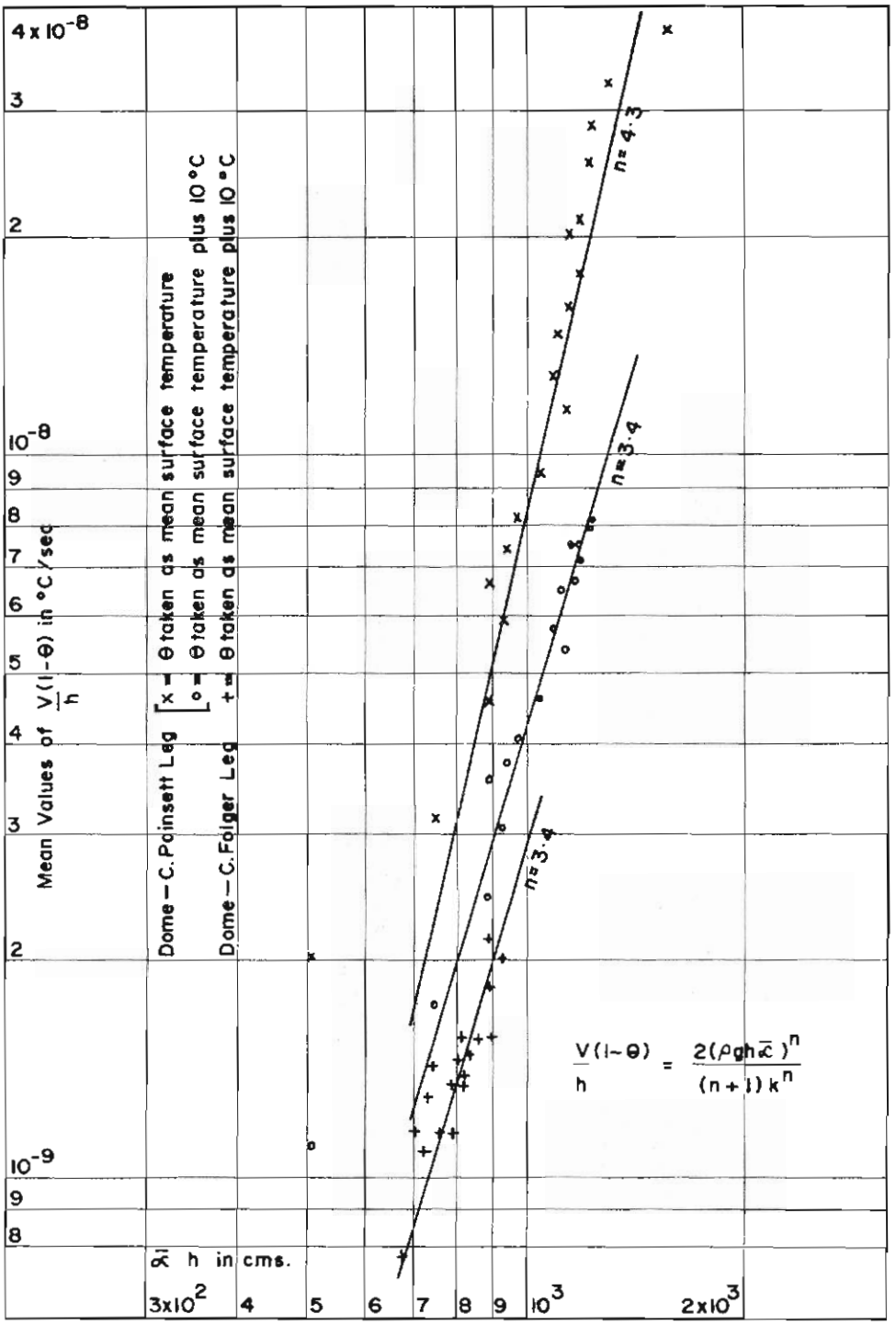

FIG. 15. Values of $(1-\theta)\frac{V}{h}$ versus $\bar{\alpha}h$ along radial legs.

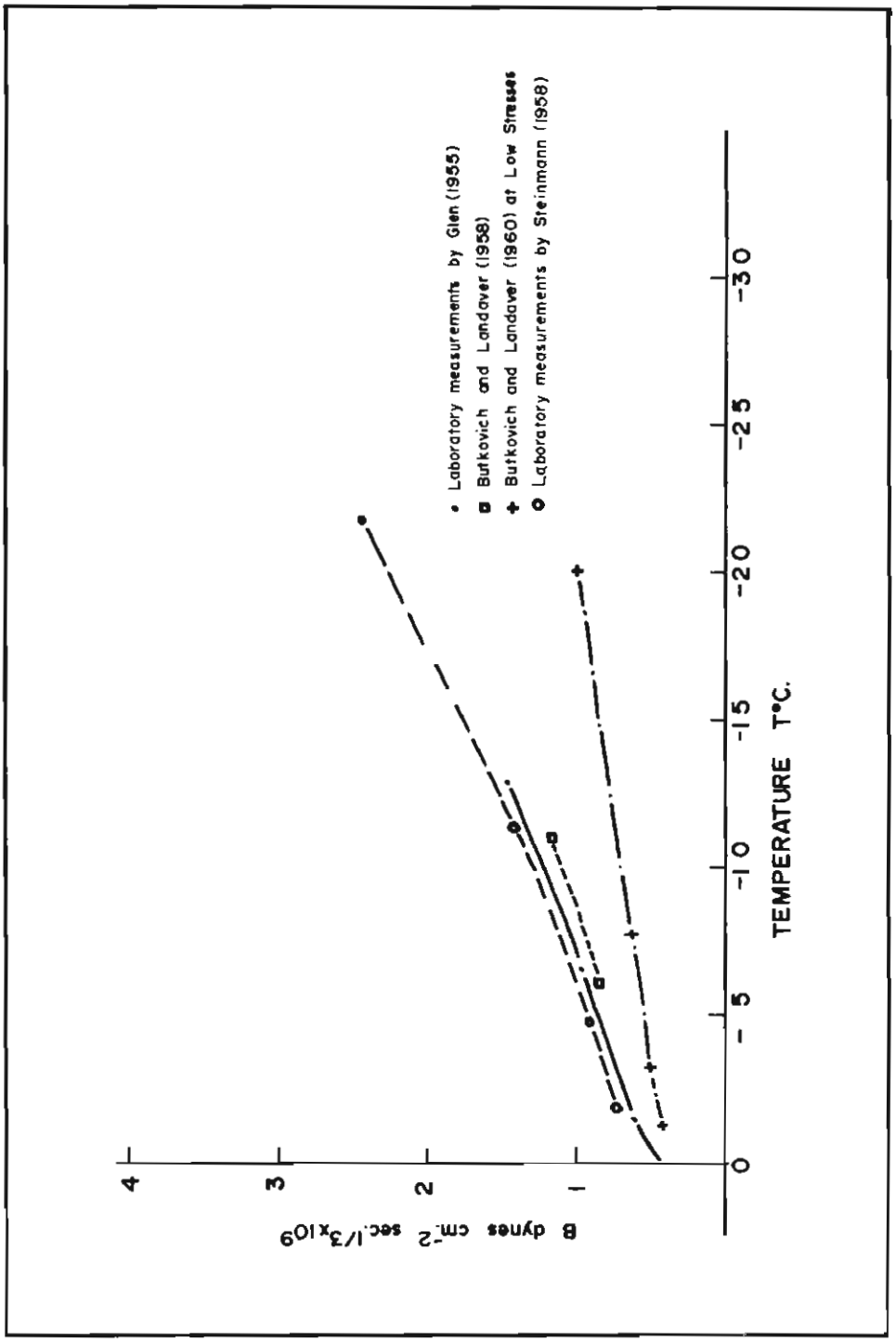

FIG. 16. The value of the flow parameter B from the flow law $\dot{E} = (\tau/B)^n$ versus temperature. (After "The Dynamics of the Amery Ice Shelf" (Budd 1966A), with additions.)

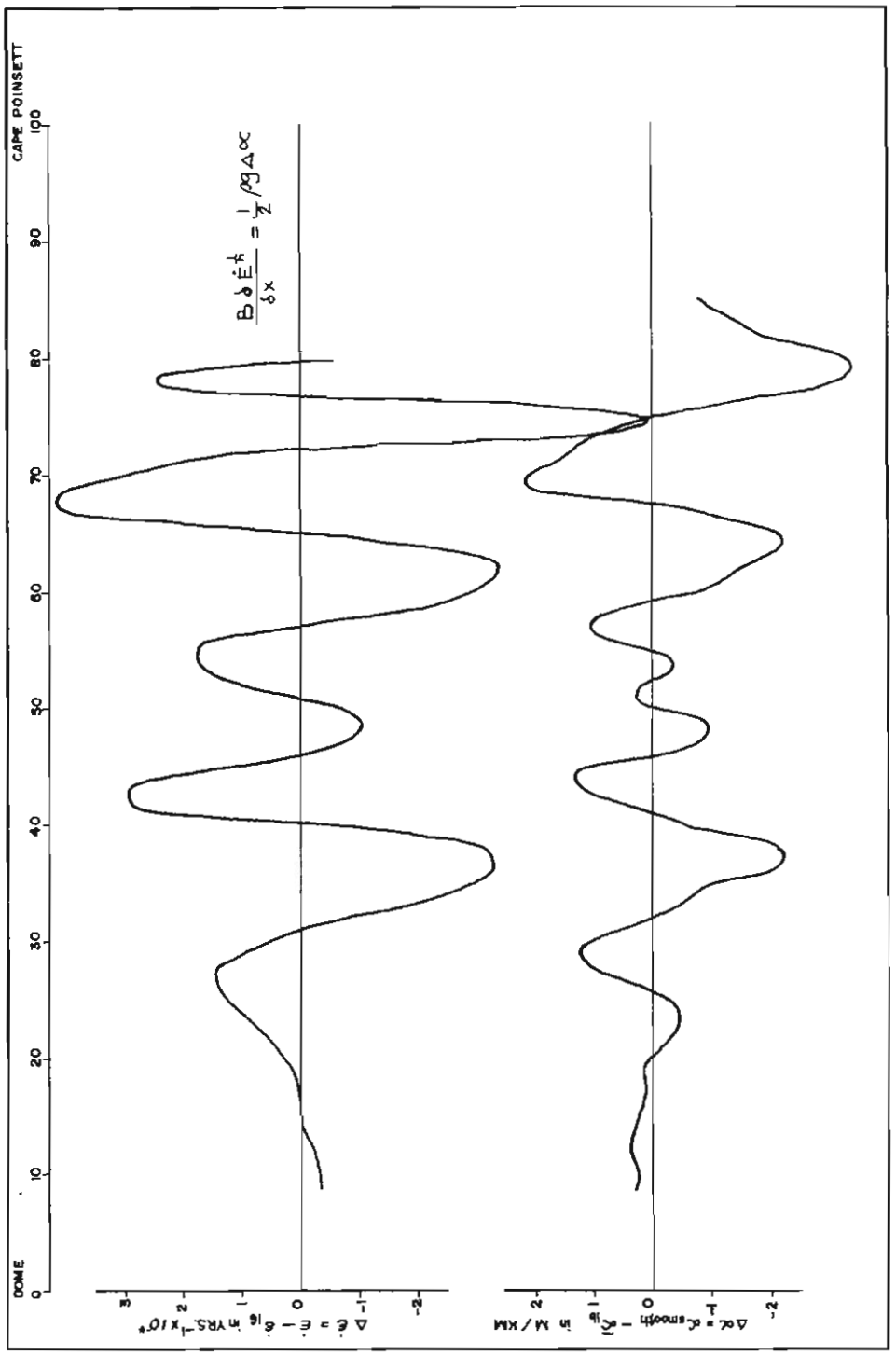

FIG. 17. Differential strain rates and surface slopes, Dome—Cape Poinsett.

D

Taking h as the mean ice thickness over each undulation, equation (5) may be written

$$B\partial E^{1/n} \simeq \tfrac{1}{2}\rho g \Delta\alpha \partial x \qquad (8)$$

Mean values of $\Delta\dot{E}_x$ for each peak and trough in Fig. 17 were multiplied by $\sqrt{3/2} \times 0{\cdot}71$ to convert to the terms of effective strain rate used by Nye (1957) (cf. Meier 1959). These were plotted (Fig. 18) against effective shear stresses calculated from $\sqrt{3/2} \times 0{\cdot}47 \times \tfrac{1}{2}\rho g \Delta\alpha \partial x$, where $\Delta\alpha$ was the mean value of the appropriate peak or trough on the $\Delta\alpha$ curve, Fig. 17, and $\partial x = 7{\cdot}5$ km, the average half-distance of the undulations. To reduce scatter caused by assuming $f = \bar{\alpha}$, the means of values between adjacent peaks and troughs were also plotted on the same graph. They showed a line whose slope gave $n = 1{\cdot}2$ and, from equation (8), a value of $B = 1{\cdot}32 \times 10^9$ dynes/cm^2 sec$^{1/3}$ at a stress of one bar.

D. ACCUMULATION AND SURFACE VERTICAL VELOCITIES

1. *Accumulation.*

Surface slopes on all three triangle legs were found from the elevations of the one-mile route markers. The surface slope at each point was taken as the mean over 1·6 km on either side. Mean elevations over 8 km on either side of each marker were calculated and the relative elevation of the point with respect to the overall slope deduced. Accumulation and surface slope values at each mile-pole were smoothed according to

$$X'_i = \frac{X_{i-1} + 2X_i + X_{i+1}}{4}.$$

These and individual readings were plotted with their relative elevations in Figs. 19, 20 and 21 and, on a more exaggerated scale, in Fig. 22.

Budd (1966B) showed that on the major continental plateau south of Wilkes, accumulation varied regularly over minor surface undulations. He and Swithinbank (1958) both found that, on comparing profiles along the prevailing wind direction, accumulation maxima coincided with surface slope minima.

Twenty of the 25 peaks in the ablation curve on the Dome—Cape Folger leg, 16 out of 21 on the Dome—Cape Poinsett leg and 16 of 17 on the coastal leg can be definitely related to minima in the corresponding slope curve. However, as the prevailing wind direction, indicated by sastrugi, is not along these legs but varies considerably over them, and as the strike direction of the undulations is unknown, this comparison was not carried further.

2. *Vertical velocities.*

The surface velocity in the vertical direction (V_z) over a given point of bedrock is given by

$$V_z = \dot{E}_z \, . \, h + A + V_x \tan(\alpha - \beta),$$

where $\dot{E}_z$ = vertical strain rate $= -(\dot{E}_x + \dot{E}_y)$;

h = ice thickness;

A = accumulation in cm of ice per year;

α and β are surface and bedrock slopes.

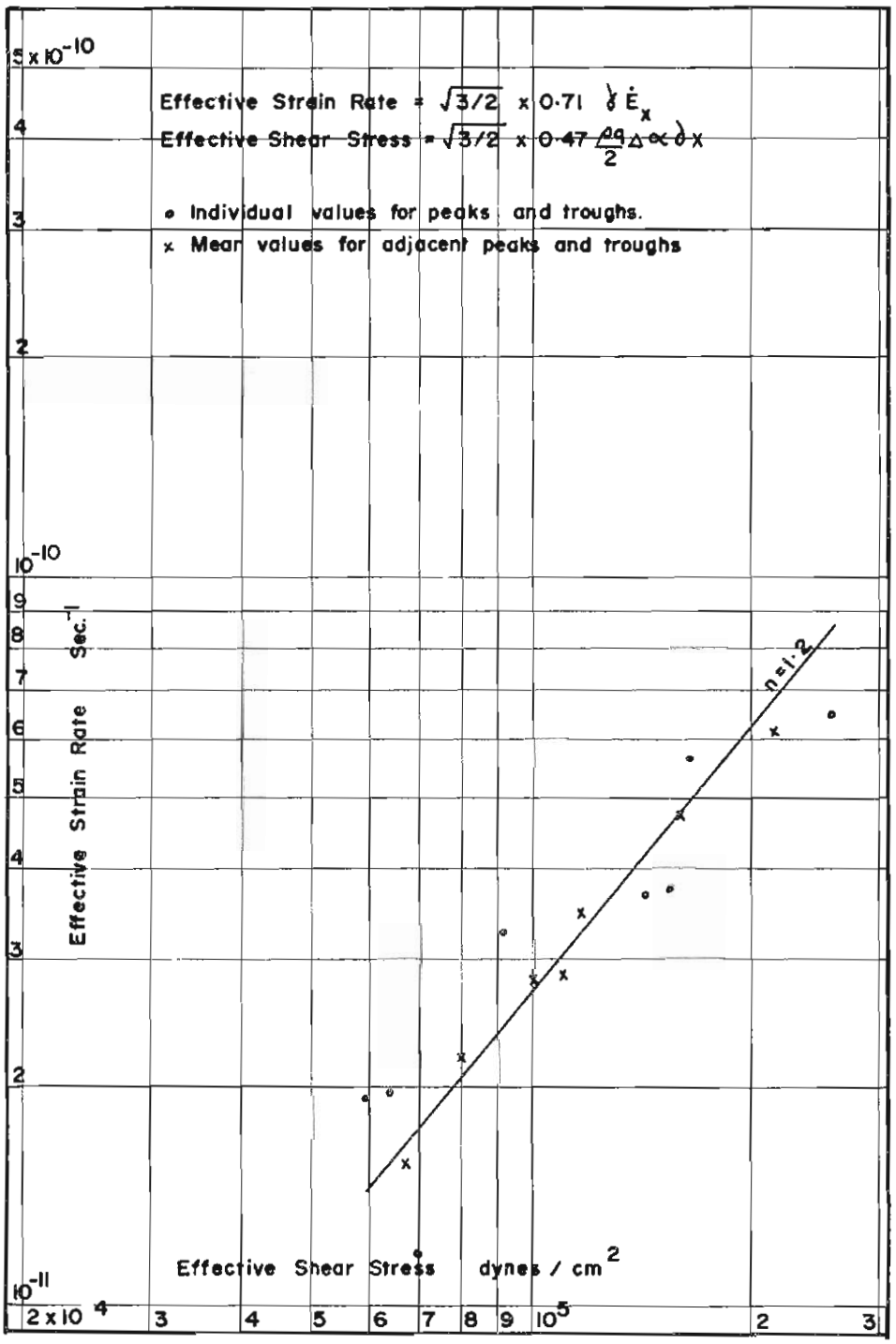

FIG. 18. Effective stress versus effective strain in upper ice, Dome—Cape Poinsett.

V_z was determined at each survey stake around the triangle and the results are shown in Fig. 23, 24 and 25. α and β were taken from the nearest uphill stake, varying in distance from 0·2 to 1·8 km. On the coastal leg, β was taken as zero and α interpolated between theodolite measurements at the strain grids. The mean accumulation over one mile on either side of each stake was converted into cm of ice to incorporate effects of snow compaction and densification. Values of $\dot{E}_x$ were meaned from tellurometer measurements on either side of the stake and $\dot{E}_y$ interpolated graphically from Figs. 8, 9 and 10. Values of V_z at each strain grid, using only the rosette measurements for $\dot{E}_x$ and $\dot{E}_y$ are shown in bar form on the graphs. Vertical velocity isolines over the triangle area are shown, as mentioned earlier, in Fig. 5.

5. DISCUSSION OF RESULTS

A. ICE FLOW

1. *Strain grids.*

As ice is practically incompressible over the range of pressures experienced (Dorsey 1940), $\Delta = 0$ in the equation $\dot{E}xx + \dot{E}yy + \dot{E}zz = \Delta$, where Δ is the dilation or ratio of change in volume to the initial volume before straining takes place (Jaeger 1962). A positive strain rate along one axis will therefore produce negative strain rates along the other two axes without indicating the presence of any compressive forces acting along these axes. Considering Figs. 2, 3 and 6, this is taken to explain the small negative strain rates at three strain grids: "C", where southerly lateral expansion occurs in the ice which has flowed past the 470 m flow-restricting ridge south of S2; at "G", where large lateral strain indicates expansion down the bedrock valley running to the east, possibly coupled with some compression resulting from the bedrock rising to the north; and possibly at "L", where east-west surface strains occur, due to the rosette's location at the centre of a north-south ridge. Rising bedrock to seaward of "L", as occurs near strain grids "A", and, presumably, "K", may also create a compressive force there, but this cannot be verified until further bedrock measurements are made in that region.

Strain vectors at "C" are in agreement with those found at the nearby S2 strain grid where continuous measurements have been made by U.S. and ANARE glaciologists since 1957. Cameron (1964) suggested that negative strain there is due to blockage of the ice flow by the Windmill Islands. This does not appear to be supported by the ice-flow vectors between "C" and stake 534 which show that flow returns to the more natural north-westerly direction perpendicular to the surface contours after passing the 470 m ridge, and that effects of blockage by the Windmill Islands and the 175 m rise east of Wilkes are not apparent until about stake 549, 12 km nearer the coast. The increased northerly component of flow in the neighbourhood of strain grid "B", and the strain tensors at that point, reflect a flow restriction caused by the 175 m rise and indicate its south-easterly extension.

Strain grids "D", "E", "H" and "J" show positive strains along both major axes, as is consistent with both surface and bedrock topography. The major strain vectors are along the general direction of greatest local surface slope. Strain grids "H" and "J" are strongly affected by their situations near the brow of steep slopes. The high strain rates measured at these points are not representative of the line as a whole.

At strain grid "A", a negative strain rate along the line of flow is due to the effect of a 60 m rise in bedrock to seaward of the rosette obstructing the natural flow of the relatively thin ice cover in that direction. The large compressive strain at "K" can only be explained by proposing a similar rise in bedrock to seaward of

that point. No east-west expansion is possible there as the rosette is located in a surface trough (cf. Fig. 21).

2. *Flow vectors.*

Considering Figs. 3 and 6, the flow vectors between the Dome and strain grid C have larger northerly components than would be expected if flow were truly radial from the summit and perpendicular to the surface contours. This is probably caused by the obstruction of the 470 m bedrock ridge south of S2 forcing the ice to flow around it. As mentioned above, the large lateral and negative longitudinal strain rates at C are caused by the horizontal widening of the flow lines after passing this obstruction. Between strain grids "C" and "B" flow is more nearly perpendicular to the contours until a northerly component is introduced between stakes 549 and 515. This is due to the blockage of normal flow by a 175 m bedrock rise 10 km east of Wilkes where the ice is only a few hundred metres thick. Between stakes 515 and 508, ice velocities increase and again become perpendicular to the contours. A velocity of 10 m/yr at bearing 265° was calculated at strain grid "A", and 11·6 m/yr at bearing 264° from other measurements near Cape Folger.

On the other two triangle legs, flow vectors have been derived from the measured extensions along the line with the addition of a lateral velocity computed from the strain grid results. As this method applies measurements from the locally affected strain rosettes over distances of many kilometres, the bearing of the vectors must be regarded with some reservation. They do, however, show an easterly component between the Dome and strain grid "H" which is in accord with the general bedrock and surface slopes in that direction. The slight deviation of flow direction from the line of maximum slope around strain grid "J" may be as much due to errors in the method of calculation as in the interpolation of contours or surface effects. Along the coastal leg, the vectors indicate a major obstruction such as a high rise of bedrock seaward of the line between stakes 587 and 590.

B. STRESS PARAMETERS

1. *Stresses near bedrock.*

Shear stresses at the base of the ice cap, calculated from the equation $\tau = \rho g h \sin \alpha$, reached a maximum level of 1·1 bars. This is of the same order as the maximum of 1·0 bars noted by Bull (1957) at 78°N in the Greenland ice cap, and the maximum of 1·5 bars found in Alpine glaciers having velocities of the same order of magnitude (Nye 1959A). Nye proposed that the shear stress is determined mainly by the roughness of the bed, the ice temperature and velocity. The ice temperatures below the Wilkes ice cap are likely to be lower than those of the Alpine glaciers but similar to those found at the base of the Greenland ice sheet. Noting this difference, and assuming that the ice velocities around the triangle are comparable to those of the Alpine glaciers considered by Nye and to the Greenland ice cap, the agreement in range of shear stresses indicates that the degree of bedrock roughness in the triangle area is similar to those of the Alpine and Greenland ice masses.

The maximum shear stress level of 1·1 bars was only reached on the Dome—Cape Poinsett leg. Along the Dome—Cape Folger leg, bottom shear stresses had a

maximum value of 0·8 bars. The difference in magnitude of the maximum shear stresses along the two legs reflects the smaller surface slopes and flow velocities between the Dome and Cape Folger as compared to those found between the Dome and Cape Poinsett.

Surface temperatures along both legs are similar, but ice temperatures in the upper layers would be expected to be warmer along the Dome—Cape Folger leg due to the lower accumulation rates (Robin 1955). The temperature gradient through the ice would be greater between the Dome and Cape Poinsett, however, due to the considerably higher flow velocities, and temperatures in the basal layers are likely to be warmer along this leg than between the Dome and Cape Folger.

2. *Velocity power law.*

Considering both a high concentration of shear in the basal layers and no longitudinal strain in the upper ice mass, Nye (1959A) proposed a flow law

$$V = \left(\frac{\tau}{A}\right)^m,$$

where V = velocity and τ = basal shear stress,

and A and m are parameters dependent on bed roughness, ice temperatures and constitution. Nye showed that m is not likely to be less than about 2, and may well be considerably more. From Weertman's (1957) calculations he showed that, when the ice in contact with the bed is at pressure melting point, $m = (n + 1)/2$, where n is one of the parameters in Glen's flow law. Taking n about 4 from Glen's (1955) experiments, Nye found that $m \simeq 2{\cdot}5$ for the case of bottom-sliding.

To test the above law, the surface velocities along both radial legs were plotted against bottom shear stresses in Fig. 14. Velocities along the Dome—Cape Folger leg showed a linear agreement with shear stresses on the log-log scale up to the maximum shear stress level of 0·8 bars. Velocities along the Dome—Cape Poinsett leg also showed a fairly consistent agreement with stresses up to 1 bar. Above these two limits, velocities appeared independent of stress, indicating either bottom-sliding as temperatures reached the pressure melting point or a change in the ice properties relating strain to stress near that point. Assuming Nye's flow law, values of $m = 2{\cdot}7$ were obtained for both legs up to the maximum, or "critical" stress limit. Applying $m = (n + 1)/2$ gives a value of $n = 4{\cdot}4$. This is found to be above the range of values determined for this stress range by other workers, as given by Budd (1966A).

The value of $m = 2{\cdot}7$, found from Fig. 14, is slightly higher than the value of 2·5 determined by Nye and Weertman for the case of bottom-sliding and suggests that the critical stresses in Fig. 14 are as likely to be due to possible changes in the ice properties as to bottom-sliding. Even allowing for the effect of unknown bottom temperatures, compositions of ice in the lower layers, and possible variations in m itself at different points along the line due to changing bedrock roughness and temperature, the amount of scatter in Fig. 14 indicates that there is an appreciable amount of longitudinal strain occurring in the ice above the basal layers. Fig. 14 shows that Nye's formula gives only a good estimate of average ice velocities up to the point of critical stress but not beyond that point.

3. *Stress parameters near bedrock.*

Surface strain rates are a combination of strain rates near the bedrock, caused by the overall shape of the ice cap, and longitudinal strains in the upper ice mass caused by local surface topography. As mentioned above, Fig. 14 indicates that there is an appreciable amount of longitudinal strain occurring in the major mass of ice above the base. This Section and the following ((4) Stress Parameters in the Upper Ice) attempt to separate the two regions of strain and determine their respective stress parameters.

Shumskiy (1961) shows that at the bedrock—ice interface,

$$\tau = \pm \rho g h \cos^2 \beta f,$$

where h is the ice thickness,

β is the bedrock slope,

and f is the coefficient of friction.

Comparing this with Nye's (1952) equation,

$$\tau = \rho g h \sin \alpha,$$

where α is the surface slope, gives us

$$\sin \alpha = \cos^2 \beta f.$$

On the Dome—Cape Poinsett leg, $\cos^2 \beta$ was always between 1·000 and 0·999, and therefore $f = \alpha$. This justifies the empirical assumption that $f = \bar{\alpha}$ used in deriving the equations of (4.C.2).

From the equation,

$$\frac{\partial}{\partial x}(hB\dot{E}^{1/n}) = \tfrac{1}{2}\rho g h(\alpha - f) \qquad \text{(4.C.2, equation 5)}$$

the relationship $f = \alpha$ is seen to be valid for cases of zero longitudinal strain or whenever $h\dot{E}^{1/n}$ is constant, as well as for cases of small bedrock slope.

Budd (1967) showed that, with no basal sliding,

$$B^n \frac{V}{h} = \frac{2(\rho g h \bar{\alpha})^n}{(n+1)} \qquad \text{(4.C.2, equation 6)}$$

If it is assumed that the temperature of the basal layers increases with the surface temperature, then the effect of variations in B along the line may be incorporated into the velocity versus basal stress relationship by letting

$$B^n = (1 - \theta)k^n,$$

where θ is the ice temperature,

and k is the stress for unit strain at 0°C (Shumskiy 1961).

This was done for two cases: (i) the basal temperature was taken as being equal to the mean surface temperature (i.e., $\theta = \theta_s$), determined from the surface elevation at each survey marker, using the relationship between surface elevation and temperature given by Cameron (1964) for the Wilkes area; (ii) after consideration of the results of (i), the basal temperature at each survey marker was taken as being 10° warmer than the mean surface temperature, $\theta = (\theta_s + 10)$.

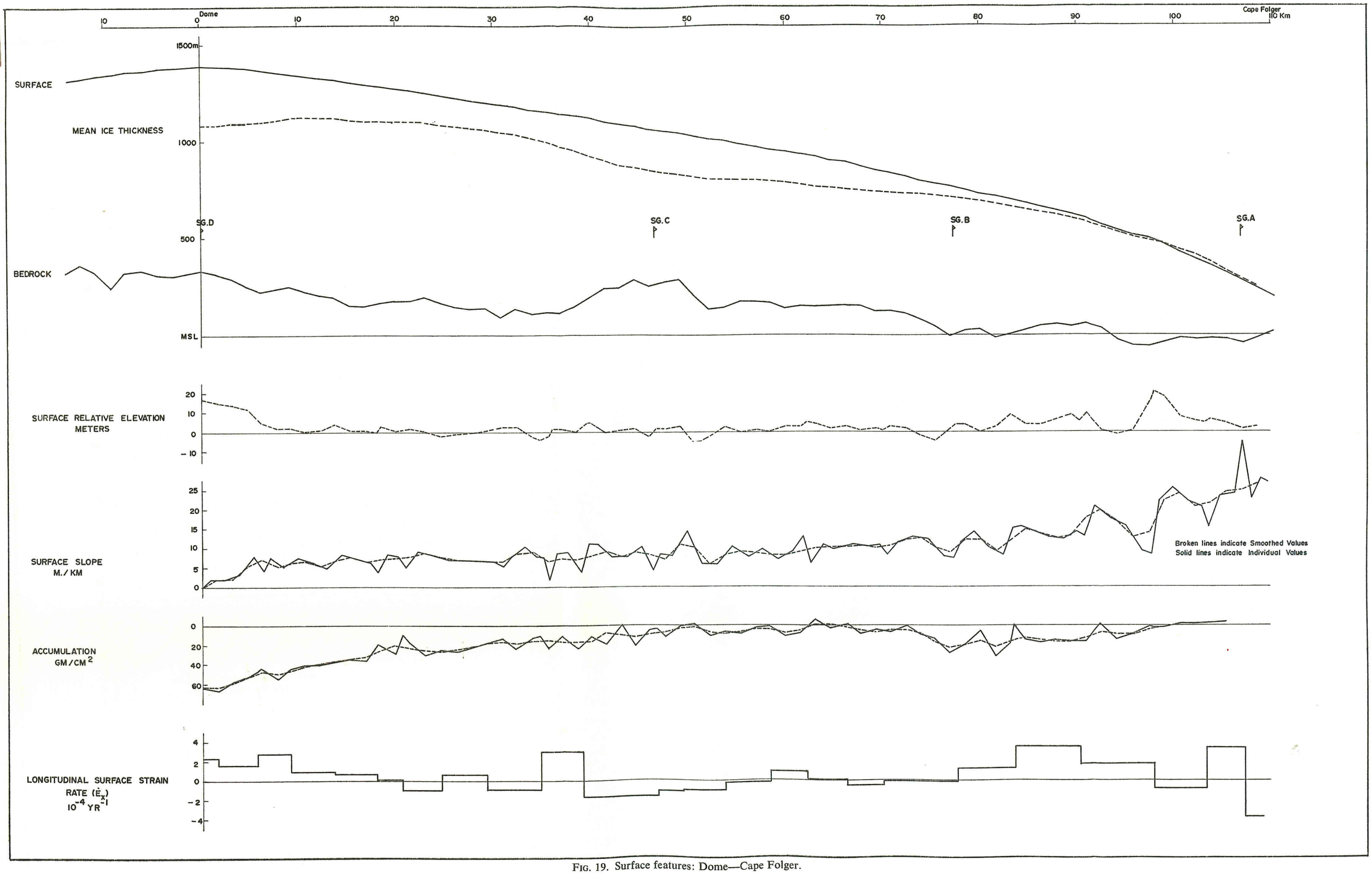

FIG. 19. Surface features: Dome—Cape Folger.

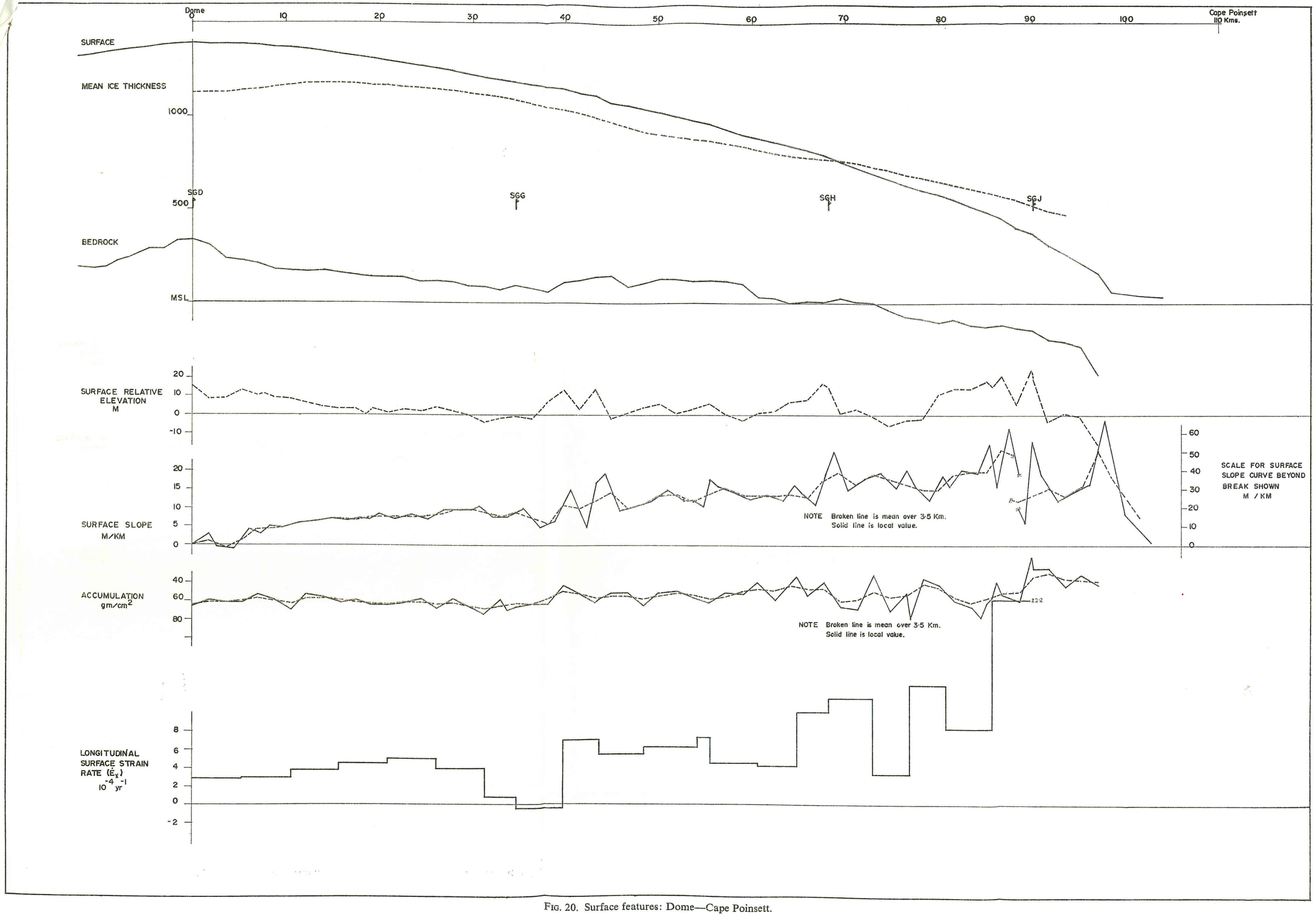

FIG. 20. Surface features: Dome—Cape Poinsett.

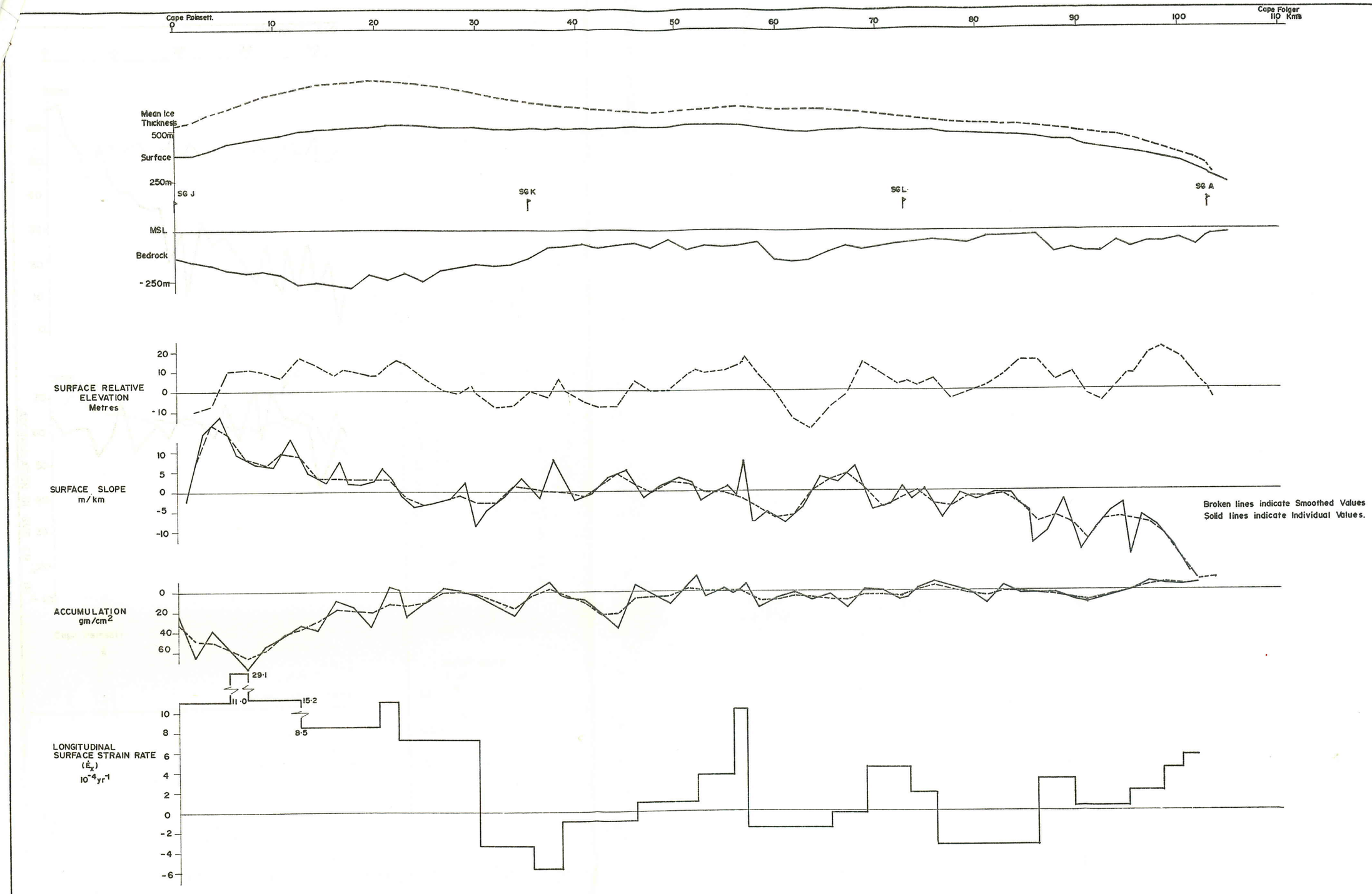

FIG. 21. Surface features: Cape Poinsett—Cape Folger.

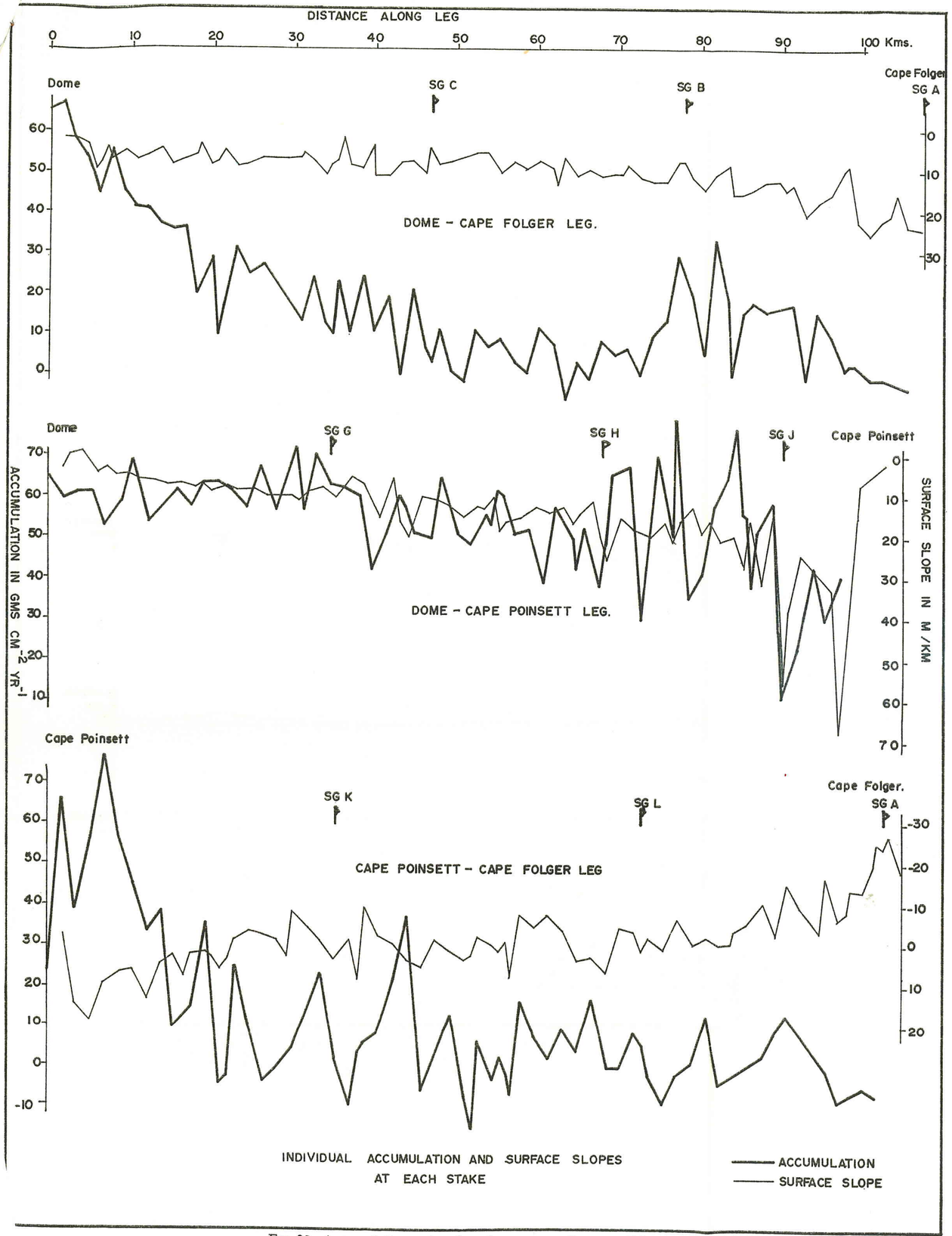

FIG. 22. Accumulation and surface slopes versus distance, all legs.

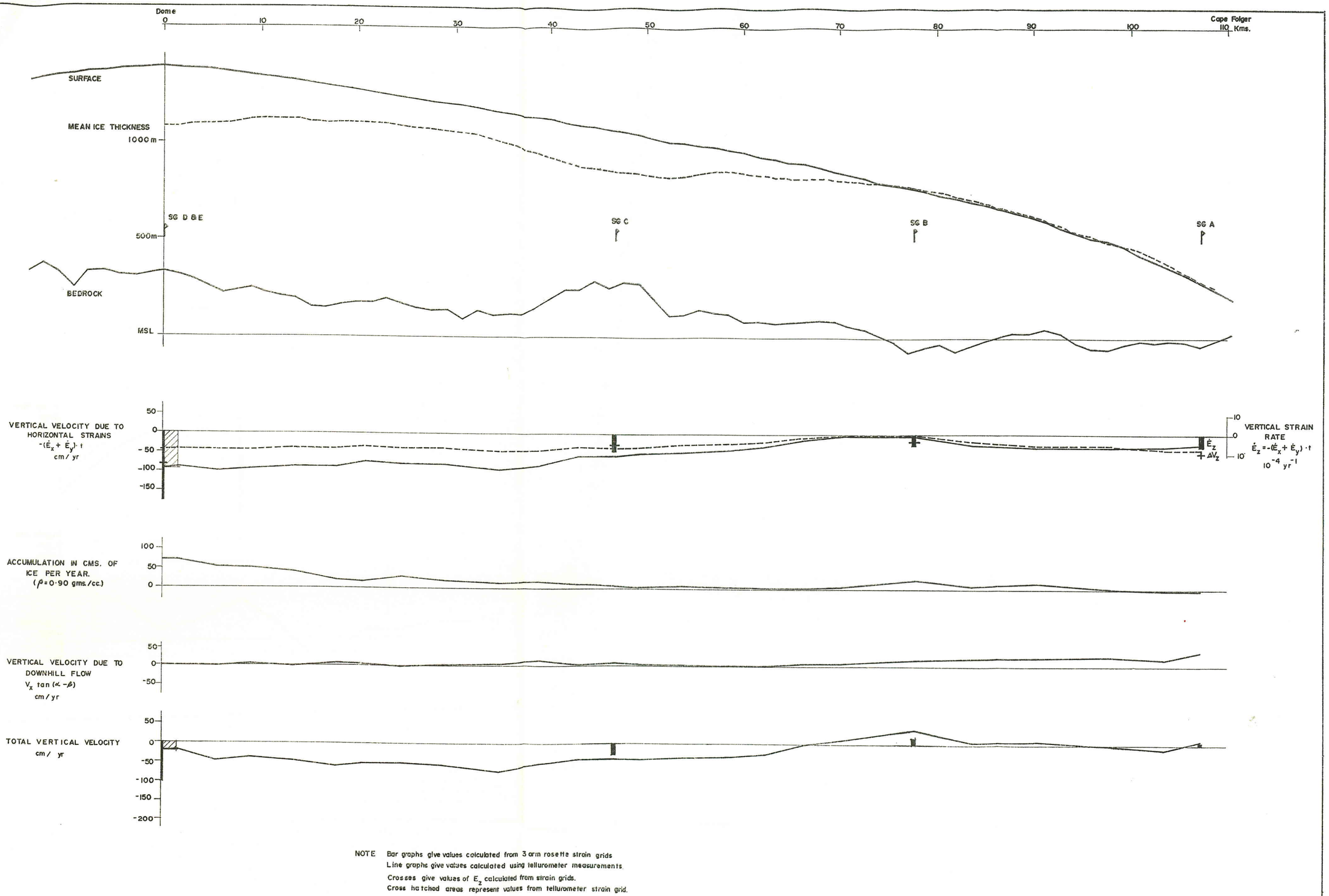

NOTE Bar graphs give values calculated from 3 arm rosette strain grids
Line graphs give values calculated using tellurometer measurements.
Crosses give values of E_z calculated from strain grids.
Cross hatched areas represent values from tellurometer strain grid.

FIG. 23. Vertical velocities: Dome—Cape Folger.

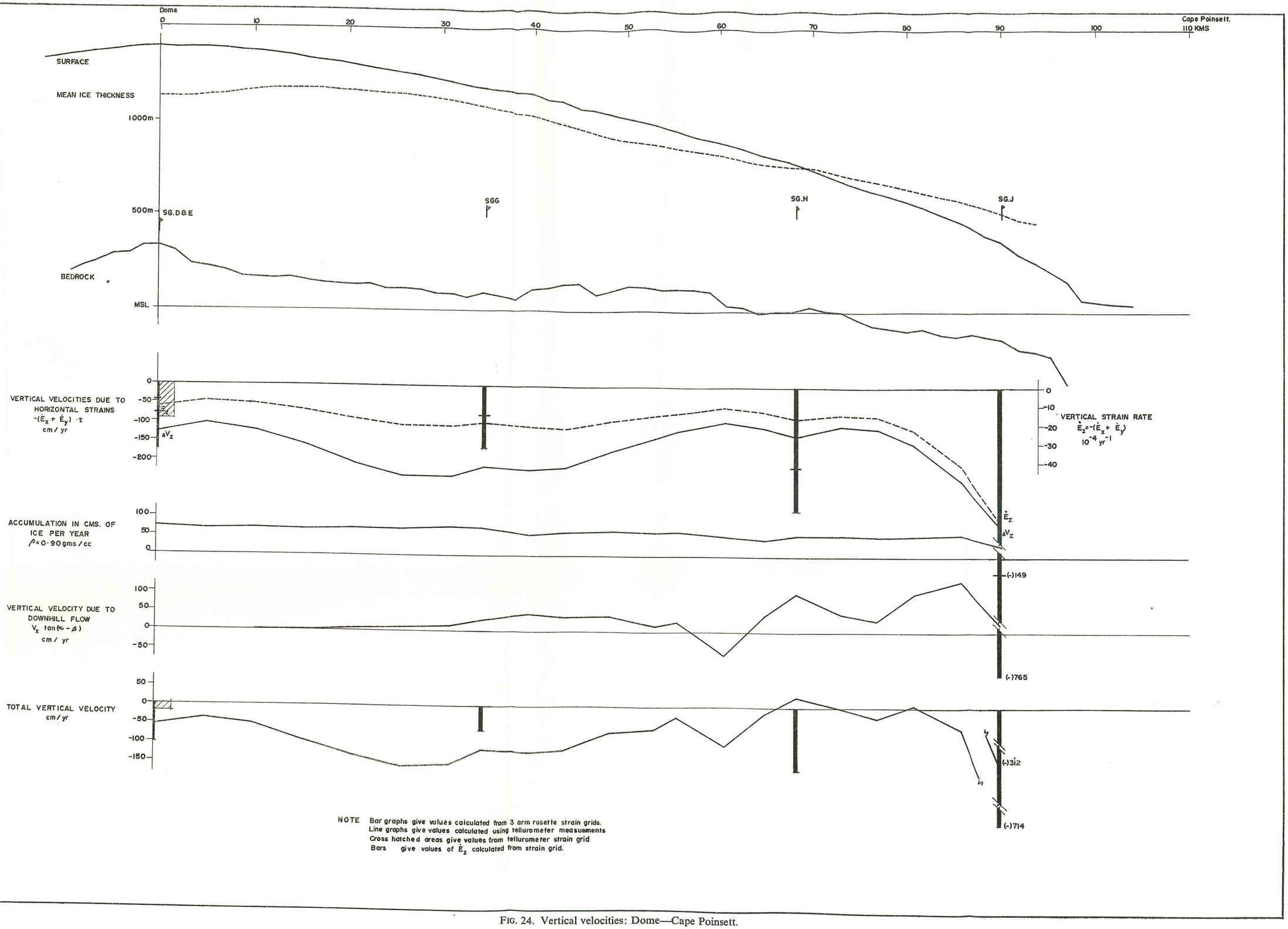

NOTE Bar graphs give values calculated from 3 arm rosette strain grids.
Line graphs give values calculated using tellurometer measuements
Cross hatched areas give values from tellurometer strain grid
Bars give values of $\dot{E}_z$ calculated from strain grid.

FIG. 24. Vertical velocities: Dome—Cape Poinsett.

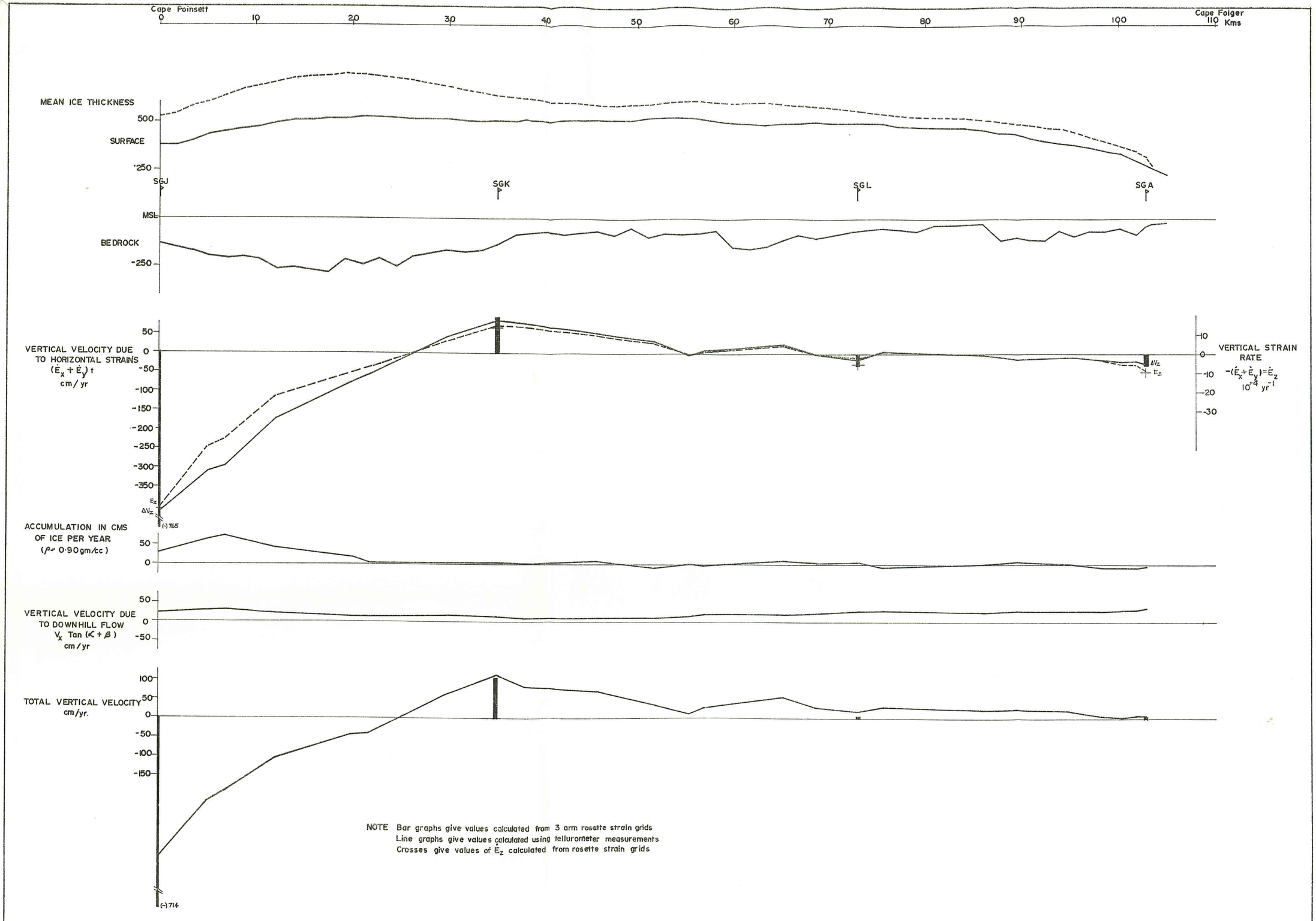

FIG. 25. Vertical velocities: Cape Poinsett—Cape Folger.

(i) Considering $\theta = \theta_s$ along the Dome—Cape Poinsett leg, values of $\bar{\alpha}h$ and $(1 - \theta)\frac{V}{h}$, smoothed over 15 km, were plotted against each other in Fig. 15. They showed a fairly linear relationship, giving a value of $n = 4{\cdot}3$ and, from equation (4.C.2, (6)), a mean value of $B = 0{\cdot}74 \times 10^9$ dynes/cm^2 sec$^{1/3}$ was calculated.

The smoothing process greatly reduced the effects of differential longitudinal strain in the upper mass of ice, though cyclical deviations from the mean line, caused by the differential strain, may still be noted. The value of $n = 4{\cdot}3$ at stresses of one bar is slightly higher than the average values found by other workers (Budd 1966A). The value of B indicates an average basal temperature of about $-3°$C (Fig. 16), or about 14° warmer than the mean of the surface temperatures which had been assumed to apply.

(ii) To investigate the effect of varying the range of assumed basal temperature, and to bring the assumed temperatures into closer agreement with those indicated by the value of B determined above, ice temperatures near the bedrock along the Dome—Cape Poinsett leg were assumed to be 10° warmer than the previously assumed surface temperatures, i.e., $\theta = (\theta_s + 10)$ in the equation $B^n = (1 - \theta)k^n$. Assuming any greater an increase in the basal temperature would have introduced too large a percentage fluctuation in the term $(1 - \theta)$ at the warmer end of the temperature range. Plotting the smoothed values of αH against the new values of $\frac{V}{h}(1 - \theta)$ (Fig. 15) gave a line of slope $n = 3{\cdot}4$ and a mean value of $B = 0{\cdot}85 \times 10^9$ dynes/cm^2 sec$^{1/3}$. These values are in good agreement with those determined by previous workers, and the value of B is consistent with the assumed range of temperatures (Fig. 16). The decreased amount of scatter among the points also indicates a more realistic temperature assumption, although it should be noted that the final two points at the Cape Poinsett end of the line were not plotted, due to the strong influence of the term $(1 - \theta)$ as it approached zero.

Basal temperatures of $\theta = (\theta_s + 10)$ were also assumed at the survey markers along the Dome—Cape Folger leg. Plotting $\bar{\alpha}h$ versus $\frac{V}{h}(1 - \theta)$ for this leg (Fig. 15) showed considerable scatter but indicated a value of $n = 3{\cdot}4$ and $B = 0{\cdot}96 \times 10^9$ dynes/cm^2 sec$^{1/3}$. The large amount of scatter and high value of B, relative to that found on the Dome—Cape Poinsett leg, result from comparing the magnitude of surface velocities which in general are in a direction away from this leg, with shear stresses calculated from slopes measured along the leg.

Of the stakes on the Dome—Cape Folger leg, flow directions at stakes 543, 605 and 534 were most nearly parallel to the line along which shear stresses were calculated. Due to the limited information on the surface slopes, it was not possible to calculate the basal shear stress in the direction of the velocity vector for any other points on this line. In Fig. 15, the plots of $\frac{V}{h}(1 - \theta)$ versus $\bar{\alpha}h$ for these three stakes closely coincide with the line of best fit obtained for the Dome—Cape Poinsett leg. This indicates that the flow along both legs is governed by the same parameters and

that values of $n = 3{\cdot}4$ and B about $0{\cdot}85 \times 10^9$ dynes/cm^2 sec$^{1/3}$ are representative for ice flow near the bedrock over the triangle area.

4. *Stress parameters in the upper ice.*

To determine the parameters governing flow in the major mass of ice above the basal region, the relation

$$B\partial\dot{E}^{1/n} = \tfrac{1}{2}\rho g \Delta\alpha \partial x \qquad \text{(4.C.3, (8))}$$

was used. This equation is only applicable where there is small degree of lateral strain (Budd, personal communication). As deseribed in (4.C.3), Fig. 17 shows the comparison of $\partial\dot{E}$ and $\Delta\alpha$ with distance along the Dome—Cape Poinsett leg. A comparison of $\partial\dot{E}$ and $\Delta\alpha$ along the Dome—Cape Folger leg showed a relationship somewhat similar to that of Fig. 17, but, due to the smaller changes in surface slope and the large amount of lateral strain, caused by the influence of bedrock topography (4.A), the investigation could not be carried further on this leg.

Fig. 18 shows the plot of effective strain rate against effective shear stress for the differential longitudinal strains in the upper ice along the Dome—Cape Poinsett line. The large amount of scatter between the plots of values for the individual peaks and troughs of Fig. 17 is greatly reduced when summed values taken between adjacent peaks and troughs are used. This would indicate that the zero line for the $\Delta\alpha$ curve in Fig. 17 is slightly too high, that is, running above the true level of mid-points between the peaks and troughs. As $\Delta\alpha = \alpha - \bar{\alpha}$, such a condition would be caused by either the value of f in equation (4.C.2, (5)) being not exactly equal to $\bar{\alpha}$ at every point but to α plus some factor dependent on local conditions (i.e., $\bar{\alpha}$ not being meaned over a sufficient distance), or, conversely, to the continual increase in the rate of change of slope going away from the Dome making the calculated value of $\bar{\alpha}$ at any point greater than it actually is (i.e., if $\bar{\alpha}$ was taken over too great a distance, the larger downslope values would not be compensated for by the lesser upslope values). The latter of these two explanations is believed to be the more correct.

The slope of the line drawn through the points in Fig. 18 gives a value of $n = 1{\cdot}2$, which is in good agreement with other works for the range of shear stress considered (Budd 1966A). Projecting the stress to one bar, a value of $B = 1{\cdot}3 \times 10^9$ dynes/cm^2 sec$^{1/3}$ was calculated from equation (8). As the effective stresses are between the range of Butkovieh and Landauer's (1960) low stress tests and their tests (1958) at higher stresses, the value of B corresponds on Fig. 16 to a mean ice temperature around $-17°$C. This is roughly the same as the mean surface temperature, or about that which would be expected to apply in the upper ice (Robin 1955; Jenssen and Radok 1963).

Due to the approximations involved in deriving the equations for this method of determining the flow parameters (Budd 1967), the amount of scatter in the results, and the lack of actual ice temperature measurements, the values of $n = 1{\cdot}2$ and $B = 1{\cdot}3 \times 10^9$ dynes/cm^2 sec$^{1/3}$ can only be taken as approximate. They do however, show that there is an appreciable difference in the parameters governing the ice flow in the upper ice mass as compared to the basal layers.

C. VERTICAL VELOCITIES AND MASS BALANCE

1. *Mass budget deduced from vertical velocities.*

Fig. 4 shows isolines connecting points with equal vertical surface velocities as calculated by

$$V_z = \dot{E}_z h + A + V_x \tan(\alpha - \beta) \qquad (4.C.3)$$

These indicate a net thinning, increasing towards the east, over the greater part of the ice cap. Vertical velocities along the easternmost arm increase from 20 cm/yr downward at the Dome to over 3 m/yr at Cape Poinsett, averaging about 80 cm/yr. These values may be somewhat high however, as values of $\dot{E}y$, used in determining $\dot{E}_z = -(\dot{E}_x + \dot{E}_y)$, were interpolated between strain grids which were, due to their positions (see Sect. 5.A.1) not representative over large areas. Shumskiy (1965) determined the rate of lowering of part of the Greenland ice cap by considering $\frac{1}{2}(\dot{E}_x + \dot{E}_y) < \dot{E}_z < (\dot{E}_x + \dot{E}_y)$. In this work, $\dot{E}_z$ is considered to be closer to $(\dot{E}_x + \dot{E}_y)$ than to $\frac{1}{2}(\dot{E}_x + \dot{E}_y)$ due to the expected high shear at the base of the ice cap (cf. Nye 1959A). The net result of using the lower values of $\dot{E}_z$ over the Wilkes ice dome would give the same qualitative result, but with larger positive and smaller negative vertical velocities throughout (see Table I).

Around Cape Folger and along most of the coastal arm a thickening of the ice is indicated. This reaches a maximum of 1 m/yr near strain grid "K" where rising bedrock is believed to retard flow towards the sea. The total decrease in volume of ice calculated from extrapolation of these results is $1{\cdot}7 \times 10^9$ m^3/yr, or an average loss of about 40 cm/yr over the entire triangle area.

Local values of V_z calculated at each strain grid, using the rosette measurements, agree generally with the above values calculated over several kilometres. The sole exception is at strain grid "H" where the rosette measurements, affected by local topography, show a very much greater downward velocity than indicated by the more general measurements.

2. *Mass balance deduced from continuity of radial flow.*

By assuming flow to be radial from the Dome summit, the velocity at any point required to maintain a state of steady mass balance can be calculated by

$$V_x = \frac{\text{(Total accumulation between Dome and that point)}}{\text{(Flow area at the point)}}$$

$$= \frac{\Sigma(d\,\text{Area} \times \text{Accumulation})}{\text{Depth} \times \text{Width}}$$

$$= \frac{\Sigma \frac{\theta}{2}(r_n^2 - r_{n-1}^2)A}{h \,.\, \theta \,.\, r}$$

$$= \frac{\Sigma(r_n^2 - r_{n-1}^2)A}{2hr_n},$$

where r_n is the distance of point n from the Dome.

TABLE I

VERTICAL VELOCITIES AT STRAIN ROSETTES $V_z = -(\dot{E}_x + \dot{E}_y)h + A + V_x(\alpha - \beta)$

Strain Grid	$\dot{E}_x + \dot{E}_y$ 10^{-4}/yr	h m	$\dot{E}_x h$ cm/yr	A ice cm/yr	V_x m/yr	$\alpha - \beta$	$V_x(\alpha - \beta)$ cm/yr	V_z cm/yr
			Taking $\dot{E}_x$ from tellurometer measurements:					
A	7·70	322	−25	−4	10·0	0·0389	+39	+10
B	0·57	834	−5	+24	5·6	0·0304	+15	+34
C	7·03	801	−56	+7	3·6	0·0228	+8	−41
D	8·80	1054	−93	+73	0·0		0	−20
G	19·84	1091	−216	+72	12·6	0·0223	+28	−116
H	16·80	771	−130	+56	29·4	0·0364	+101	+27
J	72·22	515	−372	+29	55·1	0·0040	+22	−321
K	−14·62	646	+94	+5	4·9	0·0290	+14	+113
L	2 81	563	−16	+5	8·8	0·0340	+29	+18
			Taking $\dot{E}_x$ from strain rosettes:					
A	9·44	322	−30	−4	10·0	0·0389	+39	+5
B	3·24	834	−27	+24	5·6	0·0304	+15	+12
C	5·62	801	−45	+7	3·6	0·0228	+8	−30
D	16·64	1054	−175	+73	0·0		0	−102
G	15·11	1091	−165	+72	12·6	0·0223	+28	−65
H	42·57	771	−328	+56	29·4	0·0364	+101	−171
J	148·62	515	−765	+29	55·1	0·0040	+22	−714
K	−13·17	646	+85	+5	4·9	0·0290	+14	+104
L	5·32	563	−30	+5	8·8	0·0340	+29	+4

Note: Surface slope in immediate area measured by theodolite when installing rosette.

The horizontal velocities required to balance the accumulation were calculated at each survey point along the two legs radial from the Dome, and values of V_z deduced by comparison of these with the actual velocities:

$$V_z = \frac{(\text{Required } V_x - \text{Actual } V_x) \cdot 2hr_n}{r^2_n - r^2_{n-1}}.$$

These results show an average thinning along the Dome—Cape Poinsett leg of about 50 cm/yr, and along the Dome—Cape Folger leg a thickening averaging 10 cm/yr over the entire leg. The large positive vertical velocities around strain grid "C" result from not considering the effects of lateral strain in the calculations.

For an unstable ice cap having radial flow, the horizontal velocity at any point required to cope with the local accumulation plus ice flow from the preceding stake is

$$V_x = \frac{2(V_{n-1} \cdot h_{n-1} \cdot r_{n-1}) + A(r^2_n - r^2_{n-1})}{2h_n r_n}.$$

Vertical velocities were obtained along the two radial legs by applying the required horizontal velocities given by this equation into the equation for V_z above. The results also show a net thinning along the Dome—Cape Poinsett leg and a thickening in the region between strain grid "C" and Cape Folger. The magnitudes of the vertical velocities are generally lower than those given by the assumption of a stable ice cap and by the equation $V_z = -\dot{E}_x h + A + V_x \tan(\alpha - \beta)$ of Section 4.C.1 (see Table II). The large fluctuations in V_z between neighbouring stakes is

TABLE II

COMPARISON OF METHODS FOR CALCULATING VERTICAL VELOCITY V_z

Calculated by three methods at representative stakes

Stake /65	Velocity at stake	Velocity prec. stake	Ice Thickness at stake	Ice Thickness prec. stake	Distance (r) at stake	Distance (r) prec. stake	A ice cm/yr	V_z cm/yr stable ice cap	V_z cm/yr unstable ice cap	V_z cm/yr $V_z = \dot{E}_z h + A + V(\alpha - \beta)$
SGA	10·0	8·3	322	396	107·34	103·38	−4	+57	−6	+5
542	9·4	6·7	556	689	90·53	83·81	+18	+7	+3	+9
SGB	5·6	5·6	767	725	77·67	70.20	+24	+2	+15	+12
500	5·2	4·5	737	784	66·27	62·22	+1	+1	−13	−4
526	4·5	3·6	784	796	62·22	58·52	+3	+16	−20	−26
SGC	3·6	4·2	801	852	46·82	42·99	+7	+52	+17	−30
543	4·2	4·1	852	1067	42·99	29·13	+10	+35	+4	−42
507	4·4	5·1	1070	1092	24·35	20·44	+29	−17	+27	−51
517	4·6	3·3	1130	1126	17·86	13·47	+22	−35	−41	−58
683	2·5	0·4	1099	1074	9·06	1·58	+51	−6	−10	−38
524	1·5	0·0	1162	1054	5·21	0·00	+68	+2	00	−37
527	7·4	5·1	1162	1181	20·76	15·68	+70	−35	−21	−131
G1	12·3	12·1	1091	1121	34·50	31·06	+72	−40	+33	−65
531	21·0	17·4	857	937	54·11	48·43	+61	−4	−2	−68
525	26·1	24·3	829	851	64·81	60·62	+44	−32	−12	−19
H1	29·4	26·1	775	829	68·16	64·81	+56	−58	−12	−171
584	41·2	36·1	670	703	80·81	76·89	+55	−95	−35	+5
J1	54·7	45·3	514	594	90·06	85·83	+29	−58	−31	−714

due to the application of radial flow theory to a region where flow is not radial (Fig. 6). If the centre of flow were taken to be somewhat west of the Dome, as indicated by the plotted flow vectors, the values of V_s would become much closer to those of method (1).

3. *Budget of accumulation and outflow.*

The quantity of ice flowing out of the triangle area around each survey stake was computed by multiplying the lateral velocity by the distance and mean depth between that stake and its neighbours. The summation of these values was compared with the total accumulation over the area as determined by planimeter from the accumulation isolines. This showed a net increase in volume of 442×10^6 m^3 of ice, equivalent to an overall rise in surface elevation of 10 cm.

Some error has been introduced into this method by the interpolation of accumulation isolines between peripheral measurements, but the greatest source of error is in the estimate of lateral velocities along the easternmost and coastal legs. Maximum anticipated errors in the lateral velocities along these legs average ± 16 m/yr and ± 12 m/yr. As an increase of only 1 m/yr in their estimated values would reduce the net gain over the triangle by 20% and 12% respectively, the method should not be considered to give reliable information until more accurate values of lateral velocities are determined. The results are included here solely to show that this check on the mass balance was made.

6. CONCLUSIONS

1. The Wilkes Ice Dome does not correspond to an ideal ice cap. It is unsymmetrical in outline, rests on an irregular bedrock surface, and has dissimilar cross-section profiles along different radii. It is subjected to an uneven accumulation pattern over its surface, and flow at all points is not radial from the summit. Flow velocities on the eastern side of the ice cap are considerably greater than those of the western side, and major surface strain rates vary along the coast from (+) 112 $\times$ 10^{-4}/yr at Cape Poinsett through (—) 12 $\times$ 10^{-4}/yr at Strain Grid K to (+) 10 $\times$ 10^{-4}/yr near Cape Folger. Although the foregoing conditions present drawbacks in comparing measurements made over the region with theoretical equations based on the assumption of an ideal ice cap, they also permit a broader investigation to be made into the application of such theoretical works under various ice cap conditions.

2. The Wilkes Ice Dome is not in a state of equilibrium but, lacking information on possible fluctuations of the coastline, it cannot be discerned whether it is becoming smaller, as calculations indicate, or whether it is in the process of changing form to adapt to present climatic conditions while retaining a balanced mass budget. Section 4.C shows that over the eastern side of the triangle the ice cap is becoming thinner, in some places at rates of over 1·5 m/yr. Around Cape Folger and along most of the coastal arm, however, the tendency is towards a slow thickening of the ice. The net loss over the whole triangle area has been calculated for the year 1965 to be about 40 cm of ice, or about 1·5 $\times$ 10^{9} metric tons. This corresponds very roughly to one part in 2200 of the total volume of ice under the triangle area.

3. In Section 5.A it was shown that the surface flow velocities and strain rates could be explained reasonably by considering them to be governed largely by bedrock topographical features. Shumskiy (1961) showed that the flow velocity at any point in an ice cap is a function of both the integrated basal stresses between the origin of flow and the required point, and those between the required point and the edge of the ice cap. He considered that the stresses were basically determined by the bedrock slopes, ice thickness and the varying coefficients of friction between the ice and the bedrock. Budd (1967) has extended Shumskiy's work to deduce equations (6) and (8) in Section 4.C which are seen to give consistent and reasonable results when applied to the Wilkes ice cap. Nye (1952, 1959A) assumed that, for an ice cap in a state of steady equilibrium, the flow rate at any point was a function only of the basal stress at that point, which was governed by the ice thickness and surface slope. In Section 5.B it was shown that, for the Wilkes Ice Dome, Nye's flow law gave only an estimate of average ice velocities up to the point of a limiting stress but not beyond that point. It may be concluded from this that for unstable ice caps such as the Wilkes Ice Dome, Shumskiy's approach for determining ice flow velocities is the more applicable.

4. Surface strain rates are a combination of strain rates near the bedrock, caused by the overall shape of the ice cap, and strains in the upper ice mass caused by local surface topography. It was shown in Section 5.B.3 and 5.B.4 that these effects could be examined separately. The flow parameters applicable to each region were determined from the following equations deduced by Budd (1967):

$$B^n \frac{V}{h} = \frac{2(\rho g \bar{\alpha})^n}{(n+1)}, \tag{6}$$

where V is the surface velocity,

h is the ice thickness,

α is the surface slope,

and B and n are parameters in Glen's flow law;

and

$$B\partial\dot{E}^{1/n} = \tfrac{1}{2}\rho g \Delta\alpha \partial x, \tag{8}$$

where $\partial\dot{E}$ is the mean differential strain rate,

and $\Delta\alpha$ is the mean differential surface slope over the distance ∂x.

Equation (6) gives the overall stress parameters governing the velocity throughout the total ice thickness. As most of the strain is normally the result of high shear stresses in the basal layers (Nye 1959A), the parameters given by equation (6) are considered to apply to that region. Equation (8) is applicable to the differential longitudinal strain in the upper ice mass only for situations where lateral strains are of minor importance. Values of the parameters $n = 3{\cdot}4$ and $B = 0{\cdot}85 \times 10^9$ dynes/cm^2 sec$^{1/3}$ were found for strain in the basal layers over the whole triangle area where stresses were in the neighbourhood of one bar and temperatures about -5°C, and values of $n = 1{\cdot}2$ and $B = 1{\cdot}3 \times 10^9$ dynes/cm^2 sec$^{1/3}$ were found for strain in the colder upper ice mass along the Dome—Cape Poinsett leg where stresses were about 0·1 bars and temperatures probably in the range between -15° and -20°C. These values were found to be consistent with those determined by other workers. The large degree of lateral strain along the Dome—Cape Folger leg and the lack of accurate knowledge concerning ice temperatures through the ice cap prevented this work being taken further.

7. ACKNOWLEDGEMENTS

The author wishes to thank all members of the 1965 Wilkes party of Australian National Antarctic Research Expeditions for their valuable and generous co-operation in amassing the data of this investigation. Particular thanks go to Mr. J. Lanyon, the station officer-in-charge, for his support with difficult logistics, Mr. G. A. Allen for his obtaining seismic and gravity data over the triangle area, and the station mechanics for their untiring efforts in keeping the necessary vehicles in almost continual operation.

Information on the bedrock topography and much of the surface contours was kindly supplied by the Director, Bureau of Mineral Resources, Geology and Geophysics.

Valuable assistance was rendered in the analysis of survey data by Messrs D'A. T. Gale, N. Harding, G. Cruickshank and A. G. Bomford of the Division of National Mapping, and by Messrs F. Leahy and B. T. Murphy of the Department of Surveying, University of Melbourne.

In the planning and supervision of the project the author was helped by Dr. U. Radok of the Department of Meteorology, University of Melbourne.

He is also indebted to Mr. W. F. Budd of the ANARE for his guidance in analysing the results. The assistance of Messrs P. Morgan and L. Pfitzner, ANARE glaciologists at Wilkes in 1964 and 1966, is also very much appreciated.

The help of many others in completing the description of this work is gratefully acknowledged, in particular that of Mr. G. Hawking who did the drawings. Extensive typing of drafts for this paper was done most willingly and well by the former Miss M. Neale.

The Acting Director of the Antarctic Division has approved of the publication of this work, and the author is grateful for his support.

E1

8. REFERENCES

ADMIRALTY (1938). Admiralty manual of hydrographic surveying. Hydrographic Dept., Admiralty: London.

BOGOSLOVSKIY, V. N. (1958). The temperature conditions (regime) and movement of the Antarctic glacial shield. Union Géodésique et Géophysique Internationale. A.I.H.S. Publ. No. 47. Symposium de Chamonix.

BUDD, W. F. (1966A). The dynamics of the Amery Ice Shelf. *Journal of Glaciology* **6** (45).

BUDD, W. F. (1966B). Glaciological studies in the region of Wilkes, Eastern Antarctica, 1961. *ANARE Scientific Reports* (A) **4**. Publ. No. 88.

BUDD, W. F. (1967). The longitudinal velocity profile and basal friction of large ice masses. Proceedings of Commission of Snow and Ice, A.I.H.S., Switzerland (to be published).

BULL, C. (1957). Observations in north Greenland relating theories of the properties of ice. *Journal of Glaciology* **3** (21).

BUTKOVICH, T. R., *and* LANDAUER, J. K. (1958). The flow law for ice. Union Géodésique et Géophysique Internationale. A.I.H.S. Publ. No. 47 Symposium de Chamonix.

BUTKOVICH, T. R., *and* LANDAUER, J. K. (1960). Creep of ice at low stresses. U.S. S.I.P.R.E. Research Report 72.

CAMERON, R. L. (1964). Glaciological studies at Wilkes Station, Budd Coast, Antarctica. *Antarctic Research Series* **2**. American Geophysical Union, Publ. 1197.

CLARK, D. (1961). Plane and geodetic surveying for engineers. **2**, 4th edition. Constable and Co. Ltd.: London.

DEPARTMENT OF MINES AND TECHNICAL SURVEYS (1961). Specifications for control surveys. Surveys and Mapping Branch, Technical Instruction No. 1. Ottawa.

DORSEY, N. E. (1940). Properties of ordinary water substance. Reinhold Publ. Corp.: New York.

EDWARDS, F. H. (Unpublished). Accuracies of tellurometer measurements. Thesis submitted for degree of Master of Surveying. University of Melbourne.

GLEN, J. W. (1955). The creep of polycrystalline ice. *Proceedings of Royal Society* (A) **228** (1175).

HANSEN, B. L., *and* LANGWAY, C. C. (to be published). Deep core drilling in ice and core analysis at Camp Century. Greenland, 1961-66. U.S. C.R.R.E.L. Report.

HUMPHRIES, G. J., *and* BRAZIER, H. H. (1958). First order traversing with the tellurometer. *Empire Survey Review* **14** (109).

JAEGER, J. C. (1962). Elasticity, fracture and flow, 2nd edition. Methuen and Co. Ltd.: London.

JENSSEN, D., *and* RADOK, U. (1963). Heat conduction in thinning ice sheets. *Journal of Glaciology* **4** (34).

JEWELL, F. (1962). Wilkes ice thickness measurements, Antarctica 1960. *Bureau of Mineral Resources, Geology and Geophysics Records.* No. 1962/162.

KELSEY, J. (1959A). A method for reducing ground swing on tellurometer measurements. *Empire Survey Review* **15** (112).

KELSEY, J. (1959B). The tellurometer. *The Chartered Surveyor* August, 1959.

LAZAREV, G. Ye. (1962). Elevation determination in Antarctica. *Soviet Antarctic Expedition, Information Bulletin* **4** (3).

MCLELLAN, C. D. (1959). A study of the accuraey of the tellurometer. *Canadian Surveyor* **14** (7).

MEIER, M. F. (1960). Mode of flow of Saskatchewan Glacier, Alberta, Canada. U.S. Geological Survey. Professional Paper 351.

MELLOR, M., *and* SMITH, J. H. (1966). Creep of snow and ice. U.S. C.R.R.E.L. Research Report 220.

MORGAN, P. J. (to be published). Photogrammetric and geophysical methods of determining the mass budget of an ice cap. Thesis submitted for degree of Master of Science, University of Melbourne.

NYE, J. F. (1952). The mechanics of glacier flow. *Journal of Glaciology* **2** (12).
NYE, J. F. (1957). The distribution of stress and velocity in glaciers and ice sheets. *Proceedings of the Royal Society* (A) **239** (1216).
NYE, J. F. (1959A). The motion of ice sheets and glaciers. *Journal of Glaciology* **3** (26).
NYE, J. F. (1959B). A method of determining the strain-rate tensor at the surface of a glacier. *Journal of Glaciology* **3** (25).
ROBIN, G. de Q. (1955). Ice movement and temperature distribution in glaciers and ice sheets. *Journal of Glaciology* **2** (18).
ROYEN, N. (1922). Istryek vid temperature högningar. Hyllmingskrift tilägned F. Vilk Hansen pa sectiöarsdagen. Stockholm.
SHUMSKIY, P. A. (1961). On the theory of glacier motion. Union Géodésique et Géophysique Internationale. A.I.H.S. Assemblé générale de Helsinki.
SHUMSKIY, P. A. (1965). Variation in the mass of the ice cap in central Greenland. Doklady of the Academy of Sciences, U.S.S.R. Earth Scienees Section **162** (May-June 1965). Translated and published by the Americal Geophysical Institute.
STEINMANN, S. (1954). Results of preliminary experiments on the plasticity of ice crystals. *Journal of Glaciology* **2** (16).
STEINEMANN, S. (1958). Résultats expérimentaux sur la dynamique de la glace et leurs correlations avec le mouvement et la pétrographie des glaciers. Union Géodésique et Géophysique Internationale. A.I.H.S. Symposium de Chamonix.
SWITHINBANK, C. W. M. (1958). The morphology of the inland ice sheet and nunatak areas of Western Dronning Maud Land. The regime of the ice sheet of Western Dronning Maud Land as shown by stake measurements. Norwegian-British-Swedish Antarctic Expedition 1949-1952, Scientific Results **3** (Glaciology).
TELLUROMETER PTY. LTD. (1963). Instruction manual for the operation and maintenance of the tellurometer miero-distaneer MRA-2.
TELLUROMETER PTY. LTD. (1964). Newsletter (September).
VOITKOVSKIY, K. E. (1959). Skorost' plastieheskoy deformatsii polikristallicheskogo l'da (The rate of plastic deformation of polyerystalline iee) Journal of the Siberian Department, Academy of Science, U.S.S.R. **4.**
WADLEY, T. L. (1957). The tellurometer system of distance measurement. Empire Survey Review **14** (105 & 106).
WADLEY, T. L. (1958). Electronic principles of the tellurometer. Transactions of the South African Institute of Electrieal Engineers (May).
WALKER, D. (unpublished). Preliminary report on geophysical surveys, Wilkes, Antaretica, 1962-63. (Draft submitted to Department of Meteorology, University of Melbourne.)
WEERTMAN, J. (1957). On the sliding of glaciers. *Journal of Glaciology* **3** (21).
ZUMBERGE, J. H., GIOVINETTO, M., KEHLE, R., *and* REID, J. (1960). Deformation of the Ross Ice Shelf near the Bay of Whales, Antarctica. I.G.Y. Glaciological Report No. 3. I.G.Y. World Data Center A, Glaciology. American Geographical Society.
ZUMBERGE, J. H. (1964). Horizontal strain and absolute movement of the Ross Ice Shelf between Ross Island and Roosevelt Island, Antarctica, 1958-63. *Antarctic Research Series* **2**. American Geophysical Union, Publ. 1197.

APPENDICES

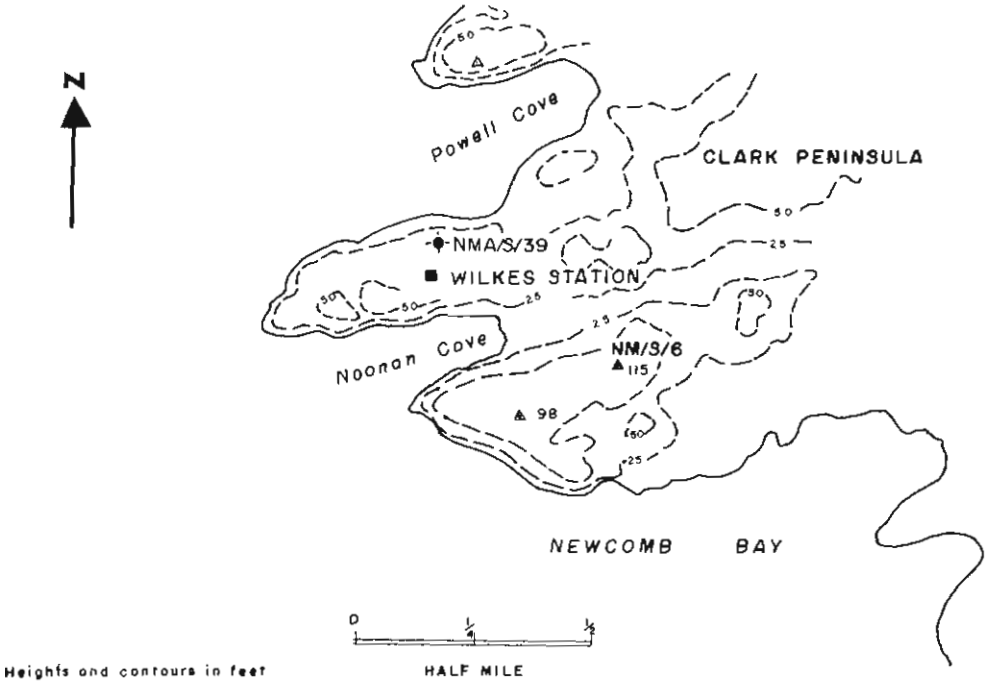
N
Powell Cove
CLARK PENINSULA
NMA/S/39
WILKES STATION
Noonan Cove
NM/S/6
115
98
NEWCOMB BAY
50
25
0
HALF MILE
Heights and contours in feet

APPENDIX I

SURVEY DATA SHEET

NM/S/6—Wilkes G-5

COMMONWEALTH OF AUSTRALIA
DEPARTMENT OF NATIONAL DEVELOPMENT
DIVISION OF NATIONAL MAPPING
TRIGONOMETRICAL STATION SUMMARY PARTICULARS

Station established by: United States Antarctic Expedition, 1957.
Station re-established by: Australian National Antarctic Research Expeditions, January 1963.
Particulars of station marking and beacon, reference marks, situation, access etc (see map): 1-inch steel rod with light on top, 4 feet out of ground.
Station name: NM/S/6 (United States Survey Station G5) Second Order.
Map name: VINCENNES BAY, ANTARCTICA.
Map number: SQ 48-49/11; Scale 1:250,000.
Map number: SQ 48-49(d); Scale 1:500,000.
Latitude: 66°15′39″.8S.
Longitude: 110°32′09″.8E.
Height: 115·21 feet (35·12 metres).
Origin of Survey: NMA/S/39 Wilkes Station (Lat. 66°15′30″S, Long. 110°31′32″E).
Datum for height: Tide gauge zero Wilkes.
Figure of Earth: International Spheroid.
Air photograph identification of station mark:
Title: Wilkes Base (film held by Division of National Mapping).
Film number: Ant 104; run number 26; photo number 8226V; quadrant A x 35·0 mm, Y 32·1 mm; diagonal 47·8 mm (film held by Division of National Mapping).
Reference books: Field book NM 2479; Calculations book 84, pages 22-35.
True azimuth for adjacent stations:
NM/S/9, Nelly Island, 280°32′43·3″ (log distance* 4·210 7090).
NM/S/7, Chappel Island, 329°21′51·3″ (log distance 4·024 4437).
NM/S/8, Midgley Island, 217°33′53·6″ (log distance 3·987 1430).
Remarks: NMA/S/39 has a possible error in latitude and longitude of ± 5 inches. Hence NM/S/6 has probable error of ± 5 inches. Azimuth of NM/S/6 to NM/S/7 has probable error of ± 10 inches. Position NMA/S/39 found from six solar position lines plus one daylight circumpolar meridian star shot.
* By tellurometer distances.

D'A. T. GALE,
Officer-in-charge,
Antarctic Mapping Branch

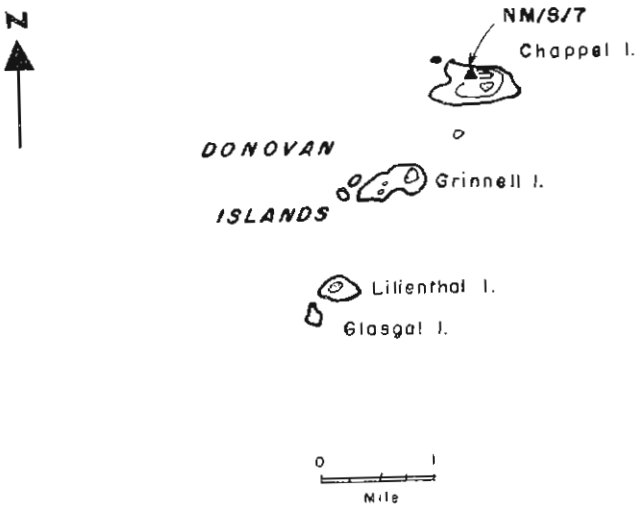
N
NM/S/7
Chappel I.
DONOVAN
ISLANDS
Grinnell I.
Lilienthal I.
Glasgal I.
0
1
Mile

SURVEY DATA SHEET

NM/S/7—Chappel I

COMMONWEALTH OF AUSTRALIA
DIVISION OF NATIONAL MAPPING
TRIGONOMETRICAL STATION SUMMARY PARTICULARS

Station established by: Australian National Antarctic Research Expeditions, January 1963.
Particulars of station marking and beacon, reference marks, situation, access etc. (see map):
2-inch galvanized iron pipe drilled into rock standing 4 feet above surface.
Station name: NM/S/7 (Chappel Island) Second Order.
Map name: VINCENNES BAY, ANTARCTICA.
Map number: SQ 48-49/11; scale 1:250,000.
Map number: SQ 48-49(d); scale 1:500,000.
Latitude: 66°10′46·0″S.
Longitude: 110°24′58·7″E.
Height: 48 metres.
Origin of survey: NMA/S/39 Wilkes Station (lat. 66°15′30″S; long. 110°31′32″E).
Datum for height: NM/S/6 (United States Survey Station G5).
Figure of Earth: International Spheroid.
Air photograph identification mark:
Title: Frazier Island to Donovan Island.
Film number: Ant 124; run number 21; photo number 805IV (film held by Division of National Mapping).
Reference books: Field books NM 2544 and NM 2530; calculations book 84, pages 22-35.
True azimuth for adjacent stations:
NM/S/6, United States Survey Station G5, 149°25′10·0″ (log distance* 4 024 4437).
NM/S/7, Midgley Island, 181°51′19·2″ (log distance 4,225 4673).
NM/S/9, Nelly Island, 239°58′05 7″ (log distance 4·087 3108).
* By tellurometer distances.

D'A. T. GALE,
Officer-in-charge,
Antarctic Mapping Branch

APPENDIX II

Survey Stake Positions

Transverse Mercator Co-ordinates

International Spheroid
False Easting 500,000·00
False Northing 1,000,000·00
A = 6,378,388·000 ms
Scale factor 0·9996
C.M. Zone 1—W177°—00′ . 00″
1/F = 297·000
Zone width 60

Positions adjusted by Bowditch's rule.

AUTUMN TRAVERSE

March-April 1965

Stake Number	Adjusted Position (m)	
	Easting	Northing
G5	479,157·71	2 650,727·46
545	492,181·24	2 661,588·98
508	495,939·24	2 666,176·17
SGA	497,590·25	2 664,861·81
623	500,581·33	2 662,261·19
504	504,547·61	2 658,713·04
542	510,412·34	2 653,976·67
620	515,587·96	2 649,717·86
518	520,370·03	2 645,867·85
544	526,181·56	2 641,166·32
500	529,270·08	2 638,751·47
526	532,427·26	2 636,215·80
549	535,310·12	2 633,896·82
511	538,959·57	2 630,966·21
534	542,560·43	2 628,077·29
605	544,437·02	2 626,571·49
543	547,420·58	2 624,176·60
547	550,473·86	2 621,721·72
505	553,944·60	2 618,927·95
677	558,206·79	2 615,490·75
507	561,927·33	2 612,485·80
653	564,970·80	2 610,027·52
517	566,969·16	2 608,415·90
535	570,389·49	2 605,651·07
683	573,808·11	2 602,884·86
533	576,523·99	2 600,687·30
E1	579,625·29	2 598,170·31
D1	580,850·37	2 597,179·32

SUMMER TRAVERSE

December 1965—January 1966

Stake Number	Adjusted Position (m)	
	Easting	Northing
G5	497,157·71	2 650,727·46
SGA	497,584·05	2 €64,865·05
623	500,577·08	2 662,265·12
504	504,543·53	2 658,717·53
542	510,410·09	2 653,981·66
620	515,587·53	2 649,722·20
518	520,370 11	2 645,871·79
544	526,181·72	2 641,170·22
500	529,269·93	2 638,755·08
526	532,426·78	2 636,218·88
549	535,309·54	2 633,899·29
511	538,958·55	2 630,968·16
534	542,559·05	2 628,079·18
605	544,435·58	2 626,573·54
543	547,419·07	2 624,179·16
637	550,024·30	2 622,086·32
644	552,935·64	2 619,744·41
689	556,793·71	2 616,631·36
677	558,205·96	2 615,493·53
507	561,927·05	2 612,488·84
653	564,970·68	2 610,031·07
517	566,968 85	2 608,419·08
535	570,388·86	2 605,653·32
683	573,807·42	2 602,886·45
660	575,780·58	2 601,286·06
E1	579,625·06	2 598,170·52
D1	580,850·37	2 597,179·32

APPENDIX II (*continued*)

Stake Number	Adjusted Position (m)	
	Easting	Northing
524	581,856·55	2 602,286·89
685	582,332·21	2 604,727·01
506	582,869·64	2 607,452·05
680	583,535·82	2 610,860·44
661	584,401·79	2 615,309·90
527	584,843·29	2 617,544 06
519	585,846·38	2 622,659·20
657	586,641·93	2 626,741·21
G1	587,484·79	2 631,029·82
503	588,482·63	2 636,135·72
530	589,220·20	2 639,962·78
502	590,158·25	2 644,688·03
593	590,485·10	2 646,345·32
509	591,534·01	2 651,681·64
523	592,515·35	2 656,653·96
525	593,325·09	2 660,766·97
H1	593,964·99	2 664,037·92
510	594,875·69	2 668,680·55
567	595,644·16	2 672,611·14
584	596,423·87	2 676,454·08
589	597,344·44	2 681,390·63
J1	598,164·83	2 685,533·78
576	593,128·50	2 684,687·50
591	591,360·72	2 684,310·14
551	586,220·42	2 683,229·41
670	581,999·91	2 682,347·71
590	576,717·93	2 681,226·74
684	569,418·88	2 679,735·43
K1	563,765·98	2 678,555·57
598	560,949·51	2 677,971·36
578	553,425·65	2 676,396·13
564	547,415·43	2 675,072·38
555	543,925·21	2 674,702·03
587	542,701·59	2 674,084·66
583	534,576·16	2 672,518·52
566	531,116·79	2 671,806·64
L1	526,826·67	2 670,924·51
580	524,265·10	2 670,398·56
690	516,105·01	2 668,718·98
682	514,316·97	2 668,353·78
599	510,762·68	2 667,624·05
613	505,311·25	2 666,497·48
616	501,962·48	2 665,824·18
602	500,141·05	2 665,451·79
561	498,719·51	2 665,171·96
SGA	497,580·09	2 664,864·35
G5	479,157·71	2 650,727·46

APPENDIX III

RESULTS FROM STRAIN ROSETTES

Line	Original Length m	Strain (m)	No. of Days	$\dot{E}_1$ 10^{-4}yr^{-1}	$\dot{E}_2$ 10^{-4}yr^{-1}	$Az.\dot{E}_1$	$\dot{E}_x$ 10^{-4}yr^{-1}	$\dot{E}_y$ 10^{-4}yr^{-1}	γ_{xy} 10^{-4}yr^{-1}
Strain Grid A.				Azimuth A_1-A_2 = 305°−12′					
A_1-A_2	98·013	+0·018	260	+10·52	−1·08	069·5°			
A_1-A_4	99·234	+0·074	260	Along Dome leg.			+1·54	+7·90	+9·71
A_1-A_3	99·643	+0·008	260	Along Cape Poinsett leg.			+10·37	−0·92	+2·01
Strain Grid B.				Azimuth B_1-B_2 = 304°−36′					
B_1-B_2	99·884	+0·020	258	+4·84	−1·61	158·5°	+3·18	+0·05	+5·64
B_1-B_3	98·668	−0·011	258						
B_1-B_4	98·402	+0·025	258						
Strain Grid C.				Azimuth C_1-C_2 = 311°−18′					
C_1-C_2	97·301	−0·017	261	+9·22	−3·60	023·8°	−2·85	+8·47	−6·02
C_2-C_3	98·629	+0·016	261						
C_3-C_4	95·834	+0·059	261						
Strain Grid D.				Azimuth D_1-D_2 = 307°−18′					
D_1-D_2	201·042	+0·118	252	+11·25	+5·39	086·2°			
D_1-D_3	200·659	+0·149	252	Along Cape Folger leg.			+8·53	+8·11	+5·85
D_1-D_4	200·693	+0·079	252	Along Cape Poinsett leg.			+5·69	+10·95	+2·57
Strain Grid E. (Tellurometer Grid at Dome)				Azimuth D_1-E_1 = 307°−18′					
D_1-E_1	1576·21	+0·26	252	+8·41	+0·39	071·8°			
D_1-E_2	1549·35	+0·63	252	Along Cape Folger leg.			+2·71	+6·09	+7·21
D_1-E_3	1923·10	+0·26	252	Along Cape Poinsett leg.			+0·80	+8·00	+2·57
D_1-E_4	2381·41	+0·48	252						
D_1-E_1	1843·66	+1·43	252						
D_1-F_2	1714·16	+0·26	252						
Strain Grid G.				Azimuth G_1-G_2 = 0·11°−30′					
G_1-G_2	97 640	−0·024	258	+22·27	−7·16	082·4°	−4·64	+19·76	+16·46
G_1-G_3	97·888	+0·032	258						
G_1-G_4	98·026	+0·149	258						

APPENDIX III (*continued*)

Line	Original Length m	Strain (m)	No. of Days	$\dot{E}_1$ $10^{-4}yr^{-1}$	$\dot{E}_2$ $10^{-4}yr^{-1}$	$Az.\dot{E}_1$	$\dot{E}_x$ $10^{-4}yr^{-1}$	$\dot{E}_y$ $10^{-4}yr^{-1}$	γ_{xy} $10^{-4}yr^{-1}$
Strain Grid H.				Azimuth H_1-H_2 = 011°–30′					
H_1-H_2	98·075	+0·255	257	+37·32	+5·25	017·9°	+36·54	+6·03	+9·91
H_1-H_3	99·599	+0·073	257						
H_1-H_4	96·988	+0·113	257						
Strain Grid J.				Azimuth J_1-J_2 = 191°–36′					
J_1-J_2	97·635	+0·721	266	+112·0	+36·61	033·7°			
J_1-J_3	97·378	+0·270	266	Along Dome leg.			+98·54	+50·07	+57·75
J_1-J_4	97·634	+0·594	266	Along Cape Folger leg.			+78·27	+70·35	+75·34
Strain Grid K.				Azimuth K_1-K_2 = 348°–42′					
K_1-K_2	97·709	−0·068	263	−1·39	−11·78	051·8°	−3·12	−10·05	+7·96
K_1-K_3	97·657	−0·061	263						
K_1-K_4	97·636	−0·010	263						
Strain Grid L.				Azimuth L_1-L_2 = 348°–48′					
L_1-L_2	99·690	−0·002	261	+5·98	−0·66	0·92·5°	+5·49	−0·17	−3·12
L_1-L_3	97·343	+0·038	261						
L_1-L_4	99·143	+0·020	261						

APPENDIX IV

STRAIN AND FLOW DATA

(A) Distances Measured on both Traverses

Stake Number /65	Autumn Distance m	Summer Distance m	No. of Days	Strain Rate $10^{-4}yr^{-1}$	Velocity m/yr V	$Az°$
Cape Folger—Dome leg.						
508	2111·12	2110·55	259	−3·83		
SGA	3965·10	3966·06	259	+3·40	10·0	298
623	5323·75	5323·42	259	−0·90	8 3	313
504	7541·40	7542·32	259	+1·72	8·7	318
542	6705·15	6706·83	258	+3·53	9·4	320
620	6141·63	6142·16	258	+1·22	6·7	355
518	7478·04	7477·95	261	−0·18	5·6	001
544	3922·00	3921·84	258	−0·58	5·6	001
500	4050·89	4050·88	258	0·00	5 2	359
526	3701 17	3701·41	257	+0·91	4 5	351
549	4682·23	4682·12	257	−0·34	3 6	347
Cape Folger—Dome leg.						
511	4618·18	4617·83	257	−1·08	3 1	333
534	2406·92	2406·72	261	−1·17	3 4	324
605	3827·25	3826·78	261	−1·72	3·6	325
543	3919·17	3918·69	261	−1·72	4·2	329
547	4457·05	4458·02	261	+2·97		
505	5477 37	5477·03	259	−0·87		
677	4784·12	4784·29	259	−0·61	4 1	343
507	3913·59	3913·32	255	−1·00	4·4	354
653	2568·10	2568·13	256	+0·14	5·1	358
517	4399·52	4399·76	256	+0·78	4·6	354
535	4399·03	4399·29	253	+0·86	3 3	344
683	3494·71	3495·39	253	+2·79	2 5	337
533	3995·41	3995·24	250	+1·60		

APPENDIX IV (*continued*)

Stake Number /65	Autumn Distance m	Summer Distance m	No. of Days	Strain Rate $10^{-4}yr^{-1}$	Velocity m/yr		
					V		$Az°$
Cape Folger—Dome leg.							
E1	1576·21	1576·47	253	+2·40	0·4		314
D1					0·0		
Dome—Cape Poinsett leg.							
					Vx	Vy	V
D1	5206·12	5207·20	258	+2·93	0·0	0·0	0·0
524	5263·90	5265·04	258	+2·99	1·5	0·1	1·7
506	5194·20	5195·54	258	+3·81	3·1	0·5	3·2
512	5088·59	5090·45	257	+4·57	5·1	1·0	5·4
527	5212·14	5214·01	257	+5·09	7·4	1·7	7·6
519	5093·20	5094·62	258	+3·96	10·1	2·3	10·3
548	3437·27	3437·43	258	+0·68	12·1	3·1	12·4
G1	5204·09	5203·90	257	−0·52	12·3	3·5	12·6
503	3898·48	3900·44	257	+7·15	12·0	4·3	12·3
530	4814·95	4816·79	256	+5·43	14·8	4·7	15·0
Dome—Cape Poinsett leg.							
502	5679·66	5682·14	257	+6·22	17·4	5·2	17·5
531	1446·65	1447·40	256	+7·25	21·0	5·5	21·0
509	5067·94	5069·55	256	+4·52	22·0	5·6	22 0
523	4191·85	4193·07	256	+4·18	24·3	5·7	24·3
525	3331·47	3333·82	256	+10·01	26·1	5·7	26·1
H1	4728·51	4732·32	256	+11·50	29·4	5·8	29·4
510	4005·12	4006·03	256	+3·24	34·8	5·9	34·8
567	3918·67	3922·22	256	+12·89	36·1	6·0	36·1
584	5020 00	5022·91	256	+8·25	41·2	6·1	41·2
589	4218·07	4224·64	256	+22·15	45·3	6·3	45·5
J1					54·7	6·7	55·1
Cape Poinsett—Cape Folger leg.							
J1	5105·12	5109·19	264	+11·01	26·7	48·2	55 1
576	1804·46	1808·26	264	+29·07	21·0	23 9	31·9

APPENDIX IV (*continued*)

Stake Number /65	Autumn Distance m	Summer Distance m	No. of Days	Strain Rate $10^{-4}yr^{-1}$	Velocity m/yr		
					Vx	*Vy*	*V*
Cape Poinsett—Cape Folger leg.							
591					15·8	20·0	25·5
	5248·83	5254·63	264	+15·25			
551					7·8	13·1	15·2
	7765·30	7770·04	262	+8·46			
595					1·2	6·9	7·0
	1942·73	1945·16	262	+11·02			
590					−0·9	5·8	5·9
	7919·69	7923·88	263	+7·25			
559					−6·7	2·0	7·0
	5307·22	5305·96	263	−3·36			
K1					−4·9	0·8	4·9
	2878·82	2877·62	263	−5·77			
598					−3·2	0·9	3·4
	7690·86	7690·28	264	−1·03			
578					−2·4	1·4	2·8
	6156·58	6156·93	263	+0·78			
564					−2·9	2·5	3·8
	3510·48	3511·37	263	+3·52			
555					−4·1	3·2	5·2
	1370·15	1371·15	263	+10·17			
587					−5·5	3·3	6·4
	8279·75	8278·69	263	−1·78			
583					−4·1	4·9	6·4
	3533·54	3533·46	260	−0·32			
566					−3·9	5·6	6·9
	4380·51	4381·86	261	+4·31			
L1					−5·8	6·6	8·8
Cape Poinsett—Cape Folger leg.							
	2615·91	2616·22	261	+1·66			
580					−6·3	6·7	9·2
	8683·99	8681·89	261	−3·53			
550					−3·2	7·4	8·0
	5108·00	5109·17	261	+3·06			
599					−4·8	7·4	8·8
	5569·06	5569·20	260	+0·34			
613					−5·0	7·3	8·8
	3416·96	3417·39	261	+1·79			
616					−5·6	7·2	9·1
	1859·42	1859·97	261	+4·13			
602					−6·3	7·1	9·3
	1605·85	1606·45	259	+5·40			
630					−7·2	7·0	10·3
SGA					−7·4	6·7	10·0

(B) Distances Measured on Summer Traverse Only

Stake Number /65	Summer Distance m	Stake Number /65	Summer Distance m
Cape Folger—Dome leg.			
543		683	
	3341·60		2541·35
637		660	
	3738·88		4949·84
644		E1	
	4959·03		
689			
	1814·16		
677			
Dome—Cape Poinsett leg.			
524		519	
	2486·76		4159·96
685		657	
	2778·32		4371·85
506		G1	
	3473·84		
680			
	4534·23		
661		502	
	2277·98		1689·62
527		593	
			5439·92
		509	
Cape Poinsett—Cape Folger leg.			
551		580	
	4313·26		8334·99
670		690	
	5401·71		1825·79
590		682	
	7452·83		3630·12
684		599	
	5777·10		
K1			
		602	
			1449·49
		561	
			1180·76
		SGA	

APPENDIX V

ICE CAP PROFILES AND ACCUMULATION

Stake Number /64	/65	Kms from orig.	Surface Elevation (m) at stake	17 km mean	relative elev'n	Bedrock elev'n (m)	Ice Thickness at stake	17 km mean	Accumulation gm/cm²/yr stake	smooth
Dome—Cape Folger										
	D1	0·00	1389	1372	+17	335	1054	1084	65·0	
052	E1	1·58	1386	1371	+15	312	1074	1088	67·3	64
695		3·07	1383	1369	+14	293	1090	1095	58·0	59
759		4·57	1378	1366	+12	258	1120	1097	53·5	53
	533	5·51	1368			232	1136		48·0	
638		6·07	1366	1361	+5	223	1143	1100	44·0	48
	660	6·53	1364			226	1138			
646		7·56	1356	1354	+2	234	1122	1110	54·8	50
683	683	9·06	1348	1346	+2	249	1099	1122	44·5	46
691		10·53	1337	1337	0	226	1111	1126	41·0	42
615		11·99	1328	1327	+1	207	1121	1125	40·5	40
613	692	13·47	1321	1317	+4	195	1126	1121	37·0	37
727		15·02	1308	1307	+1	150	1158	1110	35·3	36
602		16·58	1297	1296	+1	146	1151	1105	36·0	32
	517	17·86	1289			159	1130		19·5	
762		18·14	1288	1285	+3	163	1125	1106	20·5	26
642		19·68	1275	1274	+1	177	1098	1105	28·5	20
	653	20·44	1269			177	1092		9·5	
671		21·24	1265	1263	+2	179	1086	1101	17·0	23
614		22·79	1251	1251	0	194	1057	1101	30·5	26
750	507	24·35	1238	1240	−2	168	1070	1089	25·0	27
665		25·94	1227	1228	−1	146	1081	1079	27·0	25
705		27·54	1216	1216	0	138	1078	1070		
667	677	29·13	1205	1204	+1	138	1067	1065	18·0	18
721		30·67	1195	1192	+3	96	1099	1052	13·0	17
	689	31·04	1193			106	1087			
605		32·22	1184	1181	+3	136	1048	1044	24·0	18
624		33·75	1168	1170	−2	111	1057	1023	12·5	16
	505	34·62	1161			114	1047	1011	10·0	
700		35·28	1156	1158	−2	117	1039	1001	23·0	15
	644	35·90	1155			117	1038			
686		36·82	1147	1145	+2	116	1031	974	10·5	17
668		38·37	1133	1133	0	148	985	954	24·0	17
	547	39·64	1128			186	942			
Unnum		39·91	1125	1120	+5	194	931	928	11·0	16
754		41·46	1108	1108	0	243	865	904	19·2	8
672	543	42·99	1096	1095	+1	244	852	881	0·0	10
661		44·55	1084	1082	+2	285	799	871	21·0	12
713		46·10	1068	1070	−2	250	818	854	5·5	9
	605	46·82	1065			264	801		3·5	
628		47·65	1058	1056	−2	273	785	840	11·5	7
740	534	49·21	1046	1043	+3	286	760	830	1·0	3
714		50·74	1024	1030	−6	207	817	817	−1·8	2
748		52·29	1015	1017	−2	133	882	807	11·0	7
744	511	53·83	1006	1003	+3	146	860	808	7·0	8
656		55·39	990	990	0	178	812	809	8·8	7
681		56·95	978	977	+1	170	808	807	3·3	4
716	549	58·52	963	963	0	167	796	806	0·7	4
609		60·06	952	949	+3	137	815	795	11·7	8
637		61·62	938	935	+3	148	790	783	8·0	5
	526	62·22	930			146	784			
736		63·18	924	920	+4	144	780	769	−6·0	0

APPENDIX V (*continued*)

Stake Number /64	/65	Kms from orig.	Surface Elevation (m) at stake	17 km mean	relative elev'n	Bedrock elev'n (m)	Ice Thickness at stake	17 km mean	Accumulation gm/cm²/yr stake	smooth
662		64·73	907	905	+2	149	758	761	3·0	0
663	500	66·27	892	889	+3	155	737	755	−1·0	2
728		67·82	875	874	+1	153	722	751	8·5	5
634		69·36	859	857	+2	122	737	746	5·0	6
	544	70·20	850			125	725			
746		70·92	844	841	+3	128	716	742	6·5	4
755		72·48	826	824	+2	114	712	735	0·0	4
297		74·03	806	808	−2	84	722	732	9·7	8
723		75·57	787	791	−4	+48	739	727	13·5	16
648		77·14	775	773	+2	−6	781	717	29·0	23
	518	77·67	771			+4	767			
694		78·70	759	755	+4	+24	735	709	20·0	20
685		80·24	737	737	0	+30	707	699	5·5	16
731		81·79	721	718	+3	−17	738	683	33·0	22
684		83·35	708	699	+9	+6	702	669	18·5	17
	620	83·81	701			12	689		0·0	
664		84·91	684	680	+4	26	658	652	15·0	12
674		86·47	662	658	+4	49	613	636	18·0	17
617		88·05	642	636	+6	56	586	622	15·5	16
712		89·62	623	614	+9	42	581	608	16·5	16
	542	90·53	610			54	556			
719		91·22	601	591	+10	58	543	587	17·0	12
601		92·81	568	567	+1	+32	536	559	−1·0	8
608		94·40	540	541	−1	−30	570	531	15·0	10
644		96·00	515	514	+1	−57	572	508	9·5	9
224		97·59	500	484	+16	−58	558	490	1·5	4
	504	98·06	496			−48	544		2·5	
715		99·18	471	453	+18	−39	510	470	2·5	2
604		100·78	430	422	+8	−14	444	448	−1·0	0
735		102·37	395	389	+6	−22	417	416	−1·0	−1
	623	103·38	374			−22	396			
607		103·96	365	358	+7	−18	383	381		
676		105·57	327			−20	347		−3·5	−3·5
742		107·18	288			−41	329			
	SGA	107·34	282			−40	322			
702		108·79	249			−13	262			
	508	109·47	230			00	230			
757		110·40	205			+23	182			
Dome—Cape Poinsett										
	D1	0·00	1389	1374	+15	335	1054	1123	65·0	
300		1·74	1384	1376	+8	307	1077	1127	59·5	61
206		3·48	1385	1376	+9	237	1148	1128	61·0	61
311	524	5·21	1387	1374	+13	225	1162	1136	61·0	59
260		6·97	1380	1370	+10	206	1174	1144	52·5	56
	685	7·69	1378			193	1185			
294		8·72	1373	1364	+9	174	1199	1154	59·3	60
298	506	10·48	1365	1357	+8	169	1196	1166	69·0	63
504		12·21	1355	1349	+6	164	1191	1175	53·3	58
203	680	13·95	1344	1340	+4	165	1179	1177	56·0	57
530	512	15·68	1332	1329	+3	151	1181	1176	61·5	59
547		17·36	1321	1318	+3	144	1177	1173	58·5	61
	661	18·48	1313			138	1175			
316		19·07	1309	1306	+3	135	1174	1166	63·8	62
542	527	20·76	1295	1294	+1	133	1162	1162	63·8	63
554		22·50	1283	1280	+3	132	1151	1156	61·3	61

APPENDIX V (*continued*)

Stake Number /64	/65	Kms from orig.	Surface Elevation (m) at stake	17 km mean	relative elev'n	Bedrock elev'n (m)	Ice Thickness at stake	17 km mean	Accumulation gm/cm²/yr stake	smooth
276		24·24	1269	1267	+2	114	1155	1150	57·3	61
537	519	25·97	1257	1253	+4	118	1139	1143	67·8	62
285		27·68	1241	1239	+2	108	1133	1135	56·8	62
217		29·39	1225	1225	0	88	1137	1127	65·3	65
	657	30·13	1218			87	1131			
557	548	31·06	1208	1212	−4	87	1121	1117	73·0	67
517		32·80	1195	1197	−2	70	1125	1101	57·0	64
544	G1	34·50	1182	1183	−1	91	1091	1087	64·0	62
269		36·24	1165	1167	−2	72	1093	1066	62·5	62
519		37·98	1157	1150	+7	54	1103	1049	61·0	57
539	503	39·70	1146	1133	+13	106	1040	1036	42·2	49
290		41·45	1120	1117	+3	119	1001	1017	51·4	51
559		43·19	1112	1098	+14	107	975	995	60·8	56
	530	43·61	1105			140	965		58·0	56
512		44·95	1079	1081	−2	144	935	976	51·4	54
556		46·69	1063	1062	+1	87	976	947	50·8	54
288	502	48·43	1045	1041	+4	108	937	922	64·6	58
508	593	50·11	1025	1019	+6	128	897	903	51·7	54
546		51·87	999	998	+1	124	875	890	49·0	51
216		53·62	978	975	+3	116	862	877	55·5	54
	531	54·11	972			115	857		53·0	55
521		55·38	959	953	+6	119	840	970	61·8	58
	509	55·55	956			118	838		61·0	57
296		57·13	931	931	0	113	818	856	51·3	54
538		58·88	906	909	−3	100	806	842	52·7	49
551	523	60·62	885	884	+1	34	851	821	39·4	47
505		62·38	861	859	+2	+26	835	807	58·0	48
310		64·13	840	833	+7	−1	841	790	40·0	43
	525	64·81	829			00	829		32·5	40
289		65·89	814	806	+8	+3	811	779	53·0	46
560		67·64	795	778	+17	2	793	770	38·5	45
	H1	68·16	785			10	775		47·5	50
264		69·39	754	753	+1	24	730	765	65·5	59
500		71·15	728	725	+3	9	719	750	68	58
526	510	72·89	697	698	−1	+1	696	733	30·3	50
267		74·64	663	669	−6	−38	701	713	70·0	55
244		76·40	636	639	−3	−71	707	692	51	52
	567	76·89	626			−77	703		79	
274		78·15	606	608	−2	−88	694	671	35·3	41
502		79·90	585	574	+11	−107	692	651	41·8	44
	646	80·81	568			−102	670			
534		81·64	555	541	+14	−90	645	635	58·3	56
279		83·38	520	506	+14	−118	638	617	64·2	61
524		85·09	487	469	+18	−129	616	596	56·5	61
	589	85·83	467			−127	594		55·0	51
525		86·79	452	431	+21	−114	566	576	51·5	50
228		88·51	398	392	+6	−132	530	551	58·5	48
	J1	90·06	379			−135	514		11·0	26
528		90·22	370	350	+20	−142	512		24·0	32
231		91·93	306	310	−4	−199	505		23·3	28
278		93·64	265	264	+1	−210	475		43·3	35
548		95·35	216	217	−1	−234	450		30·0	36
281		97·06	160	176	−16	−389(?)	549(?)		40·5	
		98·5	63							
	M14	101·6	42							
		104·0	38							

APPENDIX V (*continued*)

Stake Number /64	/65	Kms from orig.	Surface Elevation (m) at stake	17 km mean	relative elev'n	Bedrock elev'n (m)	Ice Thickness at stake	17 km mean	Accumulation gm/cm²/yr stake	smooth
Cape Poinsett—Cape Folger										
	J1	0·00	379			—135	514		11·0	
540		1·70	375			—155	530		65·5	48
263		3·41	400			—168	568		38·5	50
510	576	5·10	432			—195	627		56·5	57
318	591	6·92	450	439	+11	—209	659		76·5	66
503		8·67	462	452	+10	—202	664	668	55·5	58
243		10·43	473	466	+7	—213	686	689	44·7	44
518	551	12·17	496	479	+13	—265	761	705	33·7	38
552		13·92	504	491	+8	—258	762	722	38·5	30
309		15·69	508	500		—270	778	735	9·0	18
	670	16·48	514		+10	—273	787			
205		17·45	516	506	+8	—282	798	739	15·0	19
237		19·20	519	511		—219	738	748	+35·5	20
	595	19·94	521		+13	—229	752			
272		20·95	527	514		—245	772	744	—4·7	13
	590	21·89	530			—225	755		—2·5	4
271		22·72	529	515	+14	—211	740	739	+25·0	14
275		24·50	522	515	+7	—250	772	726	+10·2	10
545		26·25	517	516	+1	—197	714	719	—3·5	1
531		28·03	514	515	—1	—179	693	700	—0·7	0
	684	29·34	517							
292	559	29·80	513	514	—1	—168	681	686	+4·7	3
229		13·58	505	513	—8	—173	678	666		14
286		33·35	503	510	—7	—168	671	652	23·5	16
555	K1	35·12	509	509	00	—137	646	636	+2·0	4
541		36·87	506	509	—3	—84	590	629	—9·7	—3
	598	38·00	515			—71	586		+3·5	1
214		38·62	509	509	00	—74	583	620	6·0	4
514		40·40	505	510	—5	—69	574	610	8·2	11
323		42·16	504	512	—8	—87	591	602	22·0	22
209		43·94	510	513	—3	—77	587	596	+37·5	22
506	578	45·69	519	514	+5	—63	582	592	—6·0	7
200		47·44	516	516	00	—86	602	591		4
235		49·20	518	517	+1	—49	567	594	+13·0	6
261		50·95	524	516	+8	—96	620	597	—7·0	—2
	564	51·84	526			—85	611		—15·0	—8
201		52·70	524	515	+9	—79	603	604	+6·0	0
505		54·46	523	513	+10	—83	606	608	—3·0	0
	555	55·35	524			—79	603		+2·5	0
215		56·21	523	510	+13	—77	600	611	—1·5	0
	587	56·73	527			—69	596		—6·8	—3
523		57·97	517	509	+8	—60	577	611	+16·5	9
536		59·72	508	509	—1	—142	650	607	7·5	8
218		61·48	494	508	—14	—155	649	603	2·0	5
293		63·25	487	506	—19	—147	634	600	9·4	6
550	583	65·00	493	502	—9	—110	603	597	4·0	9
213		66·77	497	499	—2	—80	577	594	+17·0	9
553	566	68·54	508	494	+14	—94	602	588	—0·3	4
299		70·30	500	492	+8	—79	579	579	0·0	4
532		72·03	494	491	+3	—66	560	567	+8·5	6
	L1	72·92	495			—58	553		+6·0	5
219		73·77	493	490	+3	—53	546	555	—2·0	—2
558	580	75·52	494	488	+6	—49	543	545	—9·0	—6
251		77·25	482	486	—4	—52	534	537		—2

APPENDIX V (*continued*)

Stake Number /64	/65	Kms from orig.	Surface Elevation (m) at stake	17 km mean	relative elev'n	Bedrock elev'n (m)	Ice Thickness at stake	17 km mean	Accumulation gm/cm²/yr stake	smooth
295		78·97	481	480	—1	—62	543	532	+1·0	3
324		80·69	477	475	+2	—33	510	531	+13·0	6
529		82·43	476	468	+8	—27	503	528	—4·5	2
	690	83·86	475			—24	499			
210		84·15	474	459	+15	—24	498	525	+3·0	1
	682	85·70	466			—24	490			
246		85·87	465	450	+15	—24	489	517		3
527		87·60	447	442	+5	—111	558	504	+3·0	4
211	599	89·41	443	432	+9	—91	534	496	8·7	8
245		90·86	420	422	—2	—104	524	488	13 0	11
233		92·40	405	410	—5	—110	515	477		8
265		93·95	397	394	+3	—58	455	472		4
	613	94·89	394			—69	463			
522		95·50	384	376	+8	—85	469	454	—0·8	—2
212		97·04	374	356	+18	—62	436	430	—8·5	—6
	616	98·31	363			—60	423			
543		98·60	359			—61	420		—6·0	— 6
277	602	100·17	340			—46	386		—5·0	—6
	630	101·61	311			—74	385			
291		101·77	307			—78	385		—7 0	—6
	SGA	102·80	282			—40	322			
307		103·32	268			—23	291			
239		104·93	237			—19	256			

APPENDIX VI

SURFACE AND BEDROCK SLOPES, BASAL STRESS AND VERTICAL VELOCITY

Stake Number /64	/65	Surface Slope (m/km) Local	over 3 kms	over 2 legs	$\rho gh\alpha$ bars	Local Bedrock Slope	V_s from V.C.1 cm/yr
Dome—Cape Folger							
	D1						−21
052	E1	1·9	1·9	3·6	0·346	+14·6	−18
695		2·0	2·3				
759		3·3	5·5				
	533	10·4		5 1	0·495	+27·7	−46
638		3·6	7·1				
	660	4·3					
646		7·8	5·3				
683	683	5·3	6·4	6·1	0·604	−10·0	−38
691		7·5	6·7				
615		6·2	5·4				
613	692	4·7	6·6	6·7	0·663	+8·1	−45
727		8·4	7·8				
602		7·1	6·5				
	517	6·3		7·5	0·732	−10·2	−58
762		3·6	7·2				
642		8·4	7·5				
	653	7·9		7·9	0·769	00	−52
671		5·0	7·8				
614		9·0	8·8				
750	507	8·3	7·8	7·4	0·711	+16·7	−51
665		6·9	7·0				
705		6·9	7·0				
667	677	6·9	6·7	7·5	0·705	00	−57
721		6·5	6·8				
	689	5·4					
605		7·6	8·8				
624		10·5	9·1				
	505	8·0		7·8	0·696	−3·4	−74
700		7·6	6·8				
	644	1·6					
686		8·7	7·5				
668		9·0	7·2				
	547	3·9		7·8	0·648	−29·9	−53
Unnum		11·1	8·1				
754		11·0	9·4				
672	543	7·8	7·8	8·1	0·663	−0·7	−42
661		7·7	9·1				
713		10·3	8·5				
	605	4·2		8·0	0·605	−19·4	−30
628		8·4	7·2				
740	534	7·7	11·0	8·4	0·626	−3·8	−44
714		14·4	10·1				
748		5·8	5·8				
744	511	5·8	8·1	8·9	0·659	−8·4	−37
656		10·3	9·1				
681		7·7	8·8				
716	549	9·6	8·4	9·1	0·687	+1 9	−36
609		7·1	8·1				
637		9·0	9·1				
	526	13·3		9·2	0 680	+3·3	−26
736		6·3	10·1				

APPENDIX VI (*continued*)

Stake Number /64	/65	Surface Slope (m/km) Local	over 3 kms	over 2 legs	$\rho gh\alpha$ bars	Local Bedrock Slope	V_z from V.C.1 cm/yr
662		11·0	10·4				
663	500	9·7	10·4	10·0	0·726	−3·9	−4
728		11·0	10·7				
634		10·4	10·1				
	544	10·7		10·6	0·763	−3·6	+10
746		8·3	10·7				
755		11·5	12·4				
297		12·9	12·7				
723		12·3	10·1				
648		7·6	9·1				
	518	7·5		10·9	0·745	−18·9	+12
694		11·7	12·4				
685		14·3	12·4				
731		10·3	9·4				
684		8·3	12·0				
	620	15·2		12·5	0·780	−13·0	+2
664		15·5	15·0				
674		14·1	13·7				
617		12·7	12·7				
712		12·1	13·3				
	542	14·2		14·4	0·783	−13·2	+9
719		13·0	17·9				
601		20·8	19·8				
608		17·6	17·2				
644		15·6	12·8				
224		9·4	14·1				
	504	8·5		18·3	0·788	−21·3	−2
715		22·3	22·4				
604		25·6	24·3				
735		22·0	20·8				
	623	20·8		23·0	0·800	00	−15
607		15·5	21·8				
676		23·6	24·6				
742		24·2	25·0				
	SGA	37·5		23·7	0·606	−6·2	+5
702		22·8	26·6				
	508	27·9					
757		26·8					
Dome—Cape Poinsett							
	D1						−21
300		2·9	1·1				
206		−0·6	−0·9				
311	524	−1·2	1·4	2·3	0·230	+6·9	−37
260		4·0	4·0				
	685	2·8					
294		4·9	4·3				
298	506	4·5	5·2	5·3	0·545	+2·8	−53
504		5·8	6·1				
203	680	6·3	6·7				
530	512	6·9	6·7	6·8	0·706	+8·1	−94
547		6·5	6·7				
	661	7·1					
316		6·8	7·5				
542	527	8·3	7·5	7·3	0·749	+1·2	−131
554		6·9	7·5				
276		8·0	7·5				

APPENDIX VI (*continued*)

Stake Number /64	/65	Surface Slope (m/km) Local	over 3 kms	over 2 legs	$\rho gh\alpha$ bars	Local Bedrock Slope	V_s from V.C.1 cm/yr
537	519	6·9	8·1	8·4	0·847	−2·3	−162
285		9·4	9·3				
217		9·4	9·7				
	657	9·5					
557	548	10·4	8·8	8·8	0·868	00	−155
517		7·6	7·6				
544	G1	7·6	8·7	7·2	0·691	−11·2	−65
269		9·8	7·2				
519		4·6	5·5				
539	503	6·4	10·7	8·5	0·777	−30 2	−123
290		14·9	9·9				
559		4·6	11·7				
	530	16·7		11·5	1·005	−7·1	−118
512		19·4	14·0				
556		9·2	9·9				
288	502	10·3	10·9	12·6	1·025	−12·1	−71
508	593	11·9	13·2				
546		14·8	13·4				
216		12·0	11·4				
	531	12·0		12 6	0·980	+2·0	−68
521		10·2	13·4				
	509	17·6		13·5	1·036	+5·9	−28
296		15·8	15·4				
538		14·3	13·3				
551	523	12·1	13·1	13·7	0 993	+37·9	−105
505		13·6	13·1				
310		12·0	13·6				
	525	16·1		13·3	0·923	−1·5	−19
289		13·9	13·0				
560		10·9	17·4				
	H1	19·2		16 4	1·112	−15·4	−171
264		25·2	19·4				
500		14·8	16·5				
526	510	17·8	18·9	18·2	1·178	+4·6	−3
267		19·4	17·7				
244		15·3	16·5				
	567	20·4		16 3	0·987	+12·2	−30
274		15·9	14·8				
502		12·0	14·8				
	646	18·6		17·8	1·010	−5·5	+5
534		15·7	18·9				
279		20·1	19·7				
524		19·3	19·7				
	589	27·0		20·5	1·062	−2·7	−56
525		15·6	25·8				
228		31·4	23·8				
	J1	12·3		20 9	0·972	+10 4	−714
528		56·3	26·7				
231		37·4	30·5				
278		24·0	26·1				
548		28·7	30·5				
281		32·7	49·6				
		67·4	36·8				
	M14	6·8	4·1				
		1·6					